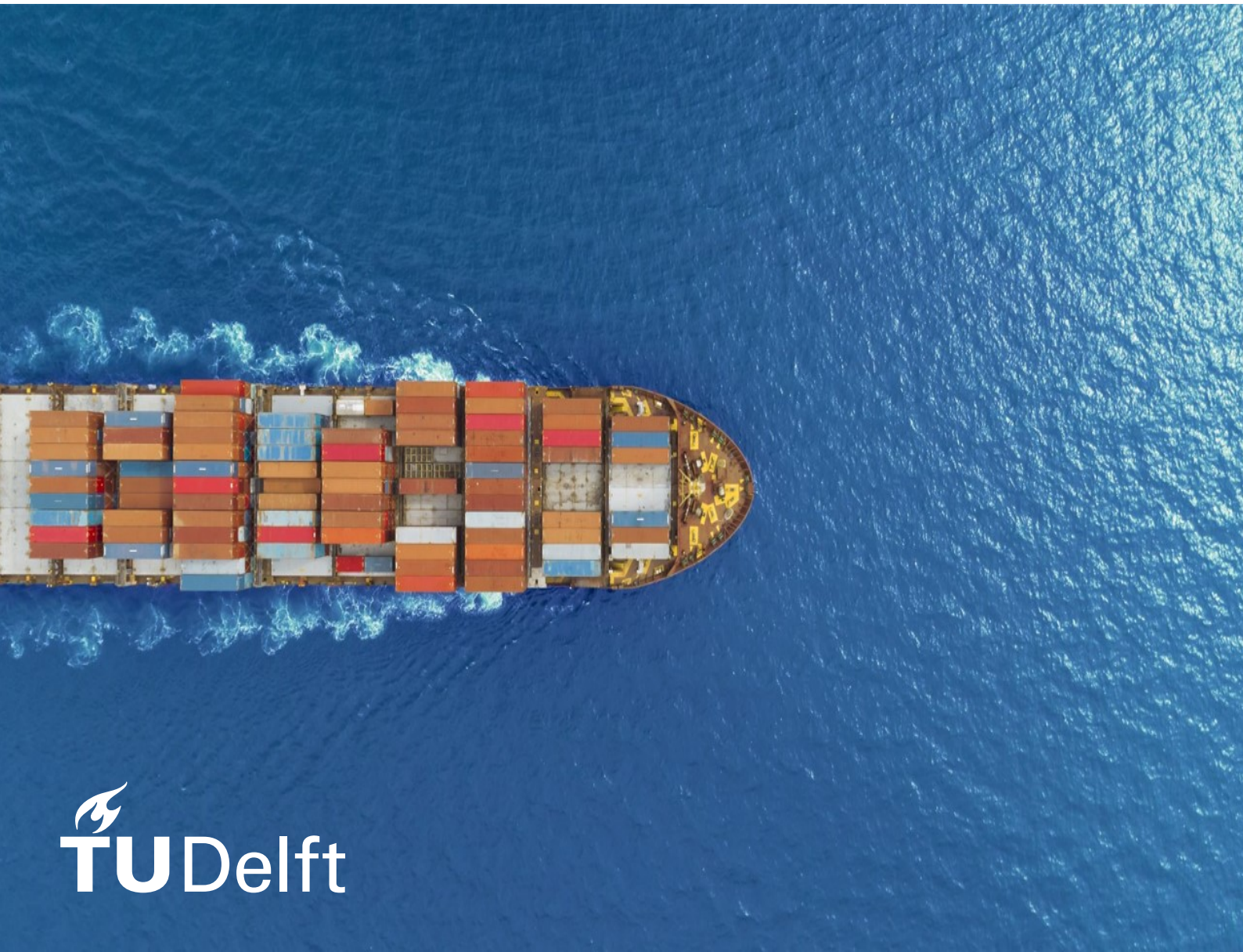


The underwater ventilation of methanol vapour

A numerical investigation

Master Thesis
C. De Boom



Thesis for the degree of MSc in Marine Technology in the specializations of Ship Design & Marine Engineering

The underwater ventilation of methanol vapour

A numerical investigation

by

C. De Boom

Performed at

TNO & Bureau Veritas

This thesis (MT.22/23.034.M) is classified as confidential in accordance with the general conditions for projects performed by the TUDelft.

To be defended publicly on Wednesday June 28, 2023 at 10:00 AM

Company supervisors

Responsible supervisor: Ir. A.W. Vredevelde (TNO)
Responsible supervisor: Ir. A. van Hoeve (Bureau Veritas)

Thesis exam committee

Chair/Responsible Professor: Dr. ir. L. van Biert
Staff Member: Dr. A.J. Bottger
Staff Member: Dr. ir. I. Akkerman
Company Member: Ir. A.W. Vredevelde (TNO)
Company Member: Ir. A. van Hoeve (Bureau Veritas)

Author details

Student number: 5379407
Faculty: 3mE. Mechanical, Maritime and Materials Engineering
Project duration: November, 2022 - July, 2023

An electronic version of this thesis is available at <http://repository.tudelft.nl/>.

Preface

Individual success is non-existent in graduation projects. To achieve success you should surround yourself with people who are outstanding in their field of expertise and that is exactly what I have done. Therefore a few words of gratitude are definitely justified.

To Lex Vredeveltdt from TNO for the day-to-day supervision. The numerous discussions on the physics and the critical questions helped greatly to successfully complete this research. I wish you all the best for your retirement.

To Aris Twerda from TNO without whom the CFD simulations would not have succeeded. The feedback on fluid dynamics helped my understanding greatly.

To Ad van Hove from Bureau Veritas for showing and guiding me in the aspects of the research which are important for rules and regulations. The received feedback help greatly in assuring the relevance of this research for the maritime industry.

To Lindert van Biert from the TU Delft for giving me the opportunity to graduate on this topic, the numerous feedback and for assuring this graduation process went smoothly.

To my parents and family for not only supporting me during this thesis, but throughout my whole education.

C. De Boom
Delft, June 2023

Abstract

In order to meet the shipping industry's emissions reduction goals, it is imperative to explore and adopt alternative marine fuels. Methanol (or methyl alcohol) is expected to play a large role in the future. However, current regulations limit the attractiveness of methanol as marine fuel due to the inability to use the space around a venting point on deck. Hazardous area zones are installed around fuel tank vapour outlets due to the flammability and toxicity of methanol vapour. Consequently, these areas become very impractical. This thesis investigates the ventilation of the fuel tank vapour below the waterline instead on deck in order to be able to limit/eliminate these areas. Therefore, the main research question is:

"What is the concentration of methanol at deck level when methanol is vented below the waterline?"

This report is divided in 2 parts. The first part is a literature study where the properties of methanol as a marine fuel are described. In this part also the physics and models of subsea venting or subsea gas releases are investigated.

In the second part an Eulerian based CFD model and a simple integral model are used to predict the methanol concentration above the waterline. The integral model predicts the gas concentration above the waterline based on the gas flow rate reaching the surface and the radial inflow rate of air. The CFD model tracks parcels (group of bubbles with the same properties) using the force balance in the discrete phase model. Both of the models are successfully validated against experimental data from the "Rotvoll experiment" wherein methane was released at the bottom of a water basin. The CFD model showed strong superiority over the integral model, o.a. due to the lack of gas dissolution in the integral model.

The numerical models are applied to the case wherein a mixture of methanol and nitrogen is vented due to an overpressure. The overpressure could be caused by for example the failure of the vapour return line when bunkering or a fire. The bunker tanks are protected by a pressure relief valve, which reduces the overpressure by directing the gases in the bunker tank towards the venting location below the waterline. The flow rate characteristic (pressure - flow rate) of the pressure relief valve determines the rate at which the gases are injected in the water. The gas dissolution showed strong dependence on the departure bubble diameter and the venting depth. Different cases with different initial bubble sizes and different venting depths were simulated. The CFD model showed that in the most critical case (lowest venting depth 0.5m and largest initial bubble size 0.08m) the gas dissolution is large enough such that no methanol vapour reaches the deck of the ship and barge. The subsea venting of methanol-nitrogen vapour proved to be a safe alternative compared to the venting above deck.

Keywords: Methanol; Nitrogen; Dissolution ; Ship; Fuel; CFD; Subsea; Venting; Tank; Bunkering; Hazardous area; Safety

Contents

| | |
|---|-------------|
| Preface | iii |
| Abstract | v |
| List of Figures | x |
| List of Tables | xii |
| Nomenclature | xiii |
| 1 Introduction | 1 |
| I Literature Review | 3 |
| 2 Methanol as marine fuel | 4 |
| 2.1 Properties of methanol | 4 |
| 2.1.1 Toxicity | 4 |
| 2.1.2 Flammability | 5 |
| 2.1.3 Methanol spill | 6 |
| 2.2 Regulations and guidelines | 6 |
| 2.2.1 Venting | 6 |
| 2.2.2 Hazardous areas and deck exclusion zones | 7 |
| 2.2.2.1 Interim guidelines for the safety of ships using methyl/ethyl alcohol as fuel | 7 |
| 2.2.2.2 The carriage of methanol in bulk onboard offshore vessels | 8 |
| 2.2.2.3 IEC-code | 10 |
| 3 Subsea venting | 12 |
| 3.1 Governing physics | 12 |
| 3.1.1 Zone of flow establishment | 12 |
| 3.1.2 Zone of established flow | 13 |
| 3.1.3 Surface zone | 14 |
| 3.1.4 Atmosphere | 14 |
| 3.2 Subsea gas release models | 14 |
| 3.2.1 Empirical models | 14 |
| 3.2.2 Integral models | 15 |
| 3.2.3 CFD models | 17 |
| 3.3 Experiment | 19 |
| 3.3.1 Gas detection on board of ships | 20 |
| 3.3.1.1 Combustible gas indicator or explosion meter | 20 |
| 3.3.1.2 Tankscope | 20 |
| 3.3.1.3 Oxygen analyzer | 20 |
| 3.3.1.4 Toxic gas detectors | 20 |
| 3.3.2 Methanol gas detection | 21 |
| 4 Conclusion | 23 |
| 4.1 Literature study conclusions | 23 |
| 4.2 Research gap analysis | 23 |
| 4.3 Research questions and methodology | 24 |
| 4.4 Boundaries research | 24 |

| | |
|--|-----------|
| II Numerical Investigation | 28 |
| 5 Methods | 29 |
| 5.1 CFD | 29 |
| 5.1.1 Basics CFD | 29 |
| 5.1.2 Geometry | 30 |
| 5.1.3 Mesh sizing | 31 |
| 5.1.4 Model | 34 |
| 5.1.4.1 Algorithms | 34 |
| 5.1.4.2 Turbulence | 35 |
| 5.1.5 Parameters | 35 |
| 5.1.6 Boundary conditions | 36 |
| 5.1.7 User defined model | 36 |
| 5.1.7.1 Drag force | 36 |
| 5.1.7.2 Bubble size distribution | 36 |
| 5.1.7.3 Gas dissolution | 38 |
| 5.1.7.4 Influence salinity | 39 |
| 5.1.7.5 Influence bubble size | 40 |
| 5.1.8 Solution method | 40 |
| 5.1.9 Software and Hardware | 40 |
| 5.2 Integral model | 40 |
| 6 Cases | 42 |
| 6.1 Rotvoll experiment | 42 |
| 6.2 Methanol full scale venting | 43 |
| 6.2.1 Release characteristic | 43 |
| 6.2.2 Geometry | 45 |
| 6.2.3 Mesh | 46 |
| 6.2.4 Boundary conditions | 47 |
| 6.2.5 Gas dissolution | 47 |
| 6.3 Methanol small scale venting | 47 |
| 6.3.1 Release characteristic | 47 |
| 6.3.2 Geometry | 49 |
| 6.3.3 Mesh | 49 |
| 6.3.4 Boundary conditions | 50 |
| 7 Results | 51 |
| 7.1 Rotvoll experiment | 51 |
| 7.1.1 Below the waterline | 52 |
| 7.1.2 Above the waterline | 56 |
| 7.1.2.1 Integral model | 56 |
| 7.1.2.2 CFD model | 56 |
| 7.2 Methanol full scale venting | 59 |
| 7.2.1 Venting depth: 2m | 59 |
| 7.2.1.1 Integral model | 59 |
| 7.2.1.2 CFD model | 61 |
| 7.2.2 Venting depth: 0.9m | 65 |
| 7.2.3 Influence initial bubble diameter | 69 |
| 7.2.4 Influence venting depth | 70 |
| 7.3 Methanol small scale venting | 72 |
| 8 Comparison underwater and on deck venting | 74 |
| 9 Conclusions and recommendations | 76 |
| 9.1 Conclusions | 77 |
| 9.2 Recommendations | 78 |
| 9.2.1 Conditions | 78 |
| 9.2.2 Bubble size | 78 |
| 9.2.3 Solubility methanol | 78 |

| | |
|---|-----------|
| 9.2.4 Mitigating measures | 78 |
| References | 80 |
| A Friedl integral model | 84 |
| B Xia’s law bubble drag | 88 |
| C UDF bubble size and gas dissolution | 89 |
| D Specifics full scale methanol-nitrogen venting | 92 |

List of Figures

| | | |
|------|--|----|
| 2.1 | Influence of loading rate on dispersion [7] | 9 |
| 2.2 | Influence of loading rate on dispersion [7] | 9 |
| 2.3 | Outlet flow at a wind speed of 1 m/s[66] | 10 |
| 2.4 | Outlet flow at a wind speed of 7 m/s [66] | 10 |
| 2.5 | Hazardous distances due to venting benzene [26] | 11 |
| 3.1 | Different zones for a subsea gas release [49] | 14 |
| 3.2 | Subsea gas release based on cone model [21] | 15 |
| 3.3 | Sketch of time-averaged bubble plume [20] | 16 |
| 3.4 | Impact of subsea gas release [38] | 18 |
| 3.5 | Relative difference between ideal gas law and the true equation of state for methane [49] | 19 |
| 3.6 | Concept drawing of experiment (from TNO) | 20 |
| 3.7 | Methanol concentrations during the ventilation of the cargo tanks [66] | 22 |
| 3.8 | Detailed graph of the methanol concentrations at various locations while ventilating the cargo tanks [66] | 22 |
| 4.1 | Concept sketch with most important parameters | 25 |
| 4.2 | Flow rate curves of PV-ECO type 4100 [7] | 27 |
| 5.1 | Control volume on a Cartesian grid [9] | 30 |
| 5.2 | Geometry Rotvoll experiment (in meter) | 31 |
| 5.3 | Velocity vectors of the mixture near the surface | 31 |
| 5.4 | Example of a polyhedral cell [5] | 32 |
| 5.5 | First meshing attempt for the Rotvoll experiment | 32 |
| 5.6 | Mesh with regional refinements | 33 |
| 5.7 | Mesh with conical regional refinements | 34 |
| 5.8 | Methane bubble equilibrium diameter in function of local gas concentration and depth | 37 |
| 5.9 | Flow model for a light gas plume, modified from [40] | 41 |
| 6.1 | Cumulative released mass in function of time | 44 |
| 6.2 | Mass release rate in function of time | 44 |
| 6.3 | Overpressure in tank in function of time | 45 |
| 6.4 | Geometry full scale methanol-nitrogen venting (blue:water, grey:air) | 45 |
| 6.5 | Used meshes | 46 |
| 6.6 | Mesh dependency | 46 |
| 6.7 | Cumulative released mass in function of time | 48 |
| 6.8 | Mass release rate in function of time | 48 |
| 6.9 | Overpressure in tank in function of time | 49 |
| 6.10 | Geometry small scale methanol venting test (blue:water, grey:air) | 49 |
| 6.11 | Mesh small scale methanol venting test | 50 |
| 6.12 | Mesh small scale methanol venting test | 50 |
| 7.1 | Particle tracks of Rotvoll experiment (0.20 kg/s release rate), seen from below | 51 |
| 7.2 | Comparison velocity at centerline between the Rotvoll experiment and integral model | 52 |
| 7.3 | Comparison velocity magnitude of water between the Rotvoll experiment and integral model near the surface, 1.75m from the centerline | 53 |
| 7.4 | Comparison velocity in function of radial position between the Rotvoll experiment and integral model for a release rate of 0.20 kg/s | 53 |
| 7.5 | Voidfraction comparison between Rotvoll experiment and integral model | 54 |

| | | |
|------|--|----|
| 7.6 | Velocity vector representation (from waterline upwards) of Rotvoll experiment | 55 |
| 7.7 | Velocity vector representation (from waterline downwards) of Rotvoll experiment | 55 |
| 7.8 | Comparison average concentrations from integral model and experiment (50m depth) | 56 |
| 7.9 | Comparison methane concentrations between the experiment and CFD for 1m above the water surface (resulting from UDF, without alteration) | 57 |
| 7.10 | Comparison methane concentrations between the experiment and CFD for 1m above the water surface (with alteration: surfacing gas reduction) | 58 |
| 7.11 | Velocity vectors Rotvoll experiment (above waterline) | 58 |
| 7.12 | Velocity vectors Rotvoll experiment (below waterline) | 59 |
| 7.13 | Mass flux of nitrogen-methanol mixture and methanol at the surface | 60 |
| 7.14 | Void fraction of nitrogen-methanol mixture and methanol at the surface | 60 |
| 7.15 | Centerline concentration of nitrogen-methanol mixture and methanol | 61 |
| 7.16 | Methanol concentration at the end of the venting process, described in function of the safety threshold IDLH (Immediately Dangerous to Life or Health) | 62 |
| 7.17 | Time-averaged methanol concentration during venting | 63 |
| 7.18 | Velocity vectors during venting | 63 |
| 7.19 | Mixture (methanol-nitrogen) vapour particles at end of venting | 64 |
| 7.20 | Methanol particle tracks, dissolution taken into account | 65 |
| 7.21 | Mesh for full scale methanol-nitrogen venting at 0.9m | 66 |
| 7.22 | Methanol concentration at the end of the venting process | 67 |
| 7.23 | Time-averaged methanol concentration during venting | 67 |
| 7.24 | Mixture (methanol-nitrogen) vapour particles at end of venting | 68 |
| 7.25 | Methanol particle tracks (initial bubble size: 0.002m), dissolution taken into account | 68 |
| 7.26 | Bubble formation regimes [59] | 69 |
| 7.27 | Methanol particle tracks (initial bubble size: 0.02m), dissolution taken into account | 69 |
| 7.28 | Methanol particle tracks (initial bubble size: 0.08m), dissolution taken into account | 70 |
| 7.29 | Methanol particle tracks (initial bubble size 0.08m) from the venting at 0.5m | 70 |
| 7.30 | Methanol concentration at 0.5m above the waterline from the venting at 0.5m (x=0: ship, x=-1.5: barge) | 71 |
| 7.31 | Comparison CFD model and similar experiment for the horizontal gas injection | 72 |
| 7.32 | Methanol particle tracks, dissolution taken into account | 73 |
| 8.1 | Concentration methanol in function of distance from release point | 74 |
| 8.2 | Comparison of methanol concentration resulting from venting above and below the waterline without taking the gas dissolution into account | 75 |

List of Tables

| | | |
|-----|---|----|
| 2.1 | Properties of methanol and diesel, modified from [57] | 4 |
| 2.2 | Exposure and lethal Limits of methanol, modified from [45] | 5 |
| 3.1 | Parameters and results of Rotvoll experiment [61] | 17 |
| 4.1 | Range parameters | 25 |
| 4.2 | Venting scenarios | 26 |
| 5.1 | Comparison calculation mass transfer coefficient | 39 |
| 6.1 | Experiments of subsea gas releases [3] | 42 |
| 6.2 | Input parameters different CFD simulations for different cases | 43 |
| 6.3 | Input for the release of methanol-nitrogen mixture | 44 |
| 6.4 | Solubility methanol-nitrogen mixture (at 20°C) | 47 |
| 7.1 | Comparison concentration measurements Rotvoll experiment and integral model at 1m above the water surface | 56 |
| 7.2 | Input for the integral model: release of methanol-nitrogen mixture | 59 |
| D.1 | Specifics full scale venting methanol-nitrogen mixture | 93 |

Nomenclature

Abbreviations

| Abbreviation | Definition |
|--------------|---|
| BLEVE | Boiling Liquid Expanding Vapor Explosion |
| CFD | Computational Fluid Dynamics |
| DPM | Discrete Phase Model |
| DMFC | Direct Methanol Fuel Cell |
| IDLH | Immediate Danger to Life and Health |
| IMDG | International Maritime Dangerous Goods |
| IMO | International Maritime Organization |
| IPCC | Intergovernmental Panel on Climate Change |
| LEL | Lower Explosive Limit |
| LFL | Lower Flammability Limit |
| MGO | Marine Gas Oil |
| PEMFC | Polymer Electrolyte Membrane Fuel cell |
| P/V | Pressure/Vacuum |
| SOFC | Solid Oxide Fuel Cell |
| TLV | Threshold Limit Value |
| TLV-C | Threshold Limit Value - Ceiling |
| TLV-STEL | Threshold Limit Value - Short Time Exposure Limit |
| TLV-TWA | Threshold Limit Value Time - Weighted Average |
| UDF | User Defined Function |

Symbols

| Symbol | Definition | Unit |
|--------------|--------------------------------------|-----------------------------------|
| b | width | [m] |
| c | Solubility | [mol/l] |
| C | Concentration | [vol%] |
| C_D | Drag coefficient | [-] |
| d | Diameter | [m] |
| E_0 | Eötvös number | [-] |
| Fr | Froude number | [-] |
| g | Gravitational constant | [m ² /s] |
| H | Water depth | [m] |
| k | Mass transfer coefficient | [mol/(sm ²)] |
| k | Turbulent kinetic energy | [m ² /s ²] |
| k | Henry's law constant | [mol/kg.bar] |
| K | Friction (pressure drop) coefficient | [-] |
| \dot{m} | Mass transfer rate | [kg/s] |
| P | Pressure | [Pa] |
| Pe_c | Compositional Peclet number | [-] |
| Q, \dot{V} | Volumetric flow rate | [m ³ /s] |
| Q_s | Release characteristic | [m ³ /s] |
| r | Radial position | [m] |
| Sc | Schmidt number | [-] |

| Symbol | Definition | Unit |
|------------|---|-----------------------------------|
| Sh | Sherwood number | [-] |
| Re | Reynolds number | [-] |
| u | Bubble speed | [m/s] |
| W | Gas release rate | [kg/s] |
| z | Height | [m] |
| β | Losses factor | [-] |
| ϵ | Turbulent kinetic energy dissipation rate | [m ² /s ³] |
| θ | Angle | [°] |
| λ | Width ratio | [-] |
| μ | Kinematic viscosity | [m ² /s] |
| ρ_g | Gas density | [kg/m ³] |
| ρ_l | Liquid density | [kg/m ³] |
| σ | Surface tension | [N/m] |
| ϕ | Void fraction | [-] |

Subscripts

| Subscript | Definition |
|-----------|------------|
| a | Air |
| b | Bubble |
| f | Fountain |
| g | Gas |
| l | Liquid |
| s | slip |

1

Introduction

In order to limit the global warming by 2°C, set by the Paris Agreement [13], every industry is looking into methods to reduce the emissions of greenhouse gases. The shipping industry's commitment to this agreement translates to a minimum reduction of 50% in annual greenhouse gas emissions by 2050, using 2008 as the reference level. In the most recent IPCC report (2022), scientist warned that the global warming will reach the 1.5°C mark before 2040 [27]. According to the energy transition outlook [44], the world is heading to a 2.2°C global warming by 2050. It is likely that in the coming years more stringent emissions reduction levels will be imposed to reach the goal set in the Paris Agreement. Using alternative fuels will be key to reach this goal. Previous research studying the applicability of various marine fuels showed the promise which methanol has. Methanol (CH₃OH) has large potential to become the main fuel in the marine fuel mix of the future. Renewable methanol (or e-methanol) reduces the emissions, from well to wake compared to conventional fuels, of CO₂ by 95%, NO_x by 80% and both SO_x and particulate matter completely (depending o.a. on engine type, source of fuel and logistics) [29]. By using methanol, the ship complies to the most stringent emission limits set out in MARPOL Annex VI. IMO tier III limit for NO_x emissions can be reached by engine modifications or after treatment.

Next to the reduction of harmful substances, methanol has other advantages. Compared to hydrogen, ammonia and LNG, methanol is easier to store and handle on board of ships. It also requires less modification to ship engines compared to for example hydrogen. Additionally, compared to other alternative fuels, it has a higher volumetric energy density (15.6 MJ/l) [63]. When packaging factors are taken into account, methanol also has a higher volumetric energy density than LNG due to o.a. its insulation, tank shapes and boil-off gas [64]. The downside of methanol is its lower gravimetric energy density (19.7 MJ/kg) compared to LNG and conventional marine liquid fuels. The main disadvantages of methanol are the following: it is corrosive, toxic to humans and poisonous to the central nervous system. The fact that methanol vapour is heavier than air makes it even more dangerous for crew on board of ships. This means that the bottom of empty, not ventilated, methanol tanks might be dangerous for the crew. Next to this also leakages and ventilation points might be dangerous. If the methanol vapour concentration is between 6-35.6 Vol% [57] of air, it becomes a flammable mixture.

Just like other marine fuels, methanol vapours might be vented due to over pressure in methanol fuel tanks, for example when bunkering or in case of fire. This might especially be the case when doing gas freeing operations. Gas freeing is defined as achieving a safe atmosphere in a methanol tank by first inerting and then by ventilating. Due to its toxicity and flammability, the IMO has taken measures for a clear area around methanol ventilation, manifold or P/V valve. These are the so-called hazardous area zone 0, 1 and 2 [28]. Consequently, that part of the ship is no longer accessible or cannot longer be used. Preventing fires in this area also necessitates the absence of any ignition sources. In order to prevent these problems, the underwater ventilation of methanol vapours will be investigated. The following research question is proposed:

"What is the concentration of methanol at deck level when methanol is ventilated below the waterline?"

If no methanol vapour is present at deck level due to a subsea gas release or if the methanol concentration is below the imposed flammability and toxicity limits, hazardous areas on deck can be reduced/eliminated, enabling the full operability of the deck space. Despite the importance of understanding the behavior of methanol vapors in water and the movements of methanol clouds after the venting at shallow depths, very limited research has been conducted in these areas. Therefore, this thesis aims to address some of these knowledge gaps by examining the behavior and concentration of methanol vapors when ventilated below the waterline. By conducting a comprehensive analysis, this study intends to contribute valuable insights into the understanding of subsea methanol ventilation and its implications. The general outline of this thesis consists out of a literature study (part I) and a numerical investigation (part II).

Part I

Literature Review

2

Methanol as marine fuel

In this chapter, a theoretical background on methanol as marine fuel is given. The literature research mainly focuses on the properties (Section 2.1) and regulations (Section 2.2) of methanol as fuel. The physics and models of subsea venting is described in more detail in the next chapter (Section 3.1 and 3.2). Also, some preliminary information is given about a subsea ventilation experiment (3.3). Chapters 2 and 3 acts as the basis for the research gap analysis, research questions and methods to be used which are described in Chapter 9.

2.1. Properties of methanol

Methanol, also called methyl alcohol, is the simplest type of the alcohol-group and has CH_3OH as chemical formula. To assess the viability of methanol as a marine fuel, first its properties should be studied. Table 2.1 shows its main properties compared to diesel. Note that both the properties of methanol and diesel will be dependent on the composition, the values in Table 2.1 are indicative.

Table 2.1: Properties of methanol and diesel, modified from [57]

| Property | Methanol | (Marine) Diesel (oil) |
|---|-----------|-----------------------|
| Molecular weight (g/mol) | 32.04 | 226 |
| Liquid density (kg/m ³) | 798 | 850 |
| Energy density (MJ/L) | 15.7 | 35.6 |
| Diesel equivalent volume | 2.54 | 1 |
| Heat of vaporization (kJ/kg) | 1098 | 250 |
| Lower heating value (MJ/kg) | 20.09 | 42.8 |
| Flash point (closed cup, 1 atm) (°C) | 12 | 52 - 96 |
| Auto-ignition temperature (°C) | 450 | 250 |
| Boiling point at 1 bar (°C) | 65 | 170 - 350 |
| Flammable range in dry air (vol%) | 6 – 36.5 | 0.5 - 7.5 |
| Heat release in case of fire (kW/m ²) | 450 | 1400 |
| Critical temperature (°C) | 239.4 | 450.0 |
| Critical pressure (bar) | 80.48 | 20 |
| Vapour pressure at 20°C (kPa) | 12.8 | 0.2 - 0.7 |
| Relative vapour density (to air) at 20°C | 1.1 | 6 |
| Cetane number | <5 | 40 - 55 |
| Octane number | 109 | 15 - 25 |
| Viscosity at 20°C (kPa) (cSt) | 0.74 | 2.5 - 3.0 |
| Solubility: methanol in water / water in methanol (%) | 100 / 100 | Negligible |

2.1.1. Toxicity

Methanol should be handled with care. According to the International Maritime Dangerous Goods (IMDG) Code [50] and material data sheets, it has the following toxicity risks: toxic if swallowed, toxic if

inhaled and toxic if contact with skin. Additionally, it may also cause damage to organs and blindness. Overall, oral ingestion, inhalation and skin contact (even when wearing protective clothing) should be avoided. Methanol, in itself, has a very limited toxicity but it is metabolised to formaldehyde and formic acid. Especially the formic acid causes the large toxic effects. The acute toxic effects of methanol are linked with relatively high concentrations. In contrast with this, methanol has a relatively low acute toxicity to marine life and other non-primate animals. It is also biodegradable and soluble in water. Consequently, methanol is not considered dangerous to the marine environment (in case of spills) which is an advantage over conventional fuels.

Table 2.2: Exposure and lethal Limits of methanol, modified from [45]

| Threshold limit values and lethal Limits | Value | Information |
|--|-----------------------------------|---|
| Time weighted average (TLV-TWA) | 200 ppm or 262 mg/m ³ | Average exposure rate without negative effects over 8-hour, day 40-hour work week |
| Short time exposure limit (TLV-STEL) | 250 ppm or 328 mg/m ³ | Acceptable average exposure over 15 minutes |
| Ceiling (TLV-C) | 763 ppm or 1000 mg/m ³ | Absolute exposure limit that should not be exceeded at any time |
| Oral LD50 (Rat) | 6200 mg/kg | Amount of oral ingested substance that kills 50% of the tested population, mg of substance per kg of body weight. |
| Dermal LD50 (Rabbit) | 15840 mg/kg | Amount of dermal ingested substance that kills 50% of the tested population |
| Inhalation LC50 (Rat) | 22500 ppm 8h | Amount of inhaled substance that kills 50% of the tested population |

Threshold limit values and lethal limits are indispensable properties of a substance. Table 2.2 shows these values for methanol. Methanol is sometimes orally ingested without knowing it. This is for example the case in beer. Concentrations of 6-27 mg/L (or 0.008-0.03 ml/l) have been measured due to distilling and fermenting errors. These low concentrations are not harmful. According to the World Health Organization (WHO) [51] methanol concentrations in blood of 500 mg/L are associated with severe toxicity, and concentrations above 1500-2000 mg/l may lead to death if untreated. Methanol also occurs naturally in the human body with a background level of 0.73 mg per kg body weight. Note that 2000 mg of methanol corresponds to 2.5 ml. This means that the lethal dose of methanol for an average crew member on board (6l of blood) is approx. 15 ml (or 12 g), which is similar to the dose of 10-30 ml (pure methanol) written in the safe handling manual [17]. Smaller amounts can already cause severe blindness. The concentrations above refer to the drinking of methanol, but as previously mentioned also the vapour inhalation is dangerous. For example, the inhalation of 40 ppm methanol for 8 hr corresponds to 145 mg added methanol in the body (assuming 85% lung absorption). Methanol does not stay in the human body forever. It is metabolised at a rate of 25 mg/kg-hr. The end products of the metabolism are carbon dioxide and water which are not harmful.

2.1.2. Flammability

Next to the toxicity, methanol second main danger is its flammability. Methanol is a low flash point fuel (see Table 2.1), which causes the formation of a flammable mixture at ambient temperature and pressure. At 20 °C, the vapour pressure is 13 kPa corresponding to approximately 13 vol% which

lies in the flammability range. This concentration will only be reached after a long time due to the slow evaporation of methanol (up to 10 kg/hr in a closed room [60]). Once there is a flammable mixture (methanol-oxygen), it is easily ignited. To illustrate this, the minimum ignition energy is lower than gasoline. Methanol vapour clouds will easily ignite by for example electrical and electrostatic discharges, but it will not self-ignite (unless reaching auto-ignition temperature). Therefore, the safety distance around a venting point on deck is necessary.

Once there has been an ignition at the venting point, there is also a danger of flash back to its source. Flame arresters should be installed on the ventilating valves. This is also mentioned in the IMO guidelines [28]: "Design and arrangement should prevent flame propagation into the fuel containment system". A different material than aluminium (alloys) should be used due to the corrosivity of methanol to aluminium alloys which can cause faulty flame arresters. Despite its solubility, methanol will keep its flammability even at very high concentrations of water [17]. Methanol fires typically have a non-luminescent flame which makes the fire difficult to detect during the day. In addition, due to the relatively low boiling point of methanol (65°C), a boiling liquid expanding vapour explosion (BLEVE) might occur. At high temperatures, the pressure inside methanol tanks on deck will rise due to evaporation. If there is a failure of the tank, the vapour will escape the tank causing a pressure drop in the tank and subsequently violent boiling inside the tank. This will cause rapidly liberation of large amounts of gas. This process might repeat itself and an explosion is possible to occur.

Methanol also has favourable flammability properties. Table 2.1 shows that methanol burns approx. 75% slower (see heat of vaporization) with approx. 12.5% the heat release (see heat release in case of fire) compared to diesel. In other words, methanol produces little vapour, needs a lot of vapour to burn (higher LFL) and burns less hot compared to diesel.

2.1.3. Methanol spill

Not many methanol spills have occurred, consequently the consequences or specific dangers are not really known. Due to its relative density being larger than 1 (compared to air), methanol vapour will move downwards after a release or spill. It will build up in enclosed spaces. If there is little or no wind it will also not move away from deck. However, after a spill, it is much more likely that a methanol-air mixture will be formed instead of pure methanol because methanol vapour mixes well with air. This mixture has a relative density of 1.01 (at 20°C), so it is naturally buoyant in air [52]. Methanol will diffuse in air at a rate of $0.155 \cdot 10^{-4} \text{ m}^2/\text{s}$ (at 25°C and 101.325 kPa) [36]. However, research has to be done on the diffusivity of a methanol-air mixture. Also, not much is known about the influence of temperature, pressure, wind speed and gas composition on the movement and behaviour of methanol vapour in air.

2.2. Regulations and guidelines

2.2.1. Venting

Due to the increased interest in methanol as marine fuel, regulations and guidelines have been developed. Methanol is categorized as a low-flashpoint fuel due to its flashpoint of 12°C, which is below the 60°C threshold. Consequently, the "International Code of Safety for Ships using Gases or other Low-flashpoint Fuels" (IGF-code) is applicable. This code describes, among others, the use of inert gas. A flammable condition in methanol fuel tanks is prevented by the injection of inert gas. Nitrogen should be used as inert gas because the reaction of carbon dioxide with methanol, in the presence of salty or moist air, causes corrosion. The amount of added inert gas should be minimized. Increasing tank pressure by adding inert gas may increase venting and therefore increase methanol vapour emissions. The pressure in the tank is the sum of the saturated vapour pressure, the unsaturated vapour pressure and pressure by the inert gas. The unsaturated vapour pressure depends on the day/night (temperature) effect. Applying a heat reflecting paint to the deck or the outside of methanol tanks can effectively reduce the heat absorption. One example of such a paint is the one used on the Euronav oil tanker "Europe". The P/V (pressure/vacuum) valve will open if the sum of these three pressures exceeds the limit [6]. The venting system is regulated by the "Interim guidelines for the safety of ships using methyl/ethyl alcohol as fuel" [28]:

- "Pressure and vacuum relief valves should be fitted to each fuel tank to limit the pressure or

vacuum in the fuel tank. The tank venting system may consist of individual vents from each fuel tank or the vents from each individual fuel tank may be connected to a common header.”

- “The fuel tank-controlled venting system should be designed with redundancy for the relief of full flow overpressure and/or vacuum. Pressure sensors fitted in each fuel tank, and connected to an alarm system, may be accepted in lieu of the secondary redundancy requirement for pressure relief.”
- “The opening pressure of the P/V valves should not be lower than 0.007 MPa below atmospheric pressure.”
- “P/V valve should vent to a safe location on open deck and should be of a type which allows the functioning of the valve to be easily checked.”

The location of the “safe location on open deck” is also further specified:

- “Fuel tank vent outlets should be situated normally not less than 3 m above the deck or gangway if located within 4 m from such gangways. The vent outlets are also to be arranged at a distance of at least 10 m from the nearest air intake or opening to accommodation and service spaces and ignition sources”
- “The outlet for gas freeing operations should be 3m above the deck or outlets underwater.”

Gas freeing in this case means to achieve a safe atmosphere in a methanol tank by first purging with inert gas (or other gas) and then by ventilating (with air). Immediate ventilation is often not done to avoid having a flammable mixture at a certain point in the gas freeing operation. Inerting means to fill up a tank with inert gas such that the oxygen concentration is below 8 vol%. Inert gas is any gas that contains less than 5 vol% oxygen. Purging is the same operation as inerting, namely introducing inert gas in the tank, but it has a different objective. Purging is done to lower the hydrocarbon concentration below which combustion is not sustained if air is introduced. Ventilation means to introduce air in the tank to increase the oxygen concentration to 21 vol%. Ventilation is also done to reduce the concentration of harmful substances below an acceptable limit. This is necessary to do tank inspections. Ventilation requirements should be such that methanol concentrations in air do not reach 200 ppm. The minimal concentrations where humans detect methanol, by smelling a sweet alcohol odour, is 2000 ppm or higher [17]. This is 10 times higher than the TWA, therefore gas detection sensors should be installed. Especially when entering methanol fuel tanks (after completing the enclosed space procedure), gas detection tubes or a portable detection device should be used. When a concentration larger than 200 ppm is detected, the area should be left or a positive pressure breathing apparatus should be used. As the lower flammable limit is 6 vol% or 60,000 ppm, which is higher than the TWA, a space safe for health is also safe for fire.

2.2.2. Hazardous areas and deck exclusion zones

When venting methanol, a safe distance should be kept from the venting point. Different regulations and guidances concerning dangerous areas and safe distances are described below.

2.2.2.1. Interim guidelines for the safety of ships using methyl/ethyl alcohol as fuel

Hazardous areas, defined by the IMO, focus on the areas where explosive gas atmospheres may occur:

- Hazardous area zone 0: includes, but is not limited to, the interiors of methyl/ethyl fuel tanks, any pipework for pressure-relief or other venting systems for fuel tanks, pipes and equipment containing methyl/ethyl fuel.
- Hazardous area zone 1 (among others):
 - Areas on open deck, or semi-enclosed spaces on deck, within 3 m of any methyl/ethyl fuel tank outlet, gas or vapour outlet, bunker manifold valve, other methyl/ethyl fuel valve, methyl/ethyl fuel pipe flange, methyl/ethyl fuel preparation space ventilation outlets.
 - Areas on open deck or semi-enclosed spaces on deck in the vicinity of the fuel tank P/V outlets, within a vertical cylinder of unlimited height and 6 m radius centred upon the centre of the outlet and within a hemisphere of 6 m radius below the outlet.

- Hazardous area zone 2 (among others): Areas on open deck or semi-enclosed spaces on deck in the vicinity of the fuel tank P/V outlets, within a vertical cylinder of unlimited height and 4 m radius centred upon the centre of the outlet and within a hemisphere of 4 m radius below the outlet.

The instrumentation and electrical apparatus installed within these areas should be of a type suitable for the zone where it is placed. As the lower flammability limit is higher than the TLV-STEL, these hazardous area zones should not only be avoided because of explosion risks but also because of toxicity risks. It is worth noting that the distances specified in the interim guidelines are independent of the ship's size. As a result, even small vessels could have a substantial risk area.

2.2.2.2. The carriage of methanol in bulk onboard offshore vessels

Next to hazardous area zones, there are also deck exclusion zones marked by the marine safety forum when carrying methanol [43]. When loading methanol, large volumes of gas are vented. Consequently, when loading, there should be a 10m (horizontal and vertical) exclusion zone around a P/V valve. When venting, a mixture of methanol vapours and inert gas is ejected vertically from an outlet and rises vertically because of its momentum. When there is no wind the plume initially keeps rising. In the case of wind it is bent downwind. The density, which is higher than air, also counteracts the momentum and pulls the plume down. After the loading and until there is no more methanol on board, this distance is reduced to 4.5m (to allow for thermal variation).

The influence of the loading rate on the vapour clouds on deck is shown in Figures 2.1 and 2.2. When loading methanol at a higher rate, the production of vapours will be increased but the vapours on deck will be more directed vertically. It should be noted that these test have been carried out for a mixture of 50 vol% propane and 50 vol% air. The density of this mixture is higher than for methanol vapour. Consequently, the expected effect might be less. The release of (methanol) vapour is also more likely to happen at the end of loading because a layer of gas is formed at the bottom which rise as the liquid surface rises. Depending on the loading rate, temperature, tank geometry etc. this gas layer will be maximal 1m (for high vapour pressure liquids) [7]. At 25°C, methanol has a vapour pressure of 0.13 bar, which gives rise to a volume concentration of 13% just above the liquid surface. Further away this concentration will be lower. In the beginning, there might be releases of mainly inert gas. When the tank is almost completely filled, the vented gas will be a mixture of methanol and inert gas.

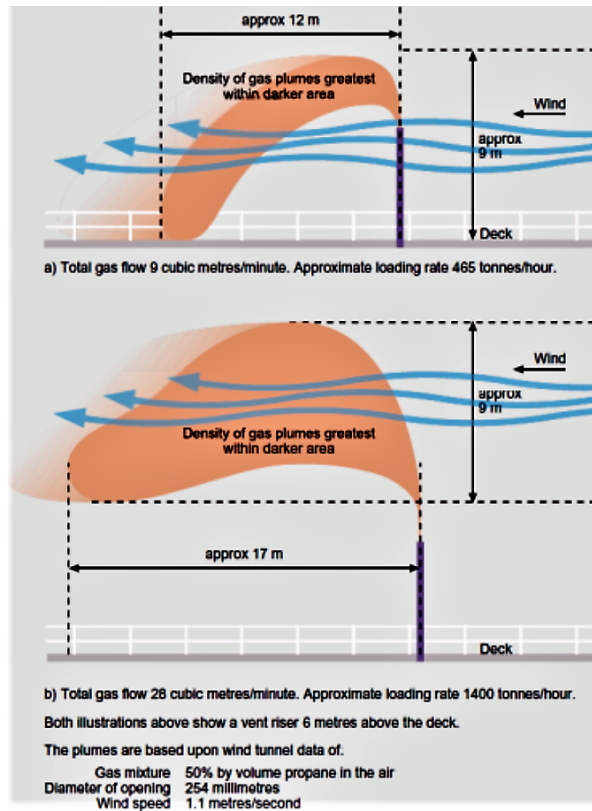


Figure 2.1: Influence of loading rate on dispersion [7]

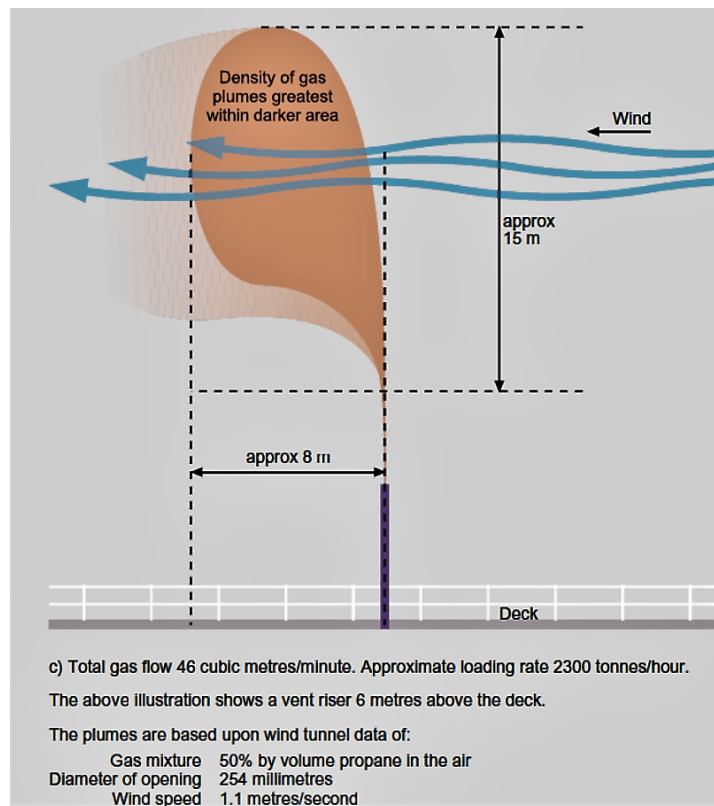


Figure 2.2: Influence of loading rate on dispersion [7]

Next to the loading rate, the wind speed and direction is also a determining factor on the danger coming from toxic gas clouds. If the relative wind direction comes from abeam, the vented vapours are blown away from the vessel. In contrast to a relative headwind, the vented vapours are direct towards the accommodation and ventilation intakes. In order to remain safe, the vented flow should be dispersed enough at the accommodation such that the concentrations are below the toxicity levels. In Figures 2.3 and 2.4 the influence of wind speed on the flow coming from the P/V valve is shown. Depending on the location of the outlet and the wind speed and direction, it is clear that venting on deck might pose a danger.

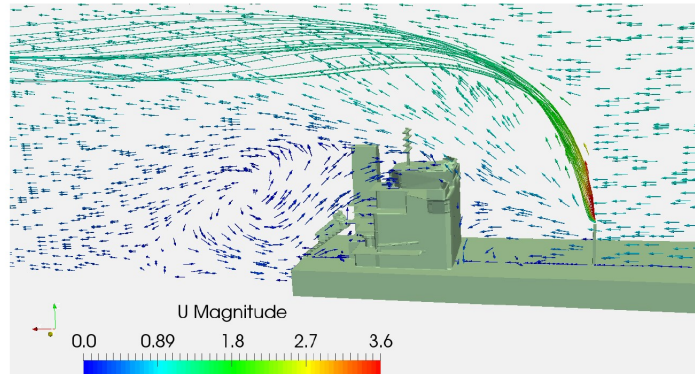


Figure 2.3: Outlet flow at a wind speed of 1 m/s[66]

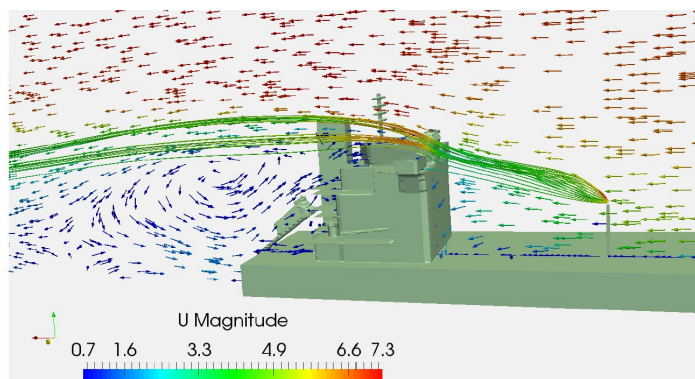


Figure 2.4: Outlet flow at a wind speed of 7 m/s [66]

2.2.2.3. IEC-code

The regulations above, by the IMO and marine safety forum, describe general safety distances when venting methanol. In contrast, the IEC (International Electrotechnical Commission) gives safe distances in function of specific venting conditions. Depending on the release rate, gas properties, release geometry, surrounding geometry and ventilation velocity dangerous areas are classified [26]. In the dangerous area the concentration of the flammable gas is higher than the LFL.

The release behaviour in the IEC-code is characterized as a heavy gas release, typically a liquid pool release, a diffusive release resulting from a low velocity gas release or a jet release resulting from a high velocity gas release [10]. The release of methanol is characterised as a diffusive release. To be considered as a heavy gas, the density of the methanol-nitrogen mixture should have a relative density of minimum 1.1 (compared to the air density). The volume percentage of methanol in methanol-nitrogen vapour mixture in a tank is a function of temperature and pressure. The following empirical equation is derived from experiments carried out in 1985 and is used to calculate the volume percentage of methanol [2].

$$\%CH_3OH = \frac{e^{82.718 - \frac{6904.5}{T} - 8.8622 \ln(T) + 7.47 \cdot 10^{-6} T^2}}{P_{tank}} \quad (2.1)$$

If the temperature is 293K (20°C) and the tank pressure 114000 Pa, which is a common opening pressure for valves, the volume percentage of methanol is 11.2%. Consequently, it is physically not possible to reach a relative density of 1.1 (at 20°C). A jet release behaviour is also not applicable, because this is typically related to sonic velocities (343 m/s). The release velocity for a high velocity P/V valve is typically 30-70 m/s. Therefore the diffusive behaviour is the most suitable.

The IEC-code is applied to the following conditions: opening pressure of P/V valve is 5 kPa, temperature of methanol-nitrogen temperature is 17 °C and the valve diameter is 0.1m. This results in a hazardous area of 1.9m around the release point. Another example is shown in Figure 2.5. This figure represents the hazardous distance for the venting of benzene vapour from a breather valve in the open air (from a process vessel). The highest hazardous distance is resulting from the filling of the process vessel (primary release) and the lowest distance is a result of the rupture of the sealing (secondary release).

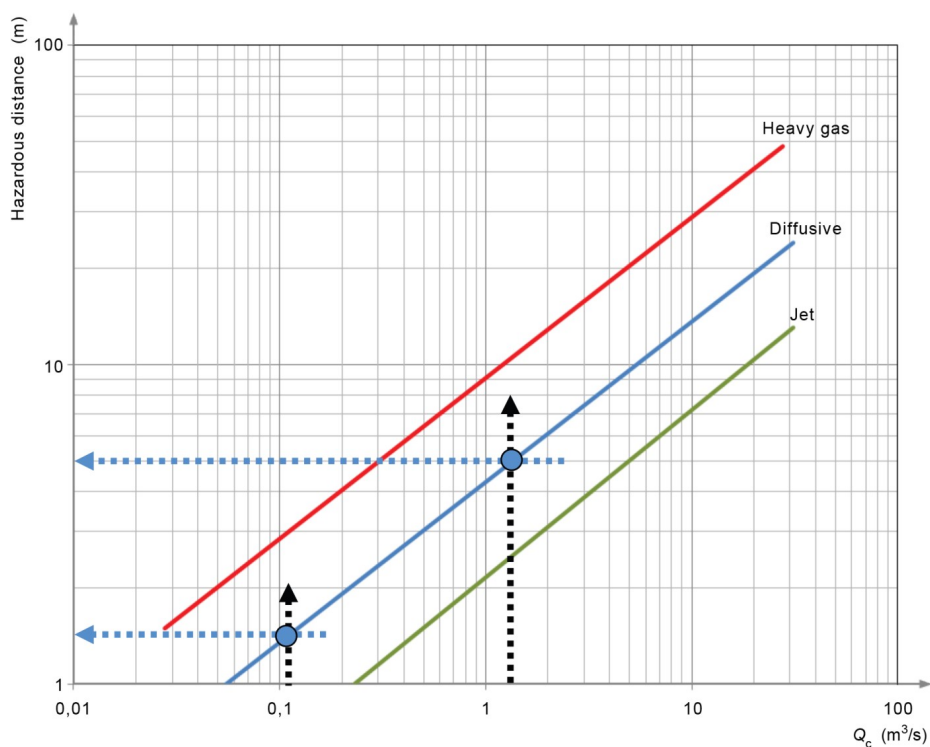


Figure 2.5: Hazardous distances due to venting benzene [26]

Q_c represents the release characteristic (in m^3/s) and is calculated as follows [10]:

$$Q_c = \frac{W_g}{LFL\rho_g} \quad (2.2)$$

Where W_g is the gas release rate (in kg/s), LFL the lower flammability limit (in volume fraction) and ρ_g the gas density (in kg/m^3). Often a safety factor is also taken into account.

3

Subsea venting

Subsea venting itself is not specifically described in regulations, but the following is mentioned in the interim guidelines [28]: "Appliances and arrangements of methyl/ethyl alcohol fuel systems may deviate from those set out in these Interim Guidelines, provided such appliances and arrangements meet the intent of the goal and functional requirements concerned and provide an equivalent level of safety to the relevant sections." If at the end the underwater ventilation has "an equivalent level of safety" as "venting to a safe location on open deck" it will be a viable alternative. Nonetheless, a risk assessment is imperative, as it is also a mandatory requirement for this design: "A risk assessment should be conducted to ensure that risks arising from the use of methyl/ethyl alcohol fuels affecting persons on board, the environment, the structural strength, or the integrity of the ship are addressed. Consideration should be given to the hazards associated with physical layout, operation and maintenance, following any reasonably foreseeable failure." An important factor in the risk assessment will be the setting of the release pressure for underwater ventilation. Depending on the opening pressure of the valve (to the underwater line) the methanol vapours will reach a different height. If a higher opening pressure is required, to overcome the hydrostatic pressure, the fuel tank should also be designed for it. On the contrary, If a lower opening pressure is needed to limit the height of methanol vapours above the water line, venting will be stimulated.

3.1. Governing physics

Very little research has been conducted on the subsea venting of vapours. Nevertheless, information can be obtained from similar scenarios. Such a scenario is the transport of gas released from gas hydrates [68]. Another similar scenario is the gas release of subsea pipeline ruptures. The latter example has been intensively studied by the U.S. Department of the Interior Minerals Management Service. They ordered studies on the risk and behaviour of wet or dry gas from a single-phase subsea pipeline release [55]. From this research different zones were chosen to represent the governing physics. After a subsea gas release, the bubbles will rise through these different zones in the water column. These are depicted in Figure 3.1. The dominating physics will change in each zone. An important driving force is the buoyancy which depends on the density of the gas. Other mechanisms governing the bubble plume are drag, turbulence and gas dissolution [49].

3.1.1. Zone of flow establishment

The zone above the release point is the zone of flow establishment. The gas enters the water column in a bubbling jet if the flow is not choked. The strength of the gas jet is represented by a modified Froude number [54]:

$$Fr^* = \frac{Q^2 \rho_g}{gd^5 \rho_l} \quad (3.1)$$

Where Q is the gas flow rate, ρ_g the gas density, ρ_l the liquid density and d the diameter of the outlet. Typical values for subsea venting are $0.25 \text{ m}^3/\text{s}$ (Q), $1.33 \text{ kg}/\text{m}^3$ (ρ_g), $1025 \text{ kg}/\text{m}^3$ (ρ_l) and 0.08 m (d) respectively. Due to the high modified Froude number (2.5), the dominant mechanism in the zone of

flow establishment is the inertia. After the release, the jet is broken up into bubbles due to interfacial shear forces.

3.1.2. Zone of established flow

The next zone is the zone of established flow. This zone starts where the dispersion appears to adopt a plume-like structure [23]. The main driving force is no longer the momentum of the jet but the buoyancy. There is also a drag force between the bubbles and the surrounding water causing the water to accelerate and move upwards along with the bubbles. The velocity of the bubbles and water along the jet is not uniform. This is shown in Figure 3.1. These velocity fluctuations cause fluctuations in the drag force. This is called turbulent dispersion and is responsible for the widening of the plume. Next to the widening, the plume will also bend downstream if currents are present. The acceleration of the spherical bubbles can be derived by Newton's second law [49]:

$$\frac{du_b}{dt} = g \left(\frac{\rho_l - \rho_b}{\rho_b} \right) + \frac{0.75\mu_l C_D Re}{\rho_b d_b^2} (u_l - u_b) \quad (3.2)$$

Where u_b is the speed of the bubble, u_l is the speed of the surrounding water, μ_l is the dynamic viscosity, C_D is the drag coefficient and Re the Reynolds number. The first term in Equation 3.2 is the buoyancy and gravity force and the second term is the drag force. The drag force is based on Stokes' law (Equation 3.3), which is valid for small spherical particles and low Reynolds numbers, together with a correction factor (X , Equation 3.4) based on the Reynolds number and drag coefficient [31].

$$F_D = 6\pi\mu \frac{d}{2} (u_l - u_b) X \quad (3.3)$$

$$X = \frac{C_D Re}{24} \quad (3.4)$$

Next to the buoyancy, gravity and the drag, there are also lift forces, virtual mass forces, pressure gradient forces and turbulent dispersion forces. These forces influence the bubbles in the plume but their effect is small (except for the turbulent dispersion) and can be neglected [30].

If the release point is deep, there will be a significant gas dissolution due to a large residence time. According to Olsen (2015), this mass transfer rate of a single bubble is represented by the Ranz-Marshall equation [65]:

$$\dot{m} = -\pi d_b^2 k (c^{sol} - c^l) \quad (3.5)$$

Where \dot{m} is the mass transfer rate for a certain gas component (for example methanol), d_b is the bubble diameter, k is the mass transfer coefficient and c^{sol} is the solubility. By applying Henry's law on the solubility of gas bubbles, the solubility can be replaced by the multiplication of the partial pressure of the gas bubble with the Henry constant of gas. In other words, Henry's law states that at a constant temperature, the amount of a gas that dissolves in a liquid is directly proportional to the partial pressure of that gas in equilibrium with that liquid [24]. c^l is the concentration in the surrounding water, this background concentration can be neglected in the case of methanol vapour. The gas dissolution is strongly dependent on the rise time of the bubble plume [42]. Previous studies showed that the gas dissolution is negligible in shallow water [30]. When 10 kg/s of methane is released at a depth of 30 m, it was observed that the percentage of gas dissolution is 0.3%. In contrast, for the same flow rate and water depth of 300m, the gas dissolution is almost 100%.

Next to the release depth, also the release rate has an influence on the mass transfer rate. In case of shallow releases, the mass transfer rate is proportional to the release rate, while it is inversely proportional for deep releases [58]. This can be explained from a saturation point of view. For shallow releases, the core might not see the ocean as the background, but the entrained water in the core which will be saturated. As a consequence, the background concentration c^l (in Equation 3.5) and mass transfer rate increase with larger release rates.

3.1.3. Surface zone

When the plume reaches the water level, it enters the surface zone. If not all gas is dissolved in the water, the rest will be released into the atmosphere. When the plume rises through the water column, it entrains some water with it. In contrast to the upward moving gas, the entrained water cannot rise out the sea level. A circular pool (of water and gas) on the sea surface is expected due to diversion of the water into a radial flow outwards from the plume eye [37].

3.1.4. Atmosphere

The dispersion process of gas in the atmosphere is dominated by the combination of buoyant force and wind. When the wind speed is small, the main driving force will be the buoyant force. However, when the wind speed is large, the wind will be the main contributor to the dispersion. Natural gas will disperse and rise in the atmosphere [38], but methanol is expected to accumulate and disperse near the water surface due to its large density.

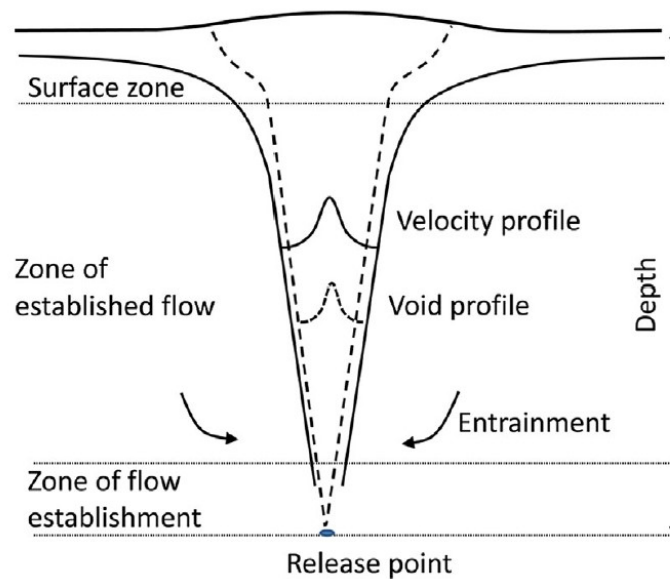


Figure 3.1: Different zones for a subsea gas release [49]

3.2. Subsea gas release models

There are 4 main methods to study the dispersion behaviour of gas through the water column and atmosphere: experiments, empirical/cone models, integral models and Computational Fluid Dynamic (CFD) models. Experiments are often expensive, time-costly and potentially dangerous.

3.2.1. Empirical models

Empirical models are the simplest models and are based on representing the dispersion of a subsea plume as a cone (see Figure 3.2). This model assumes that the plume rises with a constant angle θ which is typically 10-12° [21]. Consequently, the radius of the plume in function of the depth can be found as

$$b(z) = z \tan\left(\frac{\theta}{2}\right) \quad (3.6)$$

This model has very limited applications. It also has some limitations a.o. the radius of the plume is independent of the release rate and the dispersion into the atmosphere is not taken into account. Empirical models often use correlations fitted to experimental data. Therefore, the results of empirical models will be inaccurate in conditions other than the experiment.

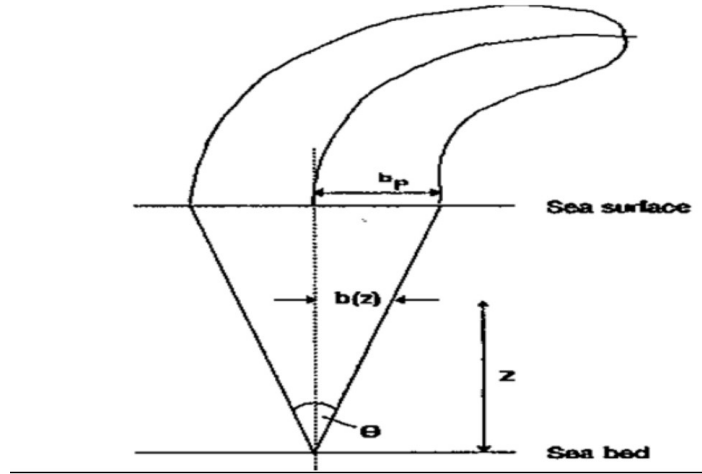


Figure 3.2: Subsea gas release based on cone model [21]

3.2.2. Integral models

Integral models assume that that plume velocities and gas fractions can be represented by certain mathematical profiles, mostly Gaussian profiles. These models are called "integral" because the governing set of equations is based on an integral over the width of the profiles [49]. Similarly to the cone model, integral models also use a constant angle θ to describe the widening of the plume.

The most used integral model is the Friedl model [20]. This is a theoretical model which mainly focuses on the fountain, which is the elevation of the water surface due to a subsea gas release.

The following assumptions are used:

- The water body is stationary and incompressible.
- The average bubble diameter is 1 cm and is constant. Good agreement with experiments is found for this value [20].
- The velocity and void fraction profile have a Gaussian distribution. The void fraction is defined as the fraction of the volume that is occupied by the gas phase.
- The entrainment hypothesis is valid: the water entrainment is proportional to the vertical plume velocity [49]. Entrainment can be explained as the horizontal transport of water into the vertical plume.

The vertical velocity profile and the void fraction profile are described as follows

$$v(r, z) = v_c(z)e^{-(r^2/b(z)^2)} \quad (3.7)$$

$$\phi(r, z) = \phi_c(z)e^{-(r^2/\lambda(z)^2)} \quad (3.8)$$

Where λ is the relative width of the velocity profile versus the bubble distribution. Subscript c represents the centerline value (see Figure 3.3). A number of parameters and dimensions are introduced. H_p is the water depth corresponding to the atmospheric pressure P_0 , H_v is the water depth, \tilde{z} is the dimensionless axial coordinate, \tilde{b} is the dimensionless width of the plume and \tilde{v} is the dimensionless vertical liquid velocity.

$$H_p = \frac{P_0}{\rho g} \quad (3.9)$$

$$\tilde{z} = \frac{z}{H_v + H_p} \quad (3.10)$$

$$\tilde{b} = \frac{b}{2\theta(H_v + H_p)} \quad (3.11)$$

$$\tilde{v} = v \left(\frac{(1 + \lambda^2)g\dot{V}_0}{2\pi\gamma\theta^2(H_v + H_p)} \right)^{-1/3} \quad (3.12)$$

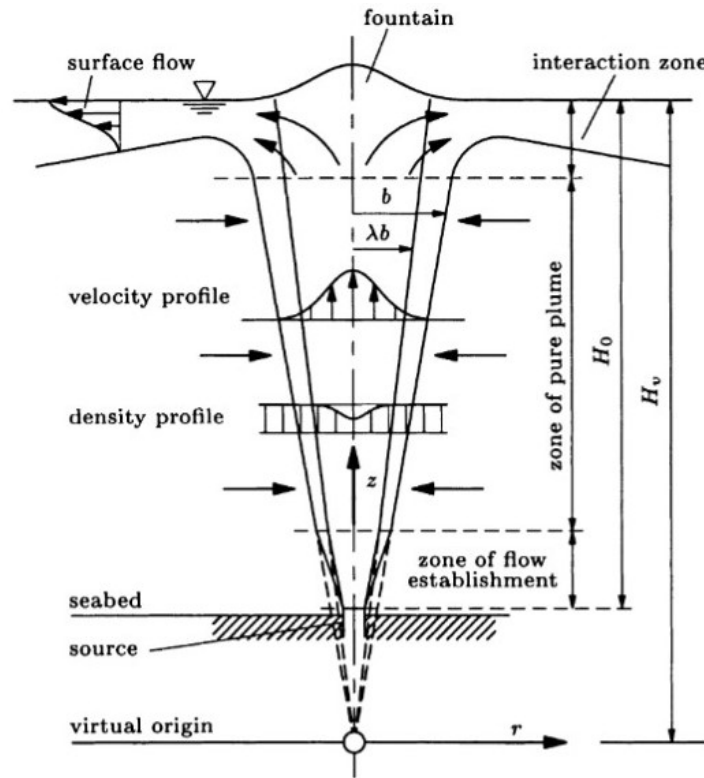


Figure 3.3: Sketch of time-averaged bubble plume [20]

The velocity and width are solved from the continuity (gas and liquid) and momentum equations. The continuity equation for the gas phase is the following

$$\tilde{\phi}_c(\tilde{z}) = \frac{1}{(1 - \tilde{z})\tilde{b}^2(\tilde{v}_c + \tilde{s})} = \phi_c \left(\frac{(1 + \lambda^2)^2\gamma\dot{V}_0^2}{2^5 g\pi^2\gamma^2\theta^4(H_v + H_p)^5} \right)^{-1/3} \quad (3.13)$$

Where $\tilde{\phi}_c$ is the dimensionless void fraction and γ is the momentum amplification factor which accounts for the added momentum due to turbulence. \tilde{s} is the dimensionless slip velocity and is given by the following equation

$$\tilde{s} = (1 + \gamma^2)v_s \quad (3.14)$$

Where v_s represents the slip velocity. The slip velocity is defined as the difference in speed between the bubbles and the entrained water and is set as 0.35 m/s in this model. The continuity equation for the liquid phase and the momentum equation are the following

$$\frac{d}{d\tilde{z}}(\tilde{b}^2\tilde{v}_c) = \tilde{b}\tilde{v}_c \quad (3.15)$$

$$\frac{d}{d\tilde{z}}(\tilde{b}^2\tilde{v}_c^2) = \frac{1}{(\tilde{v}_c + \tilde{s})(1 - \tilde{z})} \quad (3.16)$$

Equations for $\tilde{b}(\tilde{z})$ and $\tilde{v}_c(\tilde{z})$ are derived by perturbation techniques (see Appendix A) [32]. The profile of the fountain is modelled by using the momentum balance. The force momentum of the forces which acts on a control volume is [20]:

$$F_a + G_w + G_f = F_b + B \quad (3.17)$$

Where F_a is the integral of the atmospheric pressure over the water surface, F_b is the integral of the pressure at the bottom of the control volume over the bottom boundary of the control volume, G_w is the weight of the water masses below the stationary surface, G_f is the weight of the fountain and B is the total buoyancy. F_a , G_w and F_b will cancel each other out such that G_f is equal to B . B is now set as equal to the theoretical momentum flux. Next to the momentum equation, it is also assumed that the kinetic energy of a fluid element rising along the axis of the flume is converted to potential energy. By doing this the momentum equation simplifies to

$$\beta \gamma v_c^2(H_v) = gh_f \quad (3.18)$$

With h_f as the fountain height and β as a factor to account for losses. According to Friedl [20] the empirical constant $\beta = 0.39$ fits best experimental data. The profile of the fountain is given by

$$h(r) = h_f e^{-(r^2/b_f^2)} - h_{offset} \quad (3.19)$$

h_{offset} is the the offset of the Gaussian profile with respect to the still water level and can be set to zero in order to have a first estimate. The entire model is set up in Matlab (see Appendix A) [32].

3.2.3. CFD models

Most models nowadays are made by CFD, for example by Cloete et al. (2009), Olsen and Skjetne (2016b) and Olsen et al. (2017). In CFD computing power is used to make simulations of subsea plumes. CFD mainly consists out of 3 components: preprocessor, solver and post-processor [21]. A geometry is created in the preprocessor which is used as input for the solver. In the solver, different models can be used (for example the volume of fluid) which have to be adjusted for the specific scenario. The computer is able to solve a set of equations due to the chosen boundary conditions. The postprocessor presents the result in a conceivable manner.

Most of the CFD simulations are validated against the same experiment which is called "Rotvoll" [18]. In 1997 a series of experiments were conducted in a 7 meter deep (with a surface area of 6x9m) fresh water basin at Statoil's Research center in Trondheim. A mixture of helium and air was used, to obtain the same density as natural gas, to monitor the gas concentration above the surface. To measure gas concentration and velocities below the surface, air was injected. The gas was released at different flow rates from a circular opening of 0.17m diameter at 6.9m from the water surface. The plume characteristics were captured by a high-speed camera. Table 3.1 shows the parameters and results of the experiment.

Table 3.1: Parameters and results of Rotvoll experiment [61]

| Flow rates (m ³ /s) / (Nm ³ /s) | Mass flow rates (kg/s) methane / air | Inlet Velocity (m/s) | Rise time (s) | Initial fountain height (m) | Maximum fountain height (m) |
|---|--------------------------------------|----------------------|---------------|-----------------------------|-----------------------------|
| 0.05 / 0.083 | 0.03 / 0.10 | 2.2 | 6.0 | - | - |
| 0.1 / 0.17 | 0.06 / 0.21 | 4.4 | 4.8 | 0.3 | 0.65 |
| 0.45 / 0.75 | 0.3 / 0.92 | 19.6 | 3.1 | 0.45 | 1.25 |

Huser et al. (2015) came up with CFD models for the dispersion of gas from pipeline leaks [25]. They extended their research by making look-up tables for ranges of flammable gas clouds. Depending on the sea depth, release rate and wind speed; the height and distance to the gas plume, with a concentration higher than the lower flammable limit, can be found. This could be a useful tool for installing safety zones for ships operating near these gas leakages. Another method to assess the risk of subsea leakages is to incorporate the ship or offshore structure into the (CFD) model. This is what Li et al. (2019) has done [38]. The author assessed the danger depending on the length, height,

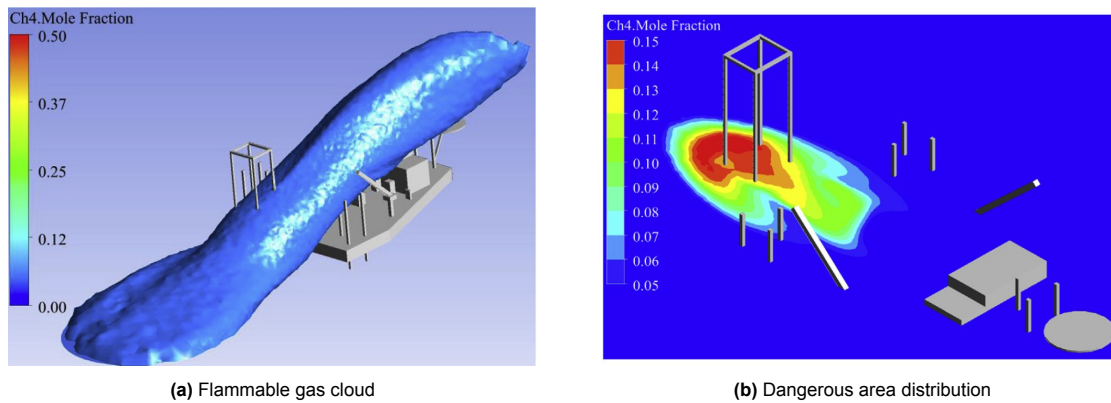


Figure 3.4: Impact of subsea gas release [38]

coverage area and volume of flammable natural gas clouds. Next to these, also the dangerous area generated on offshore platform is taken into account. The area covered by gas with a concentration within flammability limits is defined as the dangerous area. The authors concluded the following from the numerical simulations:

- The height and length of flammable gas cloud increases with surface gas release rate increasing.
- For this specific offshore structure and conditions the dangerous area size decreases with the surface gas release rate increasing.
- The distance between gas pool and offshore platform has little effect on the shape of the flammable gas cloud.
- The height of the flammable gas cloud increases with the decrease of the distance between gas pool and offshore platform.
- Wind speed has a significant effect on the spatial distribution of flammable gas cloud.
 - When the wind speed is low (1.5 m/s), flammable gas mainly disperses along the vertical direction and do not pose a threat for the offshore platform.
 - When the wind speed is large, the flammable gas disperses downwind and covers parts of the offshore platform.
- The length of flammable gas cloud increases with wind speed increasing and the height of flammable gas cloud increases with surrounding wind speed decreasing.
- The plume height decreases with increasing water depth [18].

The effect of the subsea gas release is shown in Figure 3.4. In this figure the surface gas release rate is 260 kg/s, the distance between gas pool on the sea surface and platform is 30m and the wind speed is 4.5 m/s.

From the research above a list of factors that affect the behaviour and height of the plume above the sea level can be derived:

- Gas characteristics
 - Fraction of each component
 - Mol weight of each component
 - Gas densities
 - Gas temperature
 - Gas flow rate
- Inlet (P/V valve) characteristics
 - Depth/height
 - Opening and closing pressure
- Pipeline characteristics

- Length
- Inner diameter
- Roughness coefficient
- Heat transfer coefficient
- Ambient temperature
- Outlet characteristics
 - Depth/height
 - Inner diameter

It should be noted that for shallow gas releases, the released vapour can be treated as an ideal gas. The greater the depth, the larger the influence of the pressure on the equation of state, the less accurate the consideration of ideal gas behaviour [49]. The ideal gas offset in function of the depth for methane is shown in Figure 3.5.

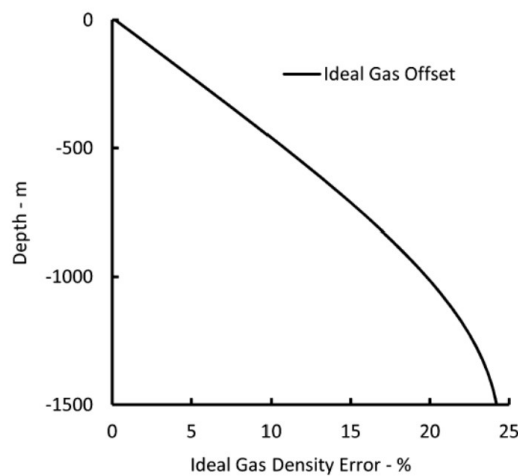


Figure 3.5: Relative difference between ideal gas law and the true equation of state for methane [49]

3.3. Experiment

A numerical model should always be validated against an experiment. TNO will conduct an experiment where a methanol-nitrogen vapour will be ventilated below the waterline. A preliminary concept is shown in Figure 3.6. Gas concentrations of methanol will be measured at certain points above the waterline. These concentrations will be compared against the concentrations (at the same point) resulting from the numeric model (CFD/integral model).

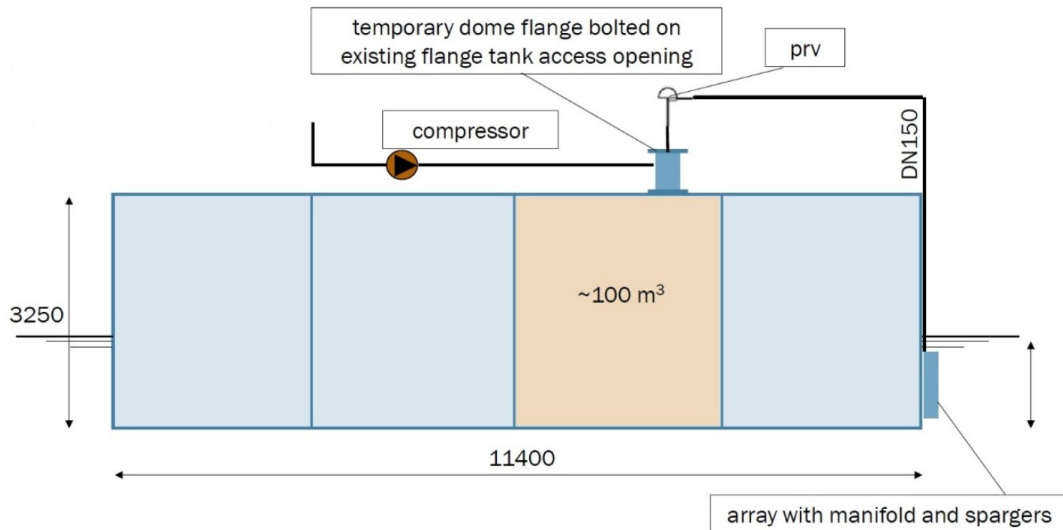


Figure 3.6: Concept drawing of experiment (from TNO)

3.3.1. Gas detection on board of ships

In order to measure gas concentrations above the waterline, gas detection sensors should be installed. On board of ships the following vapour-detection instruments are the most used:

3.3.1.1. Combustible gas indicator or explosion meter

This is an instrument which measures the composition of gas/air mixtures. It usually gives the result as a percentage of the LEL (Lower Explosive Limit). By means of a hand pump, a sample of the combustible gas is sucked into the meter. This gas is burned on the filament (resistor). The resistivity changes in function of the temperature and is in proportion to the amount of combustible gas burned. Due to the changed resistivity there is a change in current which is related to the scale in percentage of LEL. This instrument only functions if sufficient oxygen is present, at least 12% [6]. As a consequence, this instrument can not be used in inerted atmospheres.

The catalytic bead sensors works on the same principle as the explosion meter [16]. Both sensors convert a change of temperature to a sensor signal by using a wheatstone bridge. In the catalytic bead sensor a small platinum coil is embedded in a porous ceramic bead and another platinum coil stays inert. When a flammable gas oxidises, the catalyst-coated bead heats up more than the inert one. This temperature difference is measured and is proportional to the concentration of the flammable gas.

3.3.1.2. Tankscope

This is a device used for measurements of hydrocarbon gas content. On board of ships it is mainly used for measuring hydrocarbon vapours in inerted atmospheres. This instrument gives a reading in percentage of the volume of the hydrocarbon vapour. The tankscope has the same working principle as an explosion meter, they both have a wheatstone bridge. In contrast to the explosion meter, the tankscope does not heat the filament but cools it by evaporating butane in the sampled gas.

3.3.1.3. Oxygen analyzer

An instrument for determining the percentage of oxygen in a sample of the atmosphere drawn from a tank, pipe or compartment. There are different type, but most oxygen meters are based on a paramagnetic cell. Oxygen is attracted by a magnetic field resulting in a force on the nitrogen filled glass spheres. This force causes a small variation in the glass spheres which results in a deflection of the light beam. This deflection is measured and is proportional to the concentration of oxygen in the sample.

3.3.1.4. Toxic gas detectors

- Chemical detector tubes. The Tubes are made of glass with break off tips and are filled with treated chemical granules for sampling a specific substance. The tube (with broken tip) is inserted

in a hand/automatic pump. Air is drawn into the tube and reacts with the detecting reagent. The reagent changes colour if a contaminant vapour is present in the sample. The length of the discolouration stain gives a measure of the concentration of the chemical vapour which can be read from the graduated scale on the tube. The most known supplier of these tubes is Dräger.

- Electrochemical sensors. When a gas comes into contact with the sensing electrode, the gas oxidizes through a chemical reaction. A current is produced which is measured to determine the level of toxic gas present.
- Infrared sensors. Gases, which are infrared active, reduce the radiation level of emitted infrared light. This reduction is related to the gas concentration.
- Photoionization detection (PID). This detection technology is primarily used to measure volatile organic compounds (VOC). A VOC is a carbon-containing chemical, which is significantly or completely vaporised at ambient temperatures. Each VOC has an ionisation potential. VOCs are ionised (and hence detected) if light (with a photon energy greater than the ionisation potential) interacts with the gas sample [4]. An ion current is generated which can be measured by the sensor. This current is related to the gas concentration. This device is only able to detect substances that can be ionized by the UV photons.

Currently, mostly portable gas detection devices are used. Detectors like the Dräger X-am® 8000 is able to measure 7 toxic and flammable gases as well as oxygen all at once [16]. To measure different gases this device uses multiple sensor technologies: infrared, catalytic bed, photoionization detection and electrochemical sensors.

3.3.2. Methanol gas detection

The easiest and cheapest way to detect methanol vapour is by using chemical detector tubes. The following Dräger tubes can be used: Silicagel Tube Type BIA, G and NIOSH. Another method, which is more accurate, is PID. In addition to the higher accuracy, it can also detect methanol if it is only present in a low concentration. Methanol has a high ionisation potential. It requires an Argon lamp which produces a photon energy of 11.7 eV. However, this lamp is characterized by a short lifetime due to the lithium fluoride UV window, which is prone to degradation [4]. Finally, also electrochemical organic vapour sensors can be used, like the "DrägerSensor XS organic vapour" [66]. This sensor can be inserted in a portable gas detection monitor (for example PACIII or Multiwarn from Dräger) which is equipped with a data-logger.

No records of gas concentrations on board of methanol fuelled ships has been made. Nevertheless, there are records from chemical tankers transporting methanol. Figure 3.7 shows methanol concentrations on deck when tank cleaning. Due to the high vapour pressure of methanol (13 kPa at 20°C) cleaning is done by evaporation of the methanol and ventilation of the cargo tanks. When tank cleaning, large amounts of methanol are vented to the atmosphere. In Figure 3.8, the orange curve from 3.7 is shown in more detail. It should be noted that the methanol concentration exceeded the TLV-TWA (200 ppm) during a period of 6.5h at a location near the manhole which was used as tank cleaning outlet (PACIII at 3/4 deck, see Figure 3.7).

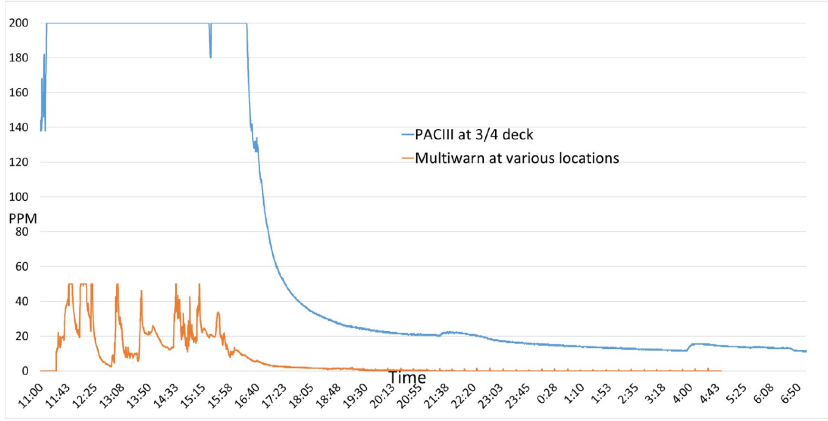


Figure 3.7: Methanol concentrations during the ventilation of the cargo tanks [66]

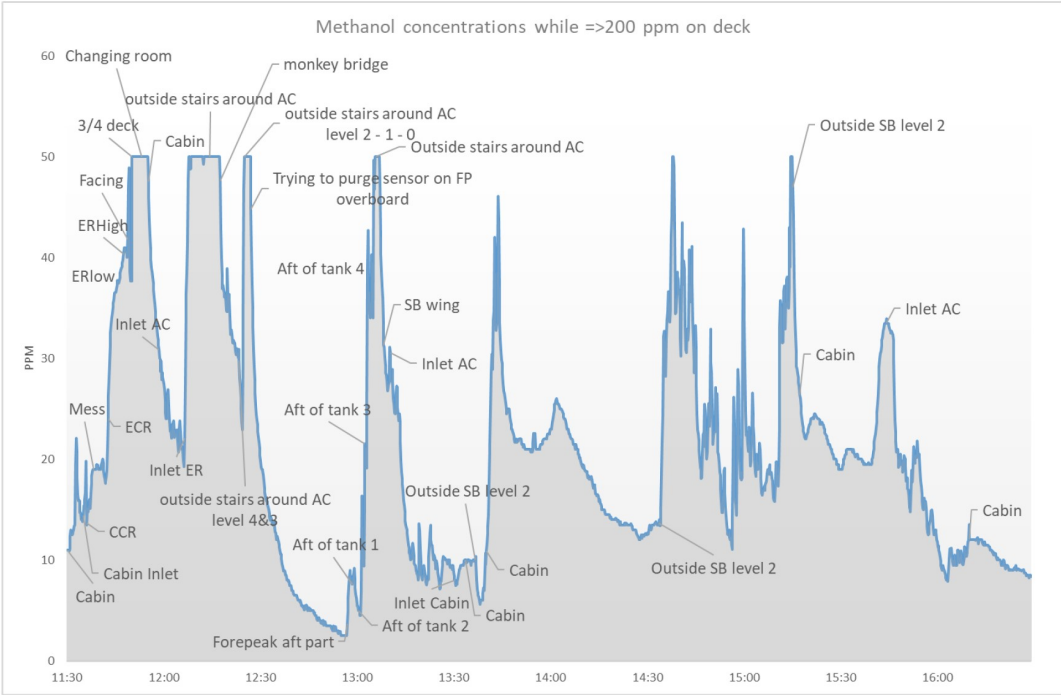


Figure 3.8: Detailed graph of the methanol concentrations at various locations while ventilating the cargo tanks [66]

4

Conclusion

This chapter acts as the basis for the research part of the thesis. Section 4.1 describes the conclusions drawn from the literature study. Section 4.2 points out the gaps between the current research and the intended research of this thesis. Finally, Section 4.3 clarifies the research questions and methods which will be used.

4.1. Literature study conclusions

In the literature study above, different general aspects of methanol as a marine fuel are described. The conclusions are as follows:

- Currently, methanol is mainly produced from gas or coal. It can also be produced from biomass or from CO₂ combined with electrolysis using renewable energy. The latter is called renewable, green or e-methanol.
- Renewable methanol leads to significant reductions in greenhouse gas emissions from well-to-wake.
- Methanol should be handled with care. Toxicity and flammability are the main dangers.
- Methanol can be used as marine fuel in internal combustion engines or in fuel cells. Both methods are available and used currently.
- Venting of methanol vapours above the waterline leads to inability to use/reach certain areas on deck due to flammability and toxicity hazards. When the use of electrical equipment in this area is unavoidable, they should be of a certified safe type.
- Subsea gas releases are represented by a multiple-zone model. In each zone, there are different dominant forces.
- Most simulations for subsea gas releases are made by CFD.
- Numerous factors (o.a. gas release rate and wind speed) affect the behaviour of the plume from subsea gas release.

4.2. Research gap analysis

The use of methanol as marine fuel is a recent development. Still many aspects should be further investigated before a wide application of methanol fuel, for example the effect of formaldehyde formic acid in the exhaust emissions. In the scope of subsea ventilation of methanol vapours, the following research gap appeared:

- Most research has focused on the gas release from ruptured pipelines or from gas hydrates. The leakage point in both cases is located at a large water depth. The governing physics, and consequently also the plume behaviour, will be different for gas releases at shallow water depths.
- Most research has focused on gases from the oil and gas industries, in particular methane. To my understanding, there has been no research published on the subsea ventilation or gas release of methanol vapours. It is expected that the dynamics of methanol vapour bubbles will behave

similarly as methane below the water line. The solubility of methane for shallow and deep releases is reasonably well investigated. This is not the case for methanol vapour. The solubility for shallow releases remains a question. Also, it is unknown how methanol's momentum and buoyancy below the waterline contribute to its behaviour above the sea level.

- Multiple risk assessment for pipeline ruptures/leakages have been made [21, 18, 38]. In these research, they mainly investigated the possibility and effects of a fire due to flammable gas reaching a platform. Such risks assessments, to my knowledge, has not been made for the subsea ventilation or gas release of methanol.

4.3. Research questions and methodology

From the research gap analysis, the research questions can be formulated. The main research question is the following:

“What is the concentration of methanol at deck level when methanol is ventilated below the waterline?”

In order to answer this question, the following sub-questions are posed:

- In subsea ventilation experiments, what is the concentration of methanol vapour above the waterline?
 - Proposed methodology: Coloured methanol vapours will be vented under the waterline of a pontoon. By means of gas detection sensors under the waterline and resistivity probes and cameras above the waterline; methanol vapour, below and at the waterline, will be detected. Also the speed of the bubbles and the void fraction of the gas below the waterline will be measured.
- How do predictions from an integral and CFD model compare with results from the experiments?
 - Methodology: First, the results from a previously conducted experiment (which is similar to the intended experiment) will be simulated by an integral model and CFD simulation. More specific this will be the Rotvoll experiment (see 3.2.3). The results which will be used for validation are the gas concentration above the waterline, the void fraction below the waterline and the speed of the bubbles below the waterline at certain positions. Next, in these models the geometry, release depth, release rate and release gas will be adjusted to the methanol experiment. In this way, the uncertainty of the results of the CFD simulation is lower. Also, If the experiment would be conducted after the simulation, predictions can be made. These predictions can help to set up the experiment (for example positioning of sensors). A CFD simulation (in Ansys Fluent) involves several steps, including geometric modelling, mesh sizing and generation, model selection, setting up boundary conditions, calculating activities. convergence and finally post-processing (results). An Eulerian–Lagrangian modelling concept is the most optimal to study the bubble movement [48].
- How do consequences of underwater venting compare to consequences of venting on deck?
 - Methodology: From the numerical models and experiments a methanol gas concentration at deck level is obtained. This concentration is compared to the gas concentration on deck due to venting above the waterline (from the IEC-code). The consequences of the methanol gas concentration in these 2 cases will be compared. Also, the conditions (o.a. draught, wind speed, fire adjacent to fuel tank) will be determined under which one should choose for underwater or above water venting.

4.4. Boundaries research

Setting boundaries is crucial to assess the viability of subsea ventilation of methanol. By defining the limits and scope of the investigation, it is possible to accurately model and predict the behaviour of methanol vapours released underwater Table 4.1 shows the ranges of the parameters depicted in Figure 4.1. Next to the outlet velocity, these are the main parameters to determine the concentration of methanol vapour on deck of the ship or bunker barge.

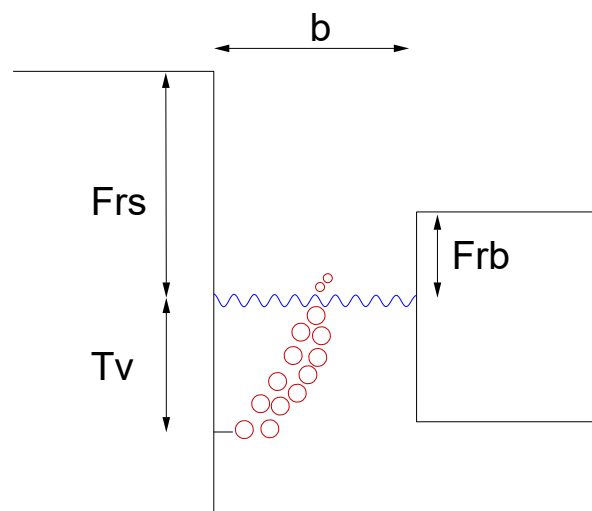


Figure 4.1: Concept sketch with most important parameters

Table 4.1: Range parameters

| Parameter | Meaning | Range (m) |
|-----------------|-------------------------------------|-----------|
| b | Width between ship and bunker barge | 0.3-2.5 |
| Fr _b | Freeboard bunker barge | 0.2-2.5 |
| Fr _s | Freeboard ship | 1-6 |
| T _v | Depth venting point below waterline | 1.5-7 |

The space between the ship and the bunker barge will be determined by the size of the fenders. Mostly pneumatic fenders will be used which can have a diameter of up to 4.5m. The freeboard of bunker barges is normally quite small and ranges from 0.2 to 2.5m. The selection of the freeboard of the methanol fuelled ship, is done with the dimensions of the ships from companies that participate in the MENENS project in mind. The freeboard is dependent on the loading condition and ranges from 1m (loaded) to 7m (in ballast). The venting point should always be located under the waterline, also in ballast condition. The depth of the venting point (measured from the waterline downwards) might be 0.7-7m. By choosing this ranges, inland ships falls outside the scope of this research. The depth of the venting point is limited by the tank design pressure. The tank should be build to withstand the hydrostatic counter pressure. For example, when the gas is vented at 10m below the waterline, the hydrostatic pressure is approx. 1 bar. Bunker tanks are not designed to withstand this overpressure.

Multiple scenarios exist in which methanol could be vented. The scenario determines how much methanol vapour is vented and what the outlet velocity is. The most common scenario will be venting when bunkering. In the future, bunkering will be mostly done by bunker barges. This is depicted in Figure 4.1. When the fuel tank is completely filled (topping off), the gas layer on top of the liquid might be vented. In this case, the venting rate will be equal to the loading rate. Assuming a filling rate of 300 t/h, this results in an average venting rate of approximately 0.10 m³/s. If the ship is fitted with a vapour return line, methanol vapours coming from the fuel tank will be returned to the quay/bunker barge. If these vapour return line fails, the PRV might open and vapour will be vented.

There are also other scenarios, next to bunkering, when venting might occur. One of these cases is the evaporation of methanol fuel due to solar radiation. This might be the case when the ship is sailing in tropical areas when the fuel is located directly under deck. Another scenario is a failure of the inert gas system. There might be a continuous, uncontrollable injecting of inert gas in the fuel tank causing venting. Fuel tanks are relatively small, therefore a topping up generator with a capacity of 500 m³/h will suffice [6]. Finally, venting might also happen in emergency situations. There might be an over pressure in the fuel tank due to a fire in an adjacent space. Similarly, there might be venting due to water ingress after a collision or grounding. The venting rate is very much dependent on the specific conditions.

Table 4.2: Venting scenarios

| Scenario | Venting rate (m ³ /s) |
|---------------------------------------|----------------------------------|
| Bunkering: failure vapour return line | 0.10 |
| Bunkering: overloading | 0.10 |
| Solar radiation | 0.10 |
| Inert gas system failure | 0.14 |
| Fire | 0.1-0.4 |
| Water ingress | 0.10 |

Fuel tanks will be equipped with a high velocity pressure relief valve. The PV-ECO type 4100 DN80 is a widely accepted standard valve for cargo tanks [7]. Such a valve has an opening pressure of 14 kPa and a closing pressure of 9 kPa. The efflux velocity will be approximately 75 m/s when opening and 30 m/s when closing. The corresponding release capacities are 900 m³/h (0.25 m³/s) and 400 m³/h (0.11 m³/s), see Figure 4.2. The ultimate capacity of this valve is 1400 m³/h (0.39 m³/s) which is enough to cover the scenarios described above. As mentioned the leading scenario will be venting when bunkering methanol. Similarly to cargo tank venting, the venting system should be able to vent gas evolution due to 1.25 times the loading rate (IBC-code) [7]. This safety factor takes into account the vapour generation due to the dropping of liquid methanol in the bunker tank and due to disturbances (for example ship movements). This corresponds to an average venting of 470 m³/h (0.13 m³/s) with an outlet velocity of 48 m/s.

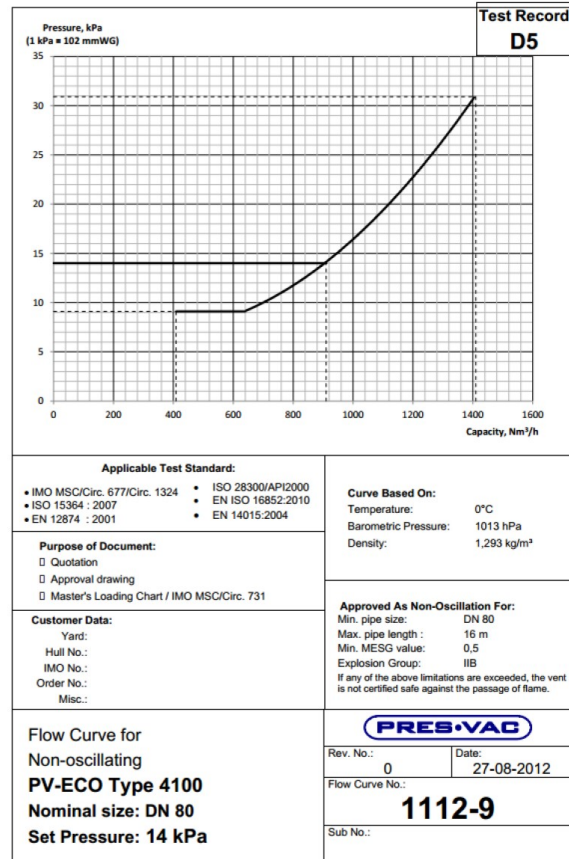
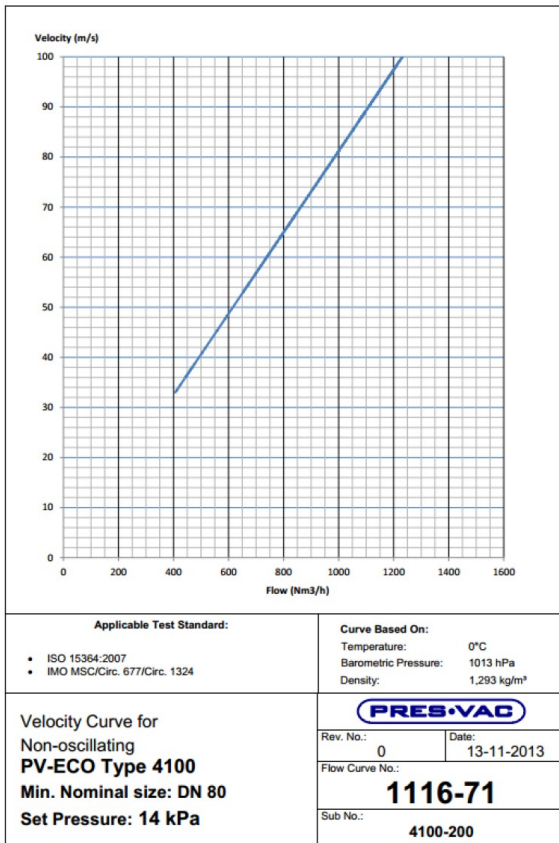


Figure 4.2: Flow rate curves of PV-ECO type 4100 [7]

Part II

Numerical Investigation

5

Methods

The aim of this research is to derive a numerical model which is able to predict the methanol concentration above the waterline due to a subsea gas release (described in Section 4.4). The methanol concentration should be sufficiently low to avoid toxicity and flammability dangers. If this is the case, dangerous areas on deck (described in Section 2.2.2) can be eliminated/reduced. Two different numerical models are proposed in this thesis: a CFD model and an integral model.

5.1. CFD

In this section, the CFD model is described by means of the Rotvoll experiment. This experiment is described in Section 6.1 and will be used as a validation for the numerical models.

5.1.1. Basics CFD

In CFD a continuous domain is transferred to a discrete domain using grid cells. Where in reality each flow variable is defined at every single point in the domain, in CFD each flow variable is defined at the grid points/centers of the discrete domain. The process of transferring a continuous domain to a discrete domain is called discretization and is done by the finite volume method. In this method the computational domain is decomposed into non-overlapping control volumes (the so-called finite volumes). Each finite volume contains the cell average of the flow variable. The governing equations (conservation of mass, momentum, energy and species) are applied in integral form to the finite volumes. By using the Gauss' theorem, volume integrals can be written as surface integrals which are consequently approximated by a sum of discrete values at one or several points at the cell surface. An example is given by the conservation of mass (also called the continuity equation) [35]:

$$\frac{\partial \rho}{\partial t} + \nabla \cdot (\rho u) = 0 \quad (5.1)$$

Where u is the velocity vector. In the case of an incompressible flow, this simplifies to

$$\nabla \cdot u = 0 \quad (5.2)$$

This differential equation can be written in an integral form over a control volume.

$$\int_V \nabla \cdot u \, dV = 0 \quad (5.3)$$

By means of the Gauss' divergence theorem the volume integral can be written as a surface integral. This theorem states that the volume integral of the divergence of a vector field over a volume enclosed by a surface is equal to the surface integral of the vector field over this closed surface.

$$\int_S u \cdot \hat{n} \, dS = 0 \quad (5.4)$$

Where \hat{n} is the normal vector (perpendicular to the surface) and S is the surface which encloses the control volume. As $u \cdot \hat{n} \, dS$ represents a flow rate, the equation describes that the net flow rate should

be equal to zero. The integration of the flow rate along the boundary of the control volume leads to the finite volume discretization for the continuity equation (Equation 5.5). The velocities at the faces are found by interpolating the velocities at the center of adjacent cells. This process can be repeated for the other conservation equations.

$$-u_1\Delta y - v_2\Delta x + u_3\Delta y + v_4\Delta x = 0 \quad (5.5)$$

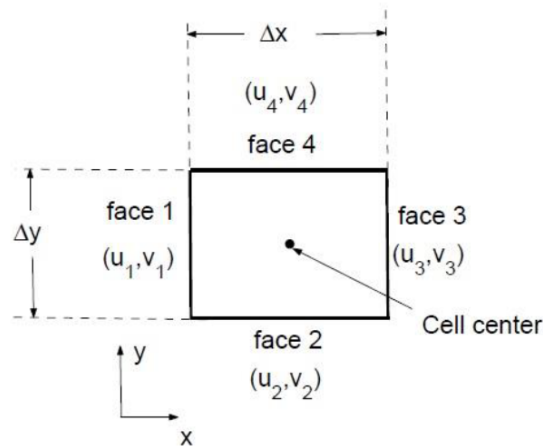


Figure 5.1: Control volume on a Cartesian grid [9]

5.1.2. Geometry

An identical geometry to the Rotvoll experiment is created in Rhinoceros. A 3D geometry is chosen in order to represent the reality as accurate as possible. The size of the water body is 9m x 6m x 7m. Methane or air is released into the water body from the release point, at the bottom of the tank, which has a diameter of 0.17m. The dimensions of the air body on top of the water were in first instance 9m x 6m x 3m. After some test runs, a circular flow seemed to appear. This is shown by Figure 5.3. The water flow just below the surface drags the gas-air mixture on top of it to the side walls. This happens due to the shear forces between the water and the atmospheric air. At the sides, this gas rises and afterwards it falls back down in the middle. Doubling the height of the air body helped to reduce this interference. Figure 5.2 shows the final geometry for the CFD simulation. The blue part represents the water body and the grey part the air body.

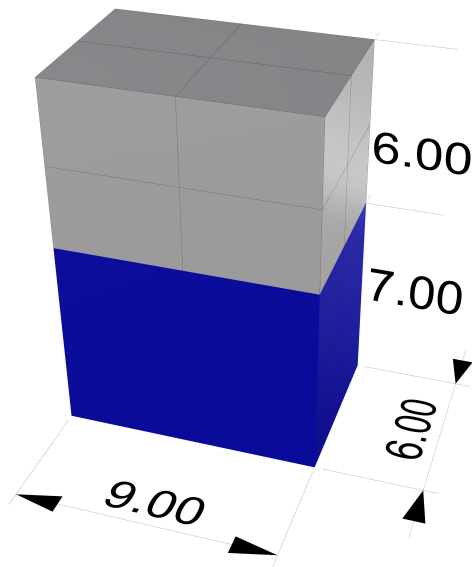


Figure 5.2: Geometry Rotvoll experiment (in meter)

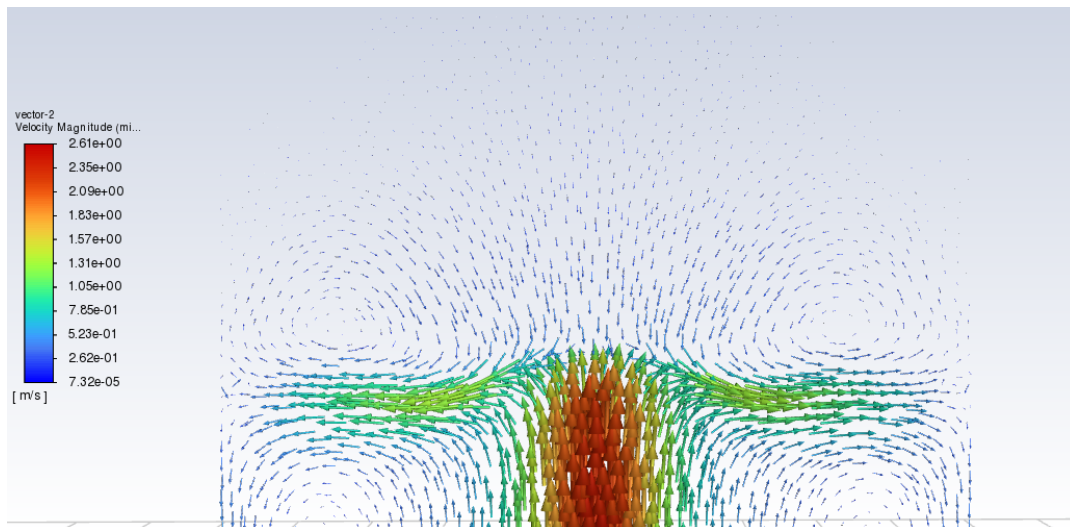


Figure 5.3: Velocity vectors of the mixture near the surface

5.1.3. Mesh sizing

In simulations the main goal is accurate and reliable results. Therefore the grid size should be as small as possible. A smaller grid size allows for a more precise approximation of the gradients in the fluid properties such as velocity and pressure, thereby reducing numerical diffusion errors. Additionally, a smaller grid size captures the fine-scale features and turbulence of the fluid flow, leading to a better representation of the flow physics. However, it is important to note that reducing the grid size also increases the computational cost and time required for the simulation. Therefore, there is always a trade-off between accuracy and computational cost when selecting a mesh size for a CFD simulation.

Initially, for means of simplicity, one uniform grid size distribution is chosen. The grid size is set as 5cm. A mesh independency study by Pan [53] showed that a finer grid did not lead to more accurate results. A total number of 322331 grid cells are used. Polyhedral cells are used as mesh type (see Figure 5.4). According to the Ansys User's Guide [5], the use of a polyhedral mesh leads to a lower cell count compared to rectangular or triangular cells for a same level of accuracy. This can be contributed to the added number of faces. Consequently, the solver can better handle gradient calculations and the system is well coupled. Next to this, the coarser grid will reduce the computational expense. Also, polyhedral cells are less sensitive to stretching (for example compared to rectangular cells) which favours numerical stability. The meshing is done in the solver (Ansys fluent) before the start of the calculations. Figure 5.5 shows the used mesh.

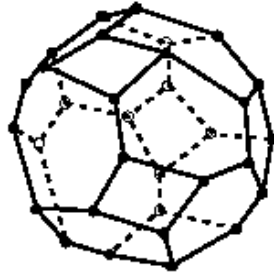


Figure 5.4: Example of a polyhedral cell [5]

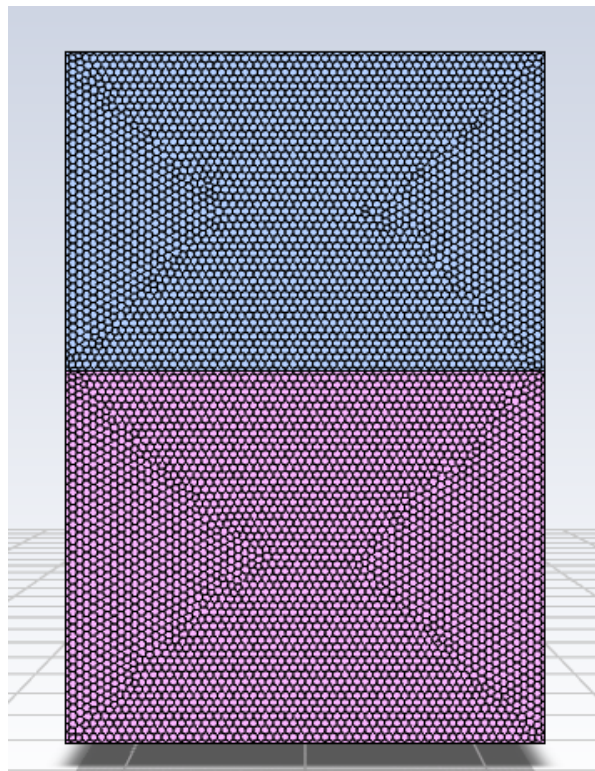


Figure 5.5: First meshing attempt for the Rotvoll experiment

Mesh independence is an essential concept in CFD that refers to the idea that the numerical solution of a CFD simulation should be insensitive to the mesh size and type. In other words, the solution should converge to a unique and accurate result as the mesh is refined, regardless of the initial mesh size or type. The importance of mesh independence lies in the fact that it ensures the reliability and accuracy

of CFD simulations. If a simulation is not mesh independent, the numerical solution can be significantly affected by the mesh size and type, which can lead to erroneous results. Mesh independence ensures that the results obtained from a CFD simulation are not affected by the mesh, but rather reflect the actual physics of the problem being studied. In order to test the dependency of the mesh on the simulation results, an additional mesh is utilized. Various grid refinements are conducted to accurately capture the details in regions of interest with significant pressure and velocity gradients. More specific, this region would be the plume region and the region around the water surface. The conical shape of the plume is not (or at least very little) affected by the shape of the mesh. This is checked by performing a simulation on a very coarse grid with cubical mesh elements. The solution should be independent of the mesh. Therefore it is investigated that a denser mesh does not lead to significant improvements in the results. Figure 5.6 shows the refined mesh with a total of 871667 number of cells. The results seemed to fit the experimental results better than for the mesh without regional refinements. However a higher turbulence level than expected occurred in the regions where the squares are connected to each other. This problem was avoided by changing the mesh to Figure 5.7. The presented results refer to this mesh, which has a lower number of cells (657399) than the mesh described above. Similarly the independence on the cell type could be examined by changing the polyhedral cells to e.g. hexahedral cells. However this falls outside the scope of this thesis because of the better support of Ansys Fluent for polyhedral cells and the described advantages of polyhedral cells over other cell types.

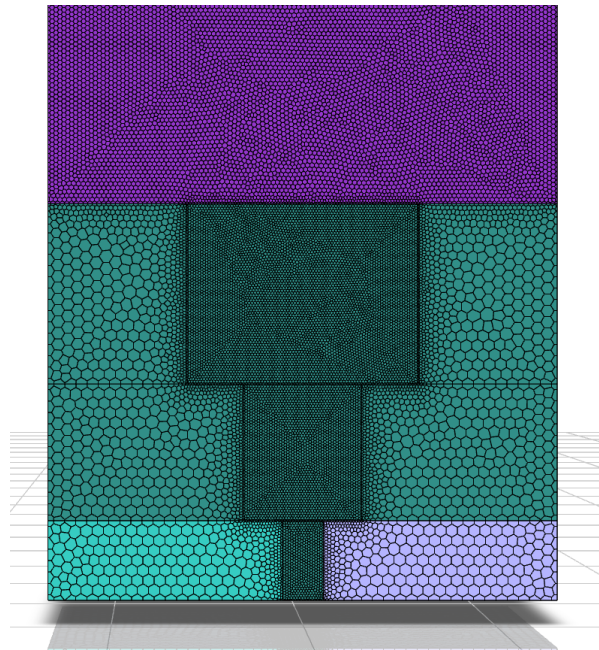


Figure 5.6: Mesh with regional refinements

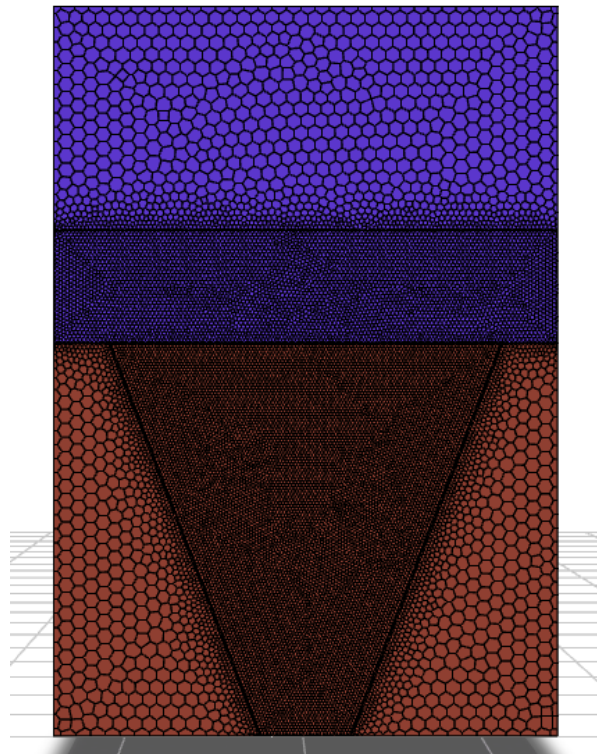


Figure 5.7: Mesh with conical regional refinements

5.1.4. Model

There are 2 ways to study single-phase fluid flows: by means of an Eulerian representation or a Lagrangian representation. In the Lagrangian frame of reference, the observer moves with one fluid element which is tracked along the way. While in the Eulerian reference frame the observer remains at a fixed position and the fluid element is tracked and described at certain locations.

Two models can solve particle transport, namely Euler–Euler and Euler–Lagrange models. In the Euler–Euler model, the particles are considered as a continuum phase, just like the water. The particles are a virtual fluid described by momentum transport equations similar to the Navier-Stokes equations. In the Euler–Lagrange model, the particles are followed individually and not as a fluid. The description for the movement of a particle is described by Newton’s second law. The Lagrangian model (in comparison to the Eulerian model) can calculate the particle size distribution with a lower computational cost [1]. As the particle size is an important variable for predicting the gas concentration, the Eulerian–Lagrangian Discrete Phase Model (DPM) is applied for the simulation of the subsea gas release. This model will track a parcel of bubbles in the Lagrangian frame and will monitor the change in properties in the Eulerian frame. A parcel is a group of bubbles which have the same properties (o.a. velocity, size, density and viscosity). The parcel is tracked by integrating the force balance (see Equation 3.2) wherein the particle inertia is equated to the forces acting on the particle. The ambient fluid is treated as a continuum by solving the Navier-Stokes equations. The surface (interface between seawater and air) is tracked by a scheme in the Volume of Fluid (VOF) model. This scheme is called the “Geo-Reconstruction scheme”. This method uses explicit discretization and represents the interface between fluids using a piecewise-linear approach [5].

5.1.4.1. Algorithms

The momentum and continuity equations in this multiphase flow problem are solved by the pressure-based solver in ANSYS FLUENT. According to Cloete et al. [14] (who used this particular solver for a similar problem): “This solution method contains multiphase models and discretization schemes which fits the present flow situation.” Next to the pressure-based solver, there is also the density-based solver. The main difference between pressure-based and density-based solvers in CFD is the way they han-

olve the governing equations of the fluid flow problem. Pressure-based solvers solve for the pressure field first and then use it to solve for the velocity field, while density-based solvers solve for the density field directly. Pressure-based solvers are typically used for incompressible flows, while density-based solvers are used for compressible (high speed) flows (for example shock wave problems).

The PISO algorithm is chosen as pressure-based solver. The PISO algorithm is a part and an extension of the SIMPLE family of algorithms which is a guess-and-correct procedure for the calculation of pressure. It is initiated by a guessed pressure field [62]. Secondly, estimated velocities are calculated by solving momentum equations. Mass fluxes at the faces of the cells are found by using these estimated velocities. Afterwards, a pressure correction equation is used (based on the mass fluxes) to find the pressure and velocity corrections [33]. The pressure correction equation is obtained by taking the divergence of the momentum equation and using the continuity equation to eliminate the pressure term. Finally, this pressure correction leads to a new pressure field which is the start of the loop. This process is repeated until the residuals are small enough and convergence is reached.

5.1.4.2. Turbulence

Normally turbulence is described by Navier-Stokes equations which describes the equation of motion for a Newtonian fluid. A Newtonian fluid (e.x. water) is characterized by a viscosity which is independent of the shear rate. These Navier-Stokes equations are ideally solved by Direct Numerical Simulation (DNS). DNS solves the full range of space and time of the Navier-Stokes equations but this requires too much computing power. It is typically limited to low Reynolds number flows and small computational domains. DNS is used primarily in academic research to study fundamental aspects of turbulent flows. In order to reduce the computational expense, Reynolds-Averaged Navier-Stokes (RANS) equations are used. In RANS equations, Reynolds decomposition is used to decompose the Navier-Stokes equations into a time averaged (time independent mean flow) and fluctuating component (time varying fluctuations around the mean). This fluctuating component is responsible for the turbulence. An alternative to RANS, Large Eddy Simulation (LES), is not chosen because it leads to only small improvements and larger computational time [14].

The RANS-model which is chosen is the standard $k-\epsilon$ model. This is a 2-equation model where the degree of turbulence is modelled by k (turbulent kinetic energy) and ϵ (turbulent dissipation). The standard $k-\epsilon$ model is known as robust, economic and reasonable accurate for a wide range of turbulent flows [62]. According to Pan [53], $k = 0.007 \text{ m}^2/\text{s}^2$ and $\epsilon = 0.001 \text{ m}^2/\text{s}^3$ gives accurate results.

The turbulence of the discrete particles in the fluid phase (water or air) is predicted using the stochastic tracking model, which is in Fluent represented by the Random Walk Model. According to the Fluent theory guide [5], the turbulent dispersion trajectory is calculated by firstly inserting the instantaneous fluid velocity (which is assumed to fluctuate according a Gaussian probability distribution) in Equation 3.2 and secondly by the integration. As this is done for numerous particles, the random turbulence effect on the particle dispersion is taken into account. The discrete particle interacts with a fluid phase eddy for a maximum time of T_L which can be approximated as [5]

$$T_L = C_L \frac{k}{\epsilon} \quad (5.6)$$

Increasing the constant C_L gives more turbulence and consequently a wider plume. The value for $k-\epsilon$ turbulence models is 0.15.

5.1.5. Parameters

As the Rotvoll experiment is carried out in fresh water, the density is 998.2 kg/m^3 . The viscosity is set to 0.001003 kg/ms . The density of air body is 1.225 kg/m^3 and the viscosity is $1.7894\text{e-}5 \text{ kg/ms}$. A uniform temperature distribution (for both the water and the air) of 15°C is assumed. Identical to the experiment, the duration of the simulation is 20s. After some test runs, it was found that a constant time step of 0.005s was small enough to reach convergence while being large enough to make the simulation computationally feasible. An overview of the input parameters for the different simulation cases is shown in Table 6.2.

5.1.6. Boundary conditions

Boundary conditions are set in order to be able to solve momentum and continuity equations. Except for the top surface of the mesh, the boundary type is designated as "wall" with a no-slip condition. Since bubbles will reflect upon hitting a wall, it is important to position these surfaces in such a way that they do not affect the results.

The inlet surface was set as a wall. This is due to the use of the DPM model, where the injection of gas particles is set as a cone with the origin at the coordinates of the inlet surface. In the experiment a horizontal plate at the inlet was used as a momentum breaker [61]. This is simulated in the CFD model by setting the inlet velocity of the discrete particles to zero. However, this does not take into account the radial velocity which the particle have after hitting the plate. Therefore the bubble plume is expected to be less wide in the CFD model compared to the experiment. The air and water have no initial velocity.

The top surface of the mesh is the outlet boundary and is set as a pressure outlet (at atmospheric pressure) with escape condition. The backflow fraction is set to zero for water and methane. Between the water and air body, an interface is created.

5.1.7. User defined model

The physics of subsea venting can not fully be implemented by custom options in Ansys Fluent. Therefore additional models are hooked to the simulation software by means of user defined models.

5.1.7.1. Drag force

In Equation 3.2 buoyancy, gravity and drag are taken into account. Buoyancy and gravity are automatically calculated in ANSYS Fluent. The drag force (more specifically the drag coefficient C_D , see Equation 3.3) can be calculated by either basic drag laws (which can be selected in ANSYS Fluent) or a user-defined function (UDF). The most used drag laws are the spherical drag law, modified spherical drag law, Xia's drag law and Tomiyama's drag law. In this thesis, Xia's drag law is chosen because this gave accurate results in similar research [14].

Xia et al. [67] derived its drag law from experiments using liquid metal. This drag law takes the shapes of bubbles into account by using the Eötvös number (see Equation 5.8) whereas the spherical drag law uses the relationship between the Reynolds number and drag coefficient for smooth, spherical bubbles. According to Olsen and Cloete [14] Xia' drag law represents the behaviour of a bubble plume. This is mainly due to the distortion of spherical bubbles in turbulent regions which are common in subsea venting scenarios. The law is given in Equation 5.7. This bubble drag is incorporated in the CFD model as a UDF (see Appendix B) and is modified from Bakli (2014) [8].

$$C_D = \frac{2}{3} \sqrt{\frac{E_0}{3}} \quad (5.7)$$

$$E_0 = \frac{g(\rho_l - \rho_g)d_b^2}{\sigma} = \frac{\text{Buoyancy forces}}{\text{Surface tension forces}} \quad (5.8)$$

5.1.7.2. Bubble size distribution

The drag coefficient is dependent on the bubble size. In addition, the gas dissolution or mass transfer from gas bubbles to the surrounding liquid is dependent on the bubble surface area. A correct bubble size distribution is therefore required to achieve accurate simulation results. The instantaneous local mean bubble diameter (d_b) is described by the balance between the local time derivative of the local bubble diameter and an equilibrium term which accounts for breakup and coalescence [14]:

$$\frac{\partial d_b}{\partial t} = \frac{(d_b^{eq} - d_b)}{\tau_{rel}} \quad (5.9)$$

τ_{rel} is the relaxation time, which is the time needed for the bubble to return to the bubble equilibrium diameter. The equilibrium bubble diameter (d_b^{eq}) is the achieved diameter when the bubble stays suf-

ficiently long at the same conditions. A mathematical expression for the equilibrium diameter, derived from experiments in a stirred tank, is given by [12]:

$$d_b^{eq} = C_1 \phi_b^{0.5} \left(\frac{\sigma}{\rho} \right)^{0.6} \left(\frac{\mu_b}{\mu} \right)^{0.25} \epsilon^{-0.4} + C_2 \quad (5.10)$$

Where ϵ is the dissipation of turbulent kinetic energy, μ_b is the viscosity of the bubble phase and σ is the surface tension between bubbles and the surrounding fluid. ϕ_b is the bubble void fraction which is the volume fraction that bubbles occupy in the water. This bubble fraction is calculated by the gas concentration (in kg/m^3) divided by the gas density which is computed by means of the ideal gas law. C_1 is a dimensionless constant and is equal to 4.0 and C_2 is the minimum bubble size and is equal to 0.0001m [53]. Methane bubbles with a void fraction of 0.10 have an equilibrium bubble diameter of approximately 0.02m. Figure 5.8 is a graphical representation of Equation 5.10 (at 20°C). It is clear that the bubble size increases if more gas is present and decreases if the depth becomes larger. If the void fraction is low (smaller than 0.10), the influence of depth is limited.

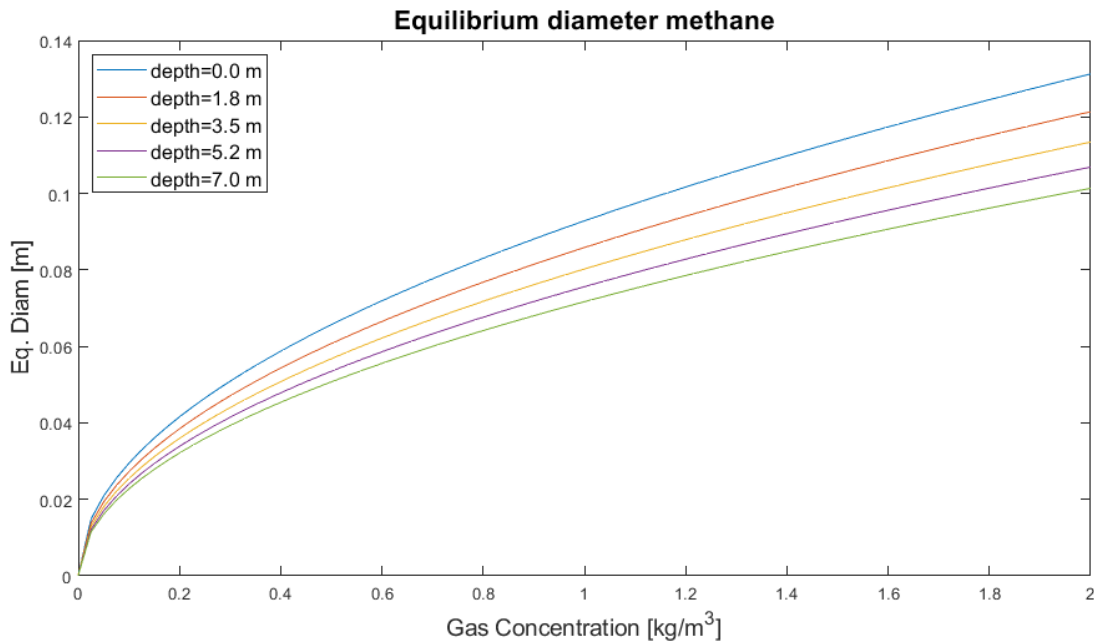


Figure 5.8: Methane bubble equilibrium diameter in function of local gas concentration and depth

The relaxation time is determined by the speed of breakup or coalescence. If the bubble diameter is smaller than the equilibrium diameter, coalescence is assumed [22]. Coalescence is the process of multiple bubbles colliding and forming one larger bubble. Otherwise, if the bubble diameter is larger than equilibrium diameter, breakup is assumed. The breaking up of the bubble occurs when the turbulent shear forces (due to turbulent eddies) are larger than the resistive tension forces. Turbulent eddies which are large compared to the bubble diameter are assumed to move the bubble around and not to break them up. Small turbulent eddies are neglected, because they are assumed not to shear bubbles. Turbulent eddies which are similar in size to the bubble will cause the most breakup. The bubbles will come in contact with turbulent eddies when there is a large mixing energy. This mainly occurs at the jet region and just beneath the water surface due to the radial flow. The relaxation time is modelled as a characteristic timescale for both processes [53, 22].

$$\tau_{rel} = \begin{cases} d_b^{2/3} \epsilon^{-1/3} & \text{if } d_b > d_b^{eq}; \text{ breakup.} \\ \frac{d_b}{1.2\sqrt{\phi_b k}} & \text{if } d_b < d_b^{eq}; \text{ coalescence.} \end{cases} \quad (5.11)$$

Where k is the turbulent kinetic energy. The breakup timescale (τ_B) is based on the third power relationship of turbulent dissipation (ϵ) with speed (u). The derivation is shown in Equation 5.12. C_B is a factor which relates the breakup timescale to the eddy timescale and is taken as 1 for simplicity reasons.

The eddy length scale (l) is replaced with the diameter of the bubble. Similarly, the coalescence time scale can be found which is based on the second power relationship of turbulent kinetic energy (k) with speed.

$$\tau_B = C_B \tau_e = 1 \frac{l}{u} = \frac{d_b}{u} = d_b^{2/3} \epsilon^{-1/3} \quad (5.12)$$

The relaxation time should always be larger than the turbulent micro scale (at which energy is dissipated by viscosity), which is the smallest time scale in a turbulent flow [22].

$$\tau_{rel} = \max(\tau_{rel}, 6\sqrt{\frac{\nu}{\epsilon}}) \quad (5.13)$$

Where ν is the kinematic viscosity. An initial bubble diameter is assumed in order to take a varying bubble distribution into account. The current bubble diameter at each time step is calculated from the previous time step by solving Equation 5.9.

$$d_b = \frac{d_{b,pre} + \frac{d_b^{eq} dt}{\tau_{rel}}}{1 + \frac{dt}{\tau_{rel}}} \quad (5.14)$$

For example, an initial methane bubble of 0.002m will have a relaxation time of 0.063s (coalescence). If the time step is 0.01s, the bubble diameter in the next time step will be 0.0045m. In reality, the coalescence is expected to be larger due to that there is no particle-particle interaction in the DPM model [8]. The particles don't occupy a volume such that they move straight through each other. As a consequence, the underwater plume will be more dispersed and have a lower velocity.

5.1.7.3. Gas dissolution

Gas dissolution is the product of the mass flux and the bubble surface area. To simplify and limit the numerical expense, the bubble shape is approximated as a sphere. The mass transfer rate through the surface of the bubble can be calculated as follows [58]:

$$\dot{m} = \pi d_b^2 k_i \rho_l n_i^{sol} \frac{M_i}{M_l} \quad (5.15)$$

Where M is the molar weight and n is the solubility of the compound in the surrounding liquid. The concentration of the dissolved gas in the surrounding liquid is assumed to be negligible. k is the mass transfer coefficient and the subscript i represents a certain chemical compound (methane or methanol). In general there is a distinction between the liquid side and the gas side of the interface [15], but the diffusion in gas is much faster than in liquid. As a consequence the liquid side becomes the rate determining side of the mass transfer and the density of the liquid is used in Equation 5.15. In addition, there is almost no theoretical or experimental knowledge on the gas-side mass transfer coefficient. Due to the importance of the (liquid-side) mass transfer coefficient, this number is determined in two different ways.

Method 1

The first method is by the Equation 5.16 [69]. This equation is a result of an experimental investigation of the gas dissolution of methane in seawater. The equation is valid for water contaminated by surfactants. Equations for pure water also exists but these are not of interest because even a small amount of impurities will affect the mass transfer coefficient.

$$k = \left[1 + (1 + Pe_c)^{1/3} \left(1 + \frac{0.096 Re^{1/3}}{1 + 7 Re^{-2}} \right) \frac{D}{d_b} \right] \quad (5.16)$$

$$Re = \frac{d_b v_s \rho_l}{\mu} = \frac{\text{Inertia forces}}{\text{Viscous forces}} \quad (5.17)$$

$$Pe_c = \frac{v_s d_b}{D} = \frac{\text{Convective transport rate}}{\text{Diffusive transport rate}} \quad (5.18)$$

Where Re is the Reynolds number, Pe_c is the compositional Peclet number and D is the diffusivity. The compositional Peclet number represents the relative importance of convective transport versus diffusive transport. Convective transport can be defined as the flow due to the motion of the bulk fluid, while diffusive transport is related to the flow of molecules from a high concentration to a low concentration. The diffusivity characterises how fast the molar flux will be in the case of a gradient in concentration.

Method 2

The second method is by means of the Sherwood number (see Equation 5.19). This number represents the ratio of (convective) mass transfer to the mass diffusion rate. The Sherwood number (in function of the Reynolds and Schmidt number) for a single sphere can be determined by the Froessling equation (see Equation 5.20). The first term represents the natural molecular diffusion (when there is no flow, $Re=0$) and the second term represents the forced convection.

The characteristic length in the Reynolds, Peclet, Sherwood and Schmidt number is replaced by the bubble diameter. Table 5.1 shows the difference in mass transfer coefficient for the different methods in function of the bubble diameter. The first method gives the lowest mass transfer coefficient which leads to a lower gas dissolution transfer rate (see Equation 5.15). Consequently, less gas will dissolve in the surrounding water and the gas concentration above the waterline will be higher. This method is used in order to have the error on the safe side.

$$Sh = \frac{k}{D/d_b} = \frac{\text{Convective mass transfer rate}}{\text{Diffusion rate}} \quad (5.19)$$

$$Sh = 2 + 0.552Re^{1/2}Sc^{1/3} \quad (5.20)$$

$$Sc = \frac{\mu}{\rho D} = \frac{\text{Viscosity}}{\text{Diffusivity}} \quad (5.21)$$

Table 5.1: Comparison calculation mass transfer coefficient

| Bubble diameter (m) | k method 1 (m/s) | k method 2 (m/s) |
|---------------------|------------------|------------------|
| 0.001 | 1.418e-04 | 1.591e-04 |
| 0.005 | 8.905e-05 | 1.002e-04 |
| 0.01 | 6.275e-05 | 7.174e-05 |
| 0.015 | 5.116e-05 | 5.938e-05 |
| 0.020 | 4.426e-05 | 5.206e-05 |

5.1.7.4. Influence salinity

The influence of salinity on the gas dissolution is not taken into account in the CFD simulations. The effect of salt on the solubility of gases can be studied using the Setschenow equation [46] which represents the solubility of non-electrolytes in electrolyte solutions

$$\ln\left(\frac{S^0}{S}\right) = k_s m \quad (5.22)$$

Where k is the salting coefficient, S is the solubility in the solution, S^0 is the solubility in water and m is the molality (number of moles of a solute per kilogram of a solvent). The salting coefficient for methane in a NaCl-solution is 0.319 and for methanol 0.152. The solubility, n_i^{sol} in Equation 5.15, can be adjusted for salinity as follows

$$n_i^{sol} = n_i^{sol} e^{\frac{-0.319s}{M_{NaCl}}} \quad (5.23)$$

Where s is the salinity of the (sea) water. In the North Sea the salinity is approx. 35 moles/kg, which causes a 17% reduction in solubility for methane. The larger the salinity, the lower the gas dissolution. This can be explained by the reduced internal circulation (in the bubble) by the salt molecules and leading to a lower mass transfer [58].

5.1.7.5. Influence bubble size

As previously mentioned, gas dissolution is dependent on the bubble size. Smaller bubble diameters lead to higher gas dissolution rates. This can mainly be explained by 2 effects. On the one side, there is the higher drag force due to smaller bubble diameter (see Equation 3.2). Consequently the rise velocities are lower and the rise time of the bubbles increase giving the bubble more time to dissolve in the water. On the other side, smaller bubbles have a larger interfacial area. Both effects cause the higher mass transfer rates for smaller bubbles.

5.1.8. Solution method

The continuity, momentum and turbulence are solved using the Second-Order Upwind Scheme. In upwind schemes the values are calculated from quantities in the cell upstream [5]. The PRESTO! scheme takes care of the discretization of the pressure. Discretization is defined as the process where the governing partial differential equations are transformed into algebraic equations (see Section 5.1.1). This is done for each cell because each cell has one set of equations. The calculations are done when convergence is reached, i.e. when the residual values are sufficiently small. The default convergence criterion of Ansys Fluent are used which means that scaled residuals should be lower than 10^{-3} for the velocity and continuity equations and 10^{-6} for the energy equation to reach convergence.

5.1.9. Software and Hardware

The latest version (2022 R2) of the commercial software Ansys Fluent is used to run the CFD simulations. The case and data files are submitted onto the high performance cluster (HPC) of TNO which was used to do the calculations. This HPC uses a Red Hat Enterprise Linux operating system. The computational time, depending on the specific simulation, usually takes up to 2-10 days. The duration (of experiment or full scale venting) and release rate, which determines the number of parcels that should be tracked, are found to be determining the computational time.

5.2. Integral model

This model is a combination of the Friedl model for the underwater plume (see 3.2.2) [20] and the model build by Loes and Fanelop for the plume above the water surface [40]. The latter is a model for a plume with excess of buoyancy. The rising gas (due to buoyancy) causes a radial inflow of air. A sketch of this phenomenon is shown in Figure 5.9. The gas concentration can be derived from a momentum balance. The general momentum equation in integral form is given below.

$$\frac{\partial}{\partial t} \int_V \rho \underline{u} dV + \int_S \rho \underline{u} \underline{u} \cdot \underline{n} dS = - \int_S p dS + \int_S \underline{\tau} \cdot \underline{n} dS + \int_V \rho \underline{F} dV \quad (5.24)$$

In words this means: the temporal change of the momentum of a (material) fluid element equals the sum of the forces that act on it. On the left hand side of the equation sign, there is respectively the local acceleration and the convective acceleration. On the right-hand side there are two surface forces and one volume force, respectively the pressure gradient, the viscous term and the body force term. The momentum balance is simplified by making the following assumptions:

- The gas which reaches the water surface is lighter than air.
- The flow is inviscid and incompressible.
- The system is stationary such that the time domain can be neglected.
- There is no change in pressure over the control volume.
- The surface integrals are approximated as the product of the integrand with the area of the control volume face.
- The volume integrals are approximated as the product of the integrand with the control volume.

Taken these assumptions into account, only the second and last term of Equation 5.24 remains. Solving the momentum balance for the vertical (z-) direction gives

$$\pi r^2 v^2 \rho - \pi r^2 v_s^2 \rho_g = g(\rho_a - \rho) \pi r^2 z \quad (5.25)$$

The multiplication of area and speed is substituted by the volumetric flow rate:

$$\dot{V} \rho v - \dot{V}_g \rho_g v_s = g(\rho_a - \rho) \pi r^2 z \quad (5.26)$$

With

$$\rho = \frac{(\dot{V}_a \rho_a + \dot{V}_g \rho_g)}{(\dot{V}_a + \dot{V}_g)} \quad (5.27)$$

$$v = \frac{(\dot{V}_a + \dot{V}_g)}{(\pi r^2)} \quad (5.28)$$

$$\dot{V} = \dot{V}_a + \dot{V}_g \quad (5.29)$$

Where r is the radius of the plume at the surface. The radius derived from the Friedl model is multiplied by 1.2-2 (depending on the depth of the release point) to account for the outward deflection of the plume near the surface. The subscripts a, g and s represent respectively air, gas and slip. The slip velocity in subsea gas release refers to the difference in velocity between the gas and the surrounding water as the gas rises through the water. From experiments it was found that the slip velocity is approx. 0.35 m/s for a wide range of bubble diameters [40]. As the water can not escape from the surface, the escape velocity of the gas is taken equal to the slip velocity. \dot{V} is the volumetric flow rate and z_0 is the height of the control volume. It is assumed that there is no gas dissolution, so \dot{V}_g is equal to the released/injected gas in order to know the average concentration in the control volume. In order to know the concentration at the centerline, \dot{V}_g is multiplied with the void fraction at the centerline at the surface. It is assumed that the concentration just above the surface is equal to the void fraction just below the surface. From the momentum balance, the only unknown, \dot{V}_a , can be calculated. Finally, the concentration is calculated as follows

$$C_g = \frac{\dot{V}_g}{\dot{V}_a + \dot{V}_g} \quad (5.30)$$

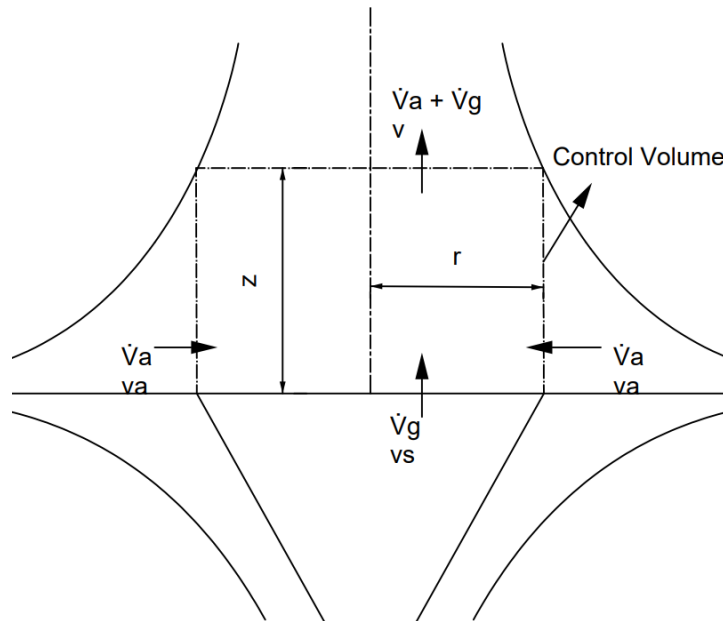


Figure 5.9: Flow model for a light gas plume, modified from [40]

6

Cases

Three cases are described in this section: the Rotvoll (validation) experiment, the full scale venting of methanol and the small scale methanol venting experiment.

6.1. Rotvoll experiment

The numerical models, described in Chapter 5, should have a solid basis. Therefore, first a model validation should be performed where the measured gas concentrations from a subsea gas release are compared to the predicted concentrations from the numerical model. This model will be afterwards adapted to the methanol venting experiment. In the past, multiple experiments of subsea gas releases have been carried out. Table 6.1 shows a summary of the relevant experiments described in the literature.

Table 6.1: Experiments of subsea gas releases [3]

| Experiments | Water depth [m] | Release rate [Nm ³ /s] |
|-----------------------------|-----------------|-----------------------------------|
| Topham (1956;1) | 23 | 0.06-0.65 |
| Topham (1956;2) | 60 | 0.30-0.40 |
| Kobus (1968) | 4.5-5 | 0.00013-0.0062 |
| Fannelop & Sjoen (1980) | 9.9 | 0.005-0.022 |
| Milgram & Van Houten (1982) | 4 | 0.00021-0.00023 |
| Milgram (1983) | 50 | 0.024-0.95 |
| Loes & Fannelop (1989) | 50 | 0.6 -1.3 |
| Rotvoll (1997) | 7 | 0.083 - 0.750 |

The following factors were considered to select the experiment: accuracy of the data, amount of available information, similar flow rate (of venting experiment) and similar depth (of venting experiment). Taking these into account, the Rotvoll experiment, carried out by SINTEF in 1997 (at the Statoil's Research center in Norway) [61], is chosen. This experiment is described in Section 3.2.3. Next to the flow rates, rise times, initial and maximum fountain height (see 3.1), they also measured the horizontal velocity profiles at 3 heights above the release point. Also, at the surface, the velocity profile of the outwelling flow was measured [49]. Additionally, they also measured gas concentrations at a height of 1m above the water surface, which is specifically interesting.

A summary of the most important parameters for the numerical models is given in the following table.

Table 6.2: Input parameters different CFD simulations for different cases

| | Rotvoll experiment | | Methanol venting | |
|------------------------------|--------------------|-----------------|-------------------|-------------------|
| | Below waterline | Above waterline | Small scale test | Full scale |
| Opening diameter (m) | 0.17 | 0.17 | 0.01 | 0.08 |
| Gas | Air | Methane | Methanol-Nitrogen | Methanol-Nitrogen |
| Density (kg/m ³) | 1.225 | 0.68 | 1.186 | 1.186 |
| Release rate (kg/s) | 0.10/0.20 | 0,068 | 0.005-0.0 | 0.32-0.25 |
| Duration (s) | 20 | 190 | 550 | 18 |

6.2. Methanol full scale venting

In this section, the venting case described in Section 4.4 is described (i.e. blockage of the vapour return line when bunkering). The input of the models described in Sections 5.1 and 5.2 are changed to the methanol venting case. First, the input, specific for the models in the case of venting of methanol due to overpressure in a bunker tank, should be calculated.

6.2.1. Release characteristic

The released mass consists out of 2 components: methanol and nitrogen. It should be noted that a good mixing is assumed between methanol and nitrogen. In reality this will probably not be the case (see Section 2.2.2.2). The Dortmund Data bank gives a relationship for the vapour pressure of methanol in function of the temperature. Following the ideal gas law and assuming a tank volume and temperature (see Table 6.3), the mass fraction of methanol and nitrogen can be determined. At 20°C, a tank with a volume of 100 m³ contains a mixture of 13% methanol and 87% nitrogen. This is consistent with the results of Equation 2.1 (11 vol% methanol). Note that the evaporation of methanol is very slow (see Section 2.1.2), consequently it takes time to reach this distribution between methanol and nitrogen.

A pressure relief valve is used to build up pressure in the bunker tank before relieving in order to overcome the hydrostatic back pressure. The pressure relief valve is connected to the sea by means of piping. The characteristics of the valve which relieves the pressure are chosen to be the same as in Figure 4.2. From the pressure drop between the opening and closing of the valve (ΔP), the release gas density (ρ) and average outflow speed (v); the friction coefficient K can be calculated by using Equation 6.1.

$$K = \frac{2\Delta P}{\rho v^2} \quad (6.1)$$

The density of the released gas is known after calculating the relief volume and relief mass. The relief volume is derived from the Boyle's law which state that for a constant temperature, the product of the pressure and volume is also constant. Consequently, the proportion of the volume of the tank and relief volume is the same as the proportion of the opening pressure and the atmospheric pressure. The relieved mass can be calculated by multiplying the molar mass of the mixture (derived from the mass fractions of methanol and nitrogen) by the number of relieved moles (derived from the ideal gas law).

The release speed can now be calculated using Equation 6.1 with the overpressure in the tank as ΔP . Multiplying this speed with the area of the valve gives the flow rate from which the mass release rate can be found. Table 6.3 shows the input of the calculations and Figures 6.1, 6.2 and 6.3 show the released mass, mass release rate and overpressure in the tank in function of time. Note that the closing pressure of the valve is reached after approx. 18s. After this time the pressure rises again until the opening pressure is reached and the release process is repeated. It should also be noted that the (mass) release rates are higher than the venting rate in case of a blocked vapour return line (described in Table 4.2, also taken into account the safety multiplication factor of 1.25). Consequently, there is no continuous venting. Figure 6.1 shows that little methanol is released. After the opening of the release valve, the mass release rate decreases (see Figure 6.2). The specifics of the venting case can be found in Appendix D. It is clear that the venting rate due to the use of this pressure relief valve is higher than the venting rates of all possible venting scenarios (described in Section 4.4).

Table 6.3: Input for the release of methanol-nitrogen mixture

| | |
|--|------|
| Tank volume [m ³] | 100 |
| Temperature [°C] | 20 |
| Relief pressure [kPa] | 14 |
| Closing pressure [kPa] | 9 |
| Diameter valve [m] | 0.08 |
| Flow rate at opening [m ³ /h] | 900 |

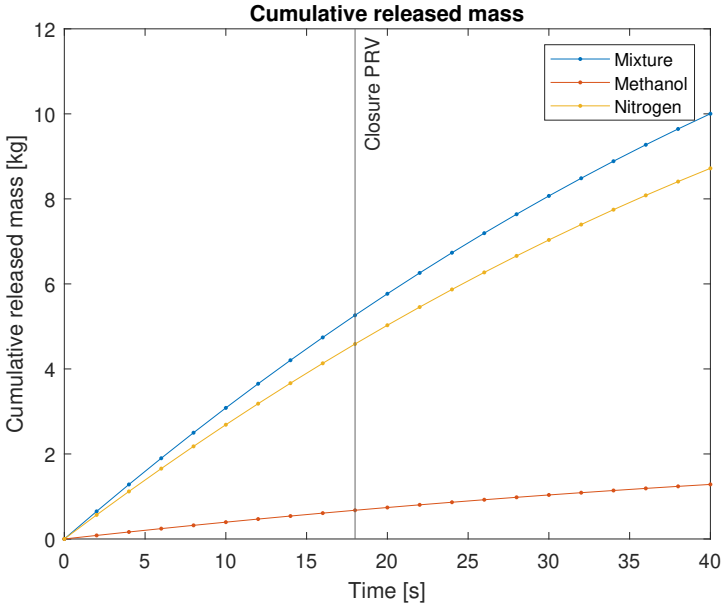


Figure 6.1: Cumulative released mass in function of time

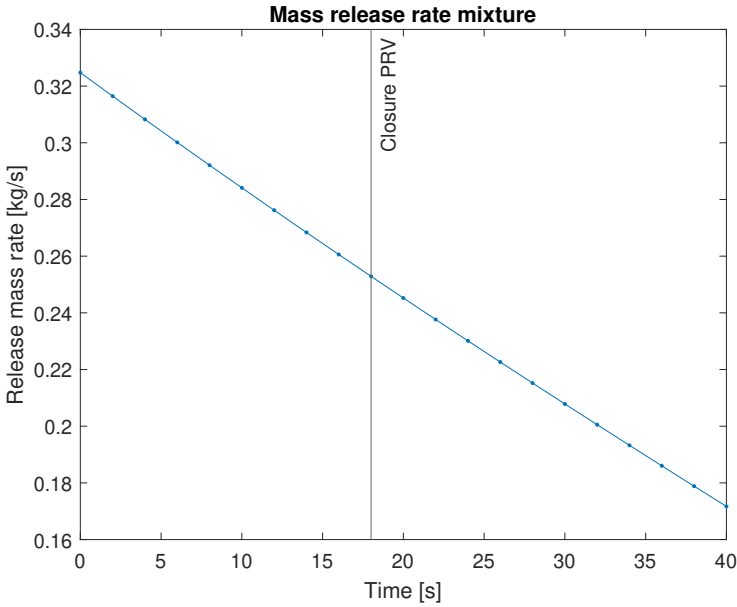


Figure 6.2: Mass release rate in function of time

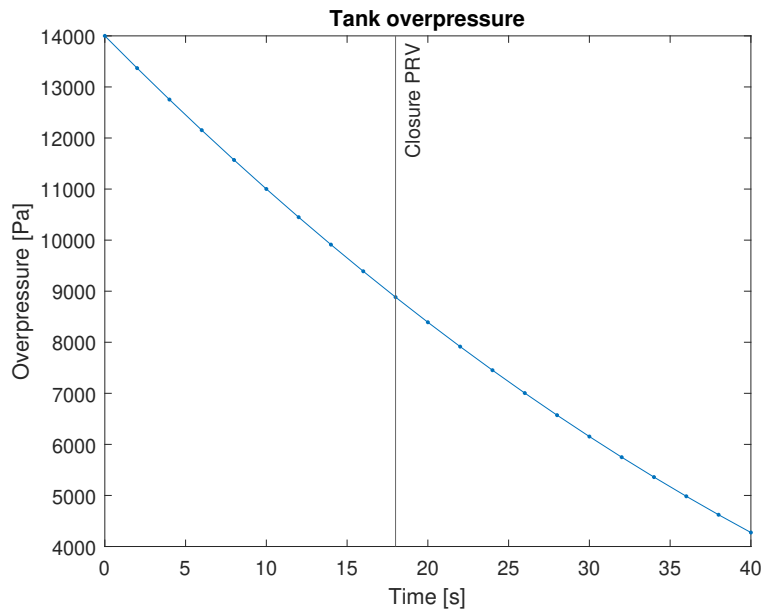


Figure 6.3: Overpressure in tank in function of time

6.2.2. Geometry

The geometry for the CFD model is based on Figure 4.1 where a bunker barge is laying next to a larger ship. Both the hull of the ship as the bunker barge are approximated by rectangular shapes. The methanol-nitrogen mixture enters the geometry at the ship's side 2m or 0.9m below the waterline. Figure 6.4 shows the used geometry in the CFD simulations. The air body is coloured grey and the water body blue.

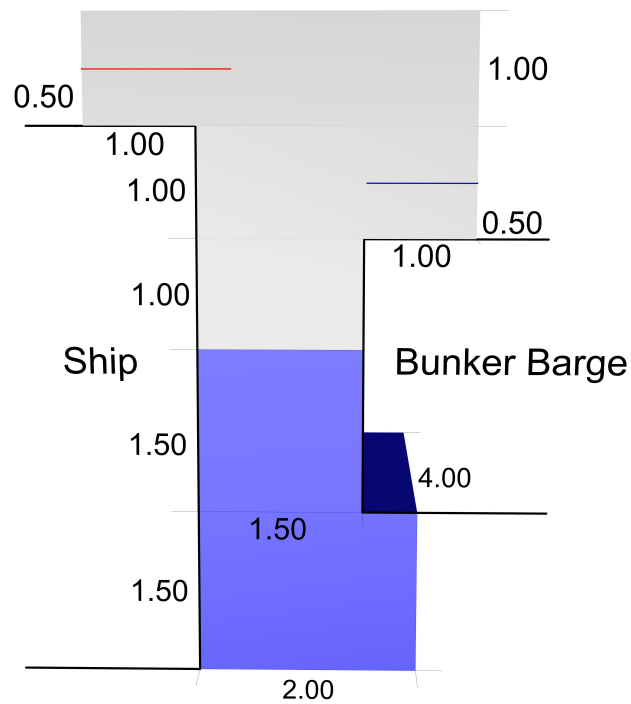


Figure 6.4: Geometry full scale methanol-nitrogen venting (blue:water, grey:air)

6.2.3. Mesh

Figure 6.5 shows the used mesh. The initial mesh consists out of 489257 cells with an average size of 4 cm. The mesh dependency is checked by the use of a refined mesh with half the grid size (974038 cells, size of 2 cm). Just like in the Rotvoll simulation, polyhedral cells are used for reasons described in Section 5.1.3. The different results generated by these meshes is shown in Figure 6.6. The results will be discussed in Section 7.2.1.2.

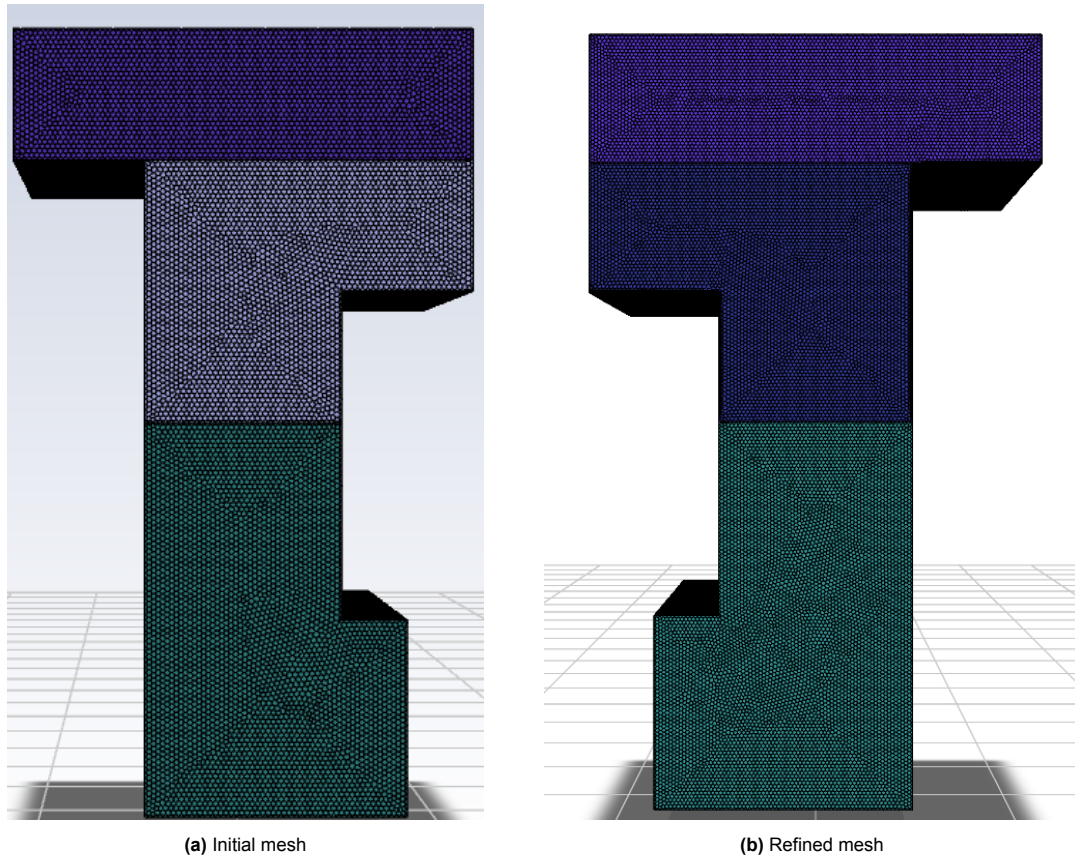


Figure 6.5: Used meshes

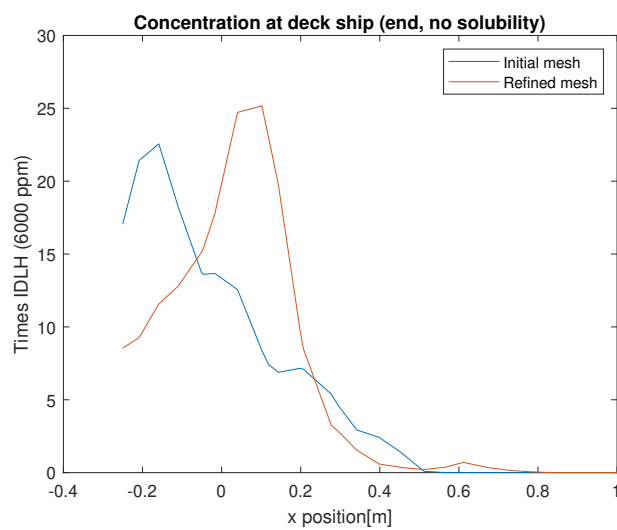


Figure 6.6: Mesh dependency

6.2.4. Boundary conditions

A careful selection of boundary conditions helps to ensure that the simulation results are physically meaningful. The boundaries (surfaces) of the geometry (see Figure 6.4) are described here. The surfaces of the ship and the bunker barge are set as walls. The interface between the water and air surface is an internal boundary type. The particles can leave the domain at the bottom surface of the geometry, below the (keel of the) bunker barge, 2m to the aft or front of the release point, above the deck of the bunker barge and above the deck of the ship. These surfaces below the waterline are walls but with the DPM escape setting and the surfaces above the waterline are pressure outlets.

6.2.5. Gas dissolution

The solubility of gas in water plays an important role in the gas dissolution. The solubility of gases in water can be calculated by Henry's law:

$$C = k \cdot P_g \quad (6.2)$$

Where C is the solubility, k the Henry's law constant and P_g is the vapour pressure of the gas. In reality k is temperature dependent, but this effect is neglected in this research because the temperature differences are small. The vapour pressures and Henry's law constants [11] are shown in Table 6.4. The solubility of methanol in water is approximately 50.000 times larger than nitrogen. The solubility of methanol can be explained by the polar OH-group which is attracted by water which is also polar. The carbon is non-polar and is repelled by water. The longer the carbon chain (ethanol, butanol etc.), the more dominant the carbon chain will be over the OH-group. Consequently, the substance will be less soluble.

Table 6.4: Solubility methanol-nitrogen mixture (at 20°C)

| | Methanol | Nitrogen |
|---|----------|----------|
| Henry's law constant (k) [mol/kg.bar] | 220 | 0.0006 |
| Vapour pressure (P_g) [Pa] | 14799 | 100527 |
| Solubility (C) [mol _{gas} / mol _{water}] | 0.5868 | 0.000011 |

Next to the solubility, also the surface tension is different in the methanol case. The surface tension of a methanol-water mixture is 0.022 N/m compared to 0.072 N/m for air and 0.062 N/m for methane. A lower surface tension leads to a lower bubble equilibrium diameter (see Equation 5.10, also shown by [34]). Physically a lower surface tension can be interpreted as a lower resistance against compressive force from the fluid and consequently a smaller bubble size. Both the lower surface tension and the higher solubility will result in a higher gas dissolution and less surfacing of methanol gas compared to methane.

6.3. Methanol small scale venting

In order to investigate the possible dangers of methanol venting, a small scale test is planned to be executed. This test is also used as an extra validation for the CFD model.

6.3.1. Release characteristic

Ideally, the full scale venting resulting from an overpressure in a bunker tank is reproduced exactly in an experiment. However, this requires open conditions which makes the measurements of gas concentrations difficult. Therefore, a small scale experiment is drawn up. A closed tank with a volume of 1 m³ will be filled with 0.9 kg methanol. A pressure relief valve, which is fitted on the tank, will open after reaching 30 kPa overpressure. Nitrogen is inserted into the tank to reach this pressure. The pressure relief valve is connected to an open water tank (1.5x0.6x0.6m) with a tube of 10mm. The tank will be completely filled with fresh water and the gas will be injected 0.4m below the water surface. Similarly to Section 6.2.1, the graphs for mass release rate and overpressure can be drawn up. Instead of 20°C, the temperature in the experiment is 40°C. Due to the larger vapour pressure of methanol at higher temperatures, there is a larger fraction methanol (35% compared to 13%) in the mixture which makes the measurements easier.

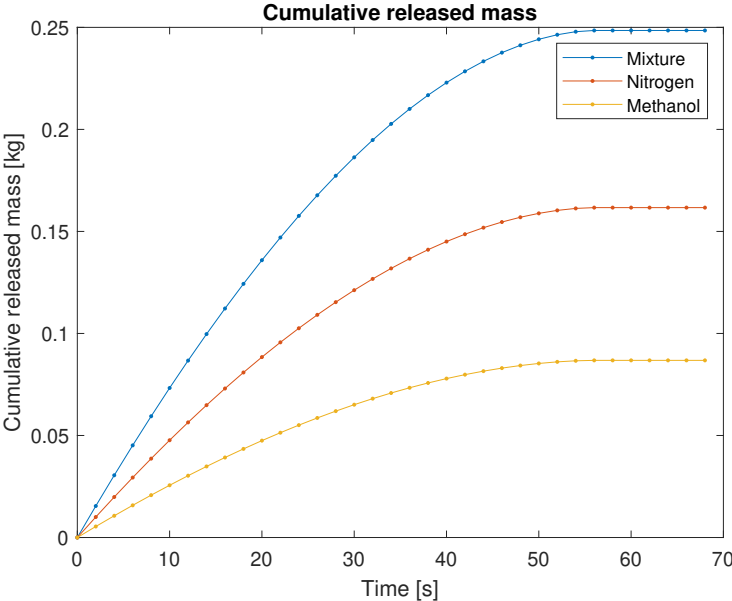


Figure 6.7: Cumulative released mass in function of time

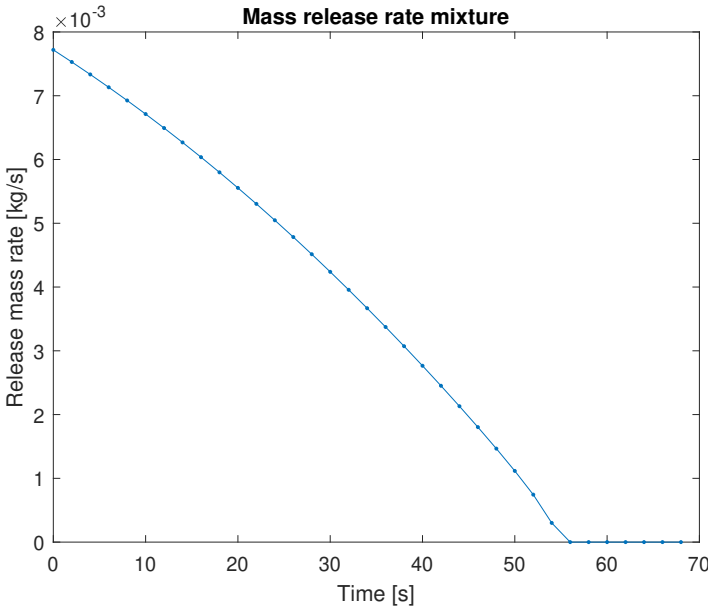


Figure 6.8: Mass release rate in function of time

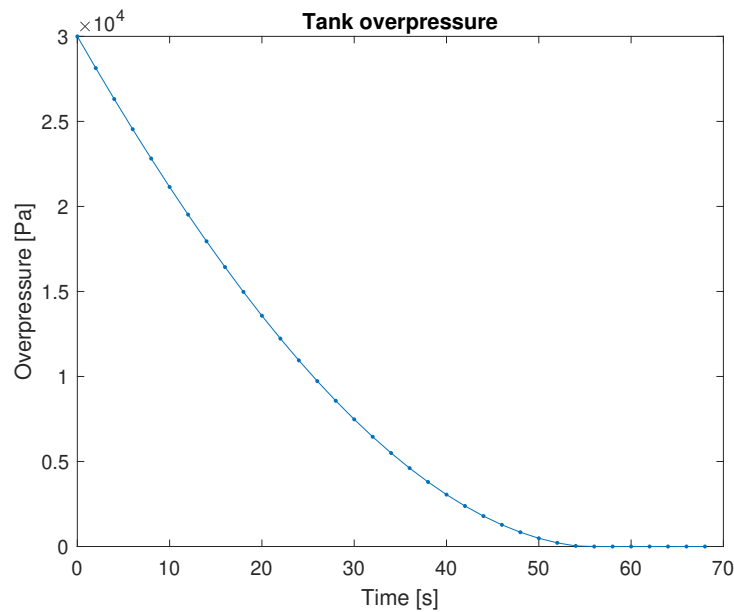


Figure 6.9: Overpressure in tank in function of time

6.3.2. Geometry

Just like the Rotvoll experiment, the geometry consists out of a water body and an air body. The dimensions of the water body are equal to that of the aquarium, 0.6x0.6x1.5m. An air body is placed on top of the water body but also around it. This is done to account for the air flow around the basin, when the released gas disperses. The water and air body are divided in multiple parts in order to give these a different mesh size. Figure 6.10 shows a cross-section of the geometry.

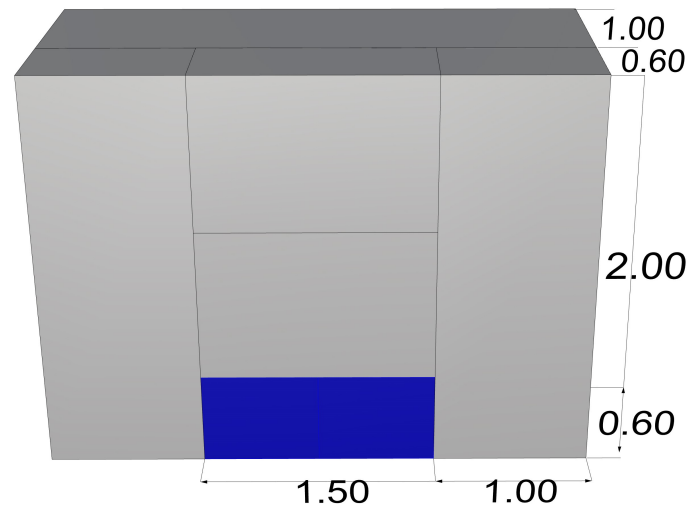


Figure 6.10: Geometry small scale methanol venting test (blue:water, grey:air)

6.3.3. Mesh

Not all regions are equally important in the mesh. Therefore, a regional refinement is chosen. Figure 6.12 shows the used mesh for the CFD simulation. A cylindrical regional refinement around the water tank is performed. Some of the gas is expected to drop next to the tank, so a margin around the tank is chosen. The mesh has a total of 461174 cells.

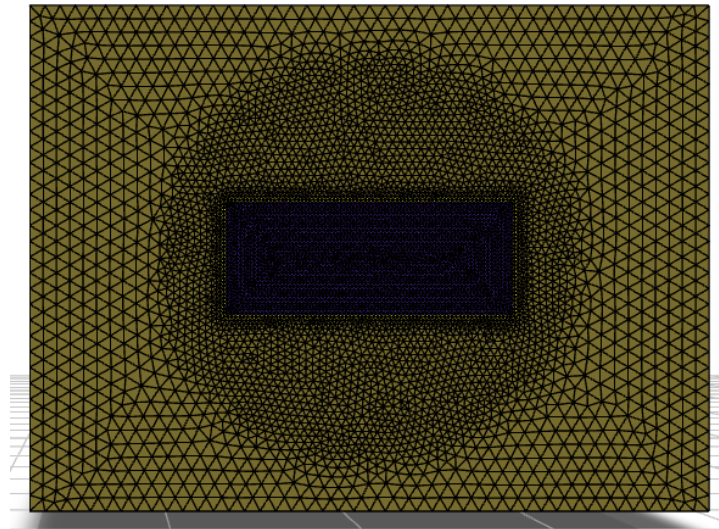


Figure 6.11: Mesh small scale methanol venting test

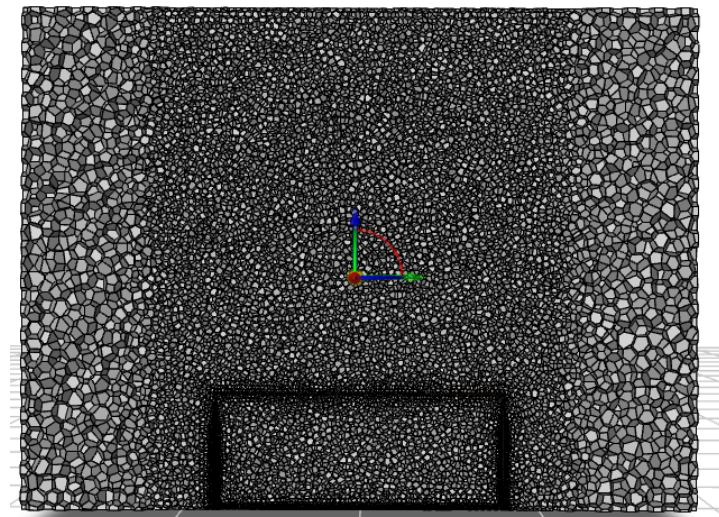


Figure 6.12: Mesh small scale methanol venting test

6.3.4. Boundary conditions

The boundary conditions are set in such a way that the model represents an aquarium with an air body around it. The boundaries between the water bodies are set as internal such that the DPM particles can pass. The boundaries between the water and the air surrounding it are set as walls, except for the water-air interface on top which is also an internal boundary. Finally, all the outer boundaries of the mesh are set as pressure outlet (except the bottom) such that the particles can leave the simulation.

7

Results

In this chapter the results of the CFD and integral model are discussed, for each of the three cases.

7.1. Rotvoll experiment

In this section the results from the Rotvoll experiment (taken from [61]) are compared to results from the integral model and the CFD model. The comparison between the 2 models and the experiment is divided in a section below the waterline (which compares velocity and void fraction profiles) and a section above the waterline (which compares gas concentration profiles). Figure 7.1 shows the developed plume for the release of air at 0.20 kg/s (from the CFD model). A conical shape can be seen, which was also noticed in the experiment and predicted by the integral model. The residence time (time particle stays at a specific location) is represented by the colour. It ranges from blue (short residence time, 0.02s) to red (large residence time, 15s).

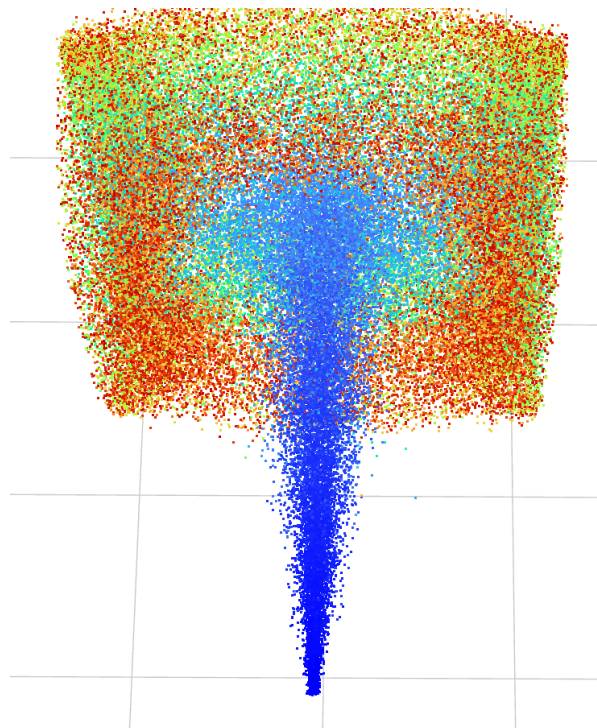


Figure 7.1: Particle tracks of Rotvoll experiment (0.20 kg/s release rate), seen from below

7.1.1. Below the waterline

Figure 7.2 shows the velocity at the centerline in function of the height, where 0 is the bottom of the basin and 7m is at the water surface. At low heights there is a large difference between the CFD model and the integral model. This is due to zero initial velocity, which is not taken into account in the integral model. After the release, the velocity increases due to the buoyancy and afterwards it decreases due to the drag force. The integral model shows a larger discrepancy near the surface due to the radial movement of the water. This can be explained due to lacking surface interaction in the model. When the gas reaches the surface there is an increasing number of turbulent eddies, leading to an erroneous velocity profile close to the surface. Both the CFD and the integral deviate more from the experiments in the case with a release rate of 0.10 kg/s. This is mainly due to the use of parameters (see 3.2.2) which are fitted to the 0.20 kg/s release rate case. The underestimation of the velocity in the CFD model is probably due to incorrect initial bubble size. When a larger bubble is injected, the buoyancy is larger and consequently also the velocity.

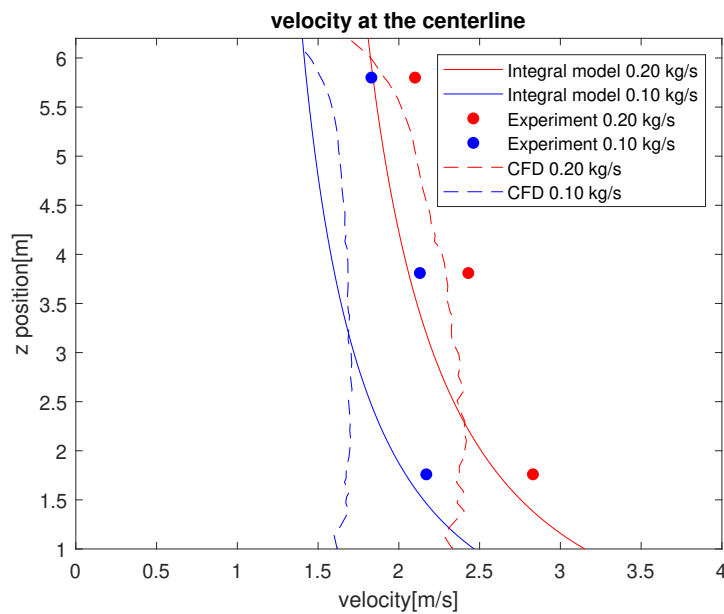


Figure 7.2: Comparison velocity at centerline between the Rotvoll experiment and integral model

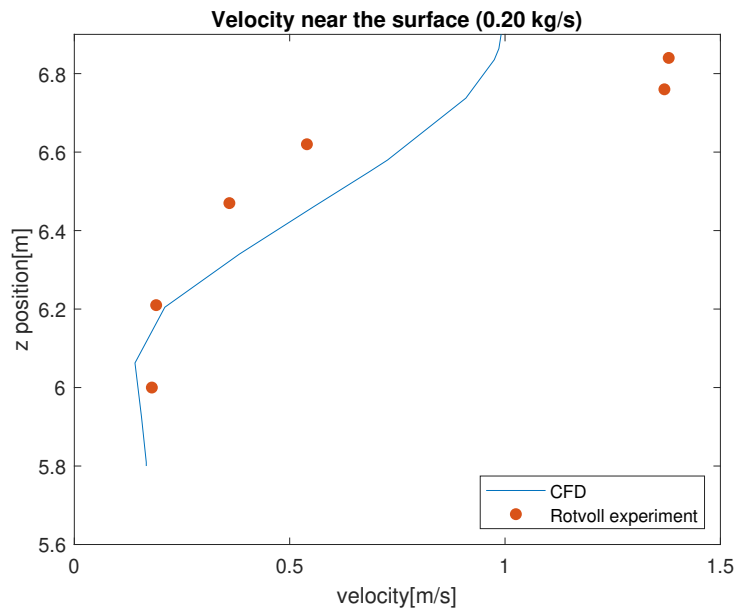


Figure 7.3: Comparison velocity magnitude of water between the Rotvoll experiment and integral model near the surface, 1.75m from the centerline

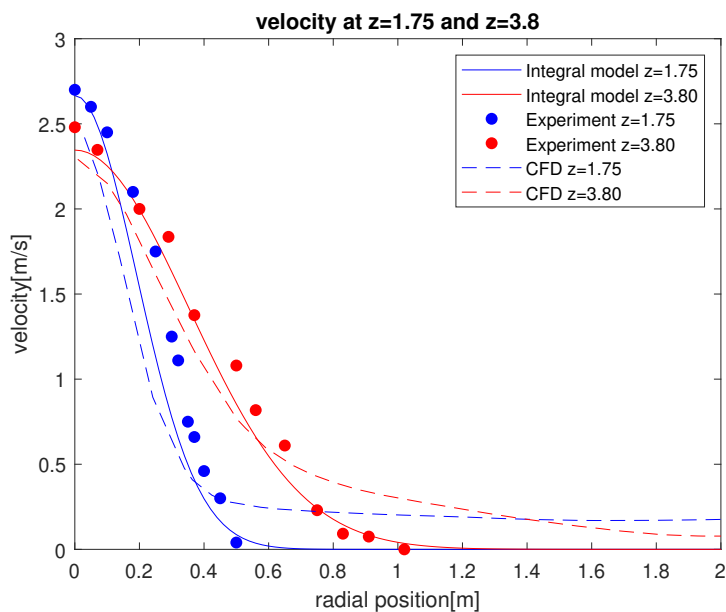


Figure 7.4: Comparison velocity in function of radial position between the Rotvoll experiment and integral model for a release rate of 0.20 kg/s

Figure 7.4 shows the velocity in function of the radial position at 2 different heights. The velocity decreases from the centerline to the sides due to the lower buoyancy. Both the integral and CFD model show good agreement with the experimental results. Closer to the surface, the velocity away from the centerline deviate more from the experiments. This is due to the use of a mono-directional velocity meter in the Rotvoll experiment. When approaching the surface, the flow becomes dominantly a radial flow. This can be seen in Figure 5.3. Very close to the surface, this also happens at the centerline, as can be seen in Figure 7.3. The standard $k-\epsilon$ model does not account sufficiently for turbulence damping near the water surface. An explanation can be found in the fluent theory guide. The standard $k-\epsilon$ model assumes a isotropic grid turbulence, which means it properties are equal in all directions. However,

in reality there is a higher radial turbulence relative to axial turbulence near the free surface [8]. This leads to errors in the representation of the plume near the surface in the CFD simulation. The results of the models can be compared to the experimental results with the RMSE (root-mean-square error). The RMSE is the square root of the average of squared errors, where the error is defined as the difference between the experimental and numerical result. The average of the RMSE (for $z=1.75$ and 3.80) for the integral model is 0.17 compared to 0.24 for the CFD model. This is caused by the discrepancy of the CFD far away of the centerline and can be explained by the use of the vertical velocity measurements in the experiment compared to the multi-directional velocity magnitude in the CFD. Further away from the centerline, the vertical velocity diminishes to zero but there is still some velocity in the x- and y-direction.

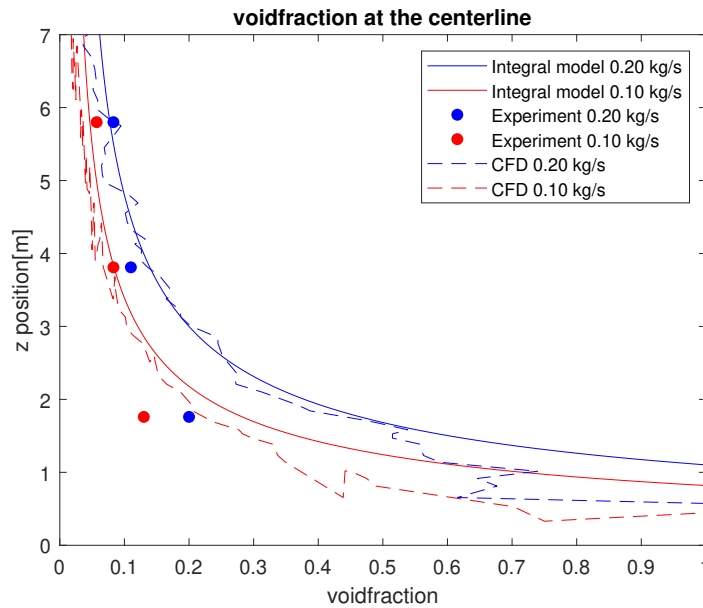


Figure 7.5: Voidfraction comparison between Rotvoll experiment and integral model

Figure 7.5 shows the void fraction at the centerline in function of the height for the experiment, integral model and CFD model. Due to the widening of the plume at increasing heights, the void fraction decreases when nearing the water surface. At small depths, the models seem to predict the void fraction well. The Gaussian distribution in the integral model seems to be a good approximation. In the CFD model, the DPM (Discrete Phase Model) is used. The fluent manual specifies that the DPM gives accurate results when the volume fraction of the discrete phase (injected gas) in the continuous phase (water or air) is low (less than 10%). This is in order to be able to neglect the interaction of the discrete particles on each other. The CFD results seem to show some spikes around a general trend. The curve represent the void fraction at a single cell for each z value of the centerline. These variations could be smoothed by averaging the void fraction at positions close around the centerline. An alternative could be the use of a coarser mesh. The use of a structured mesh with the same cell size as the unstructured mesh would not reduce these variations.

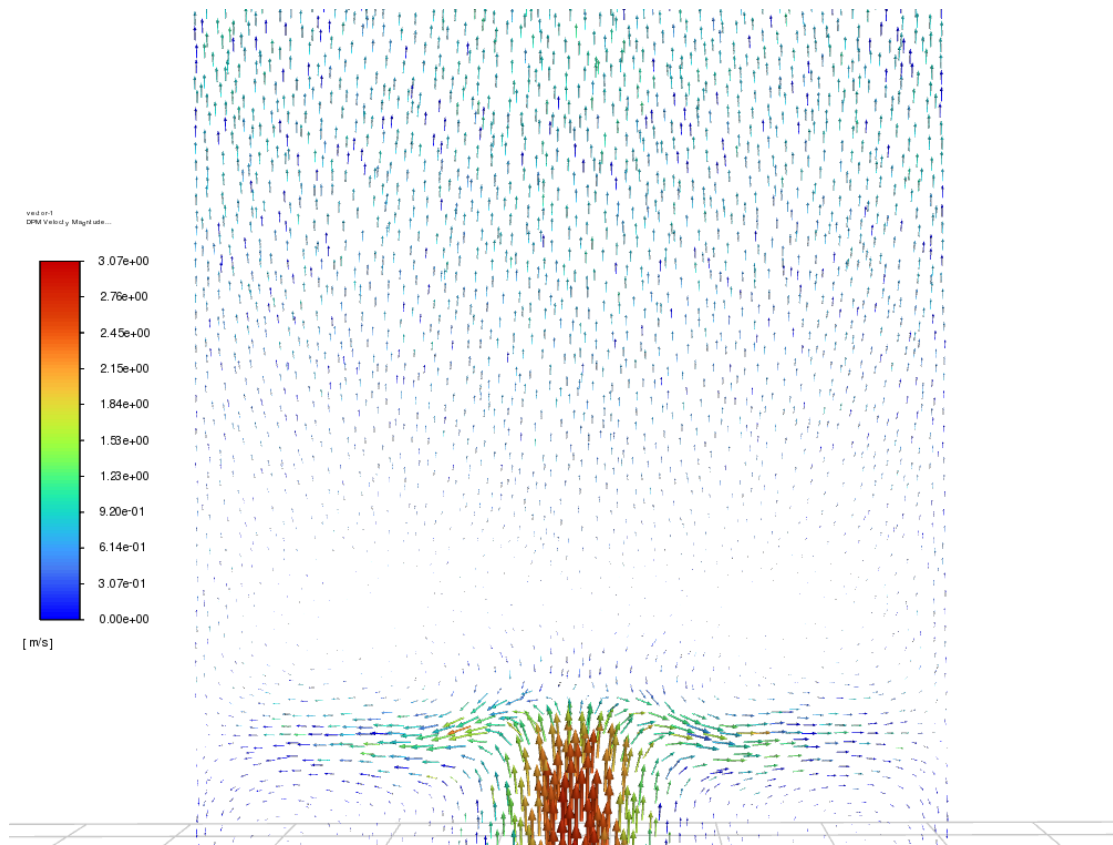


Figure 7.6: Velocity vector representation (from waterline upwards) of Rotvoll experiment

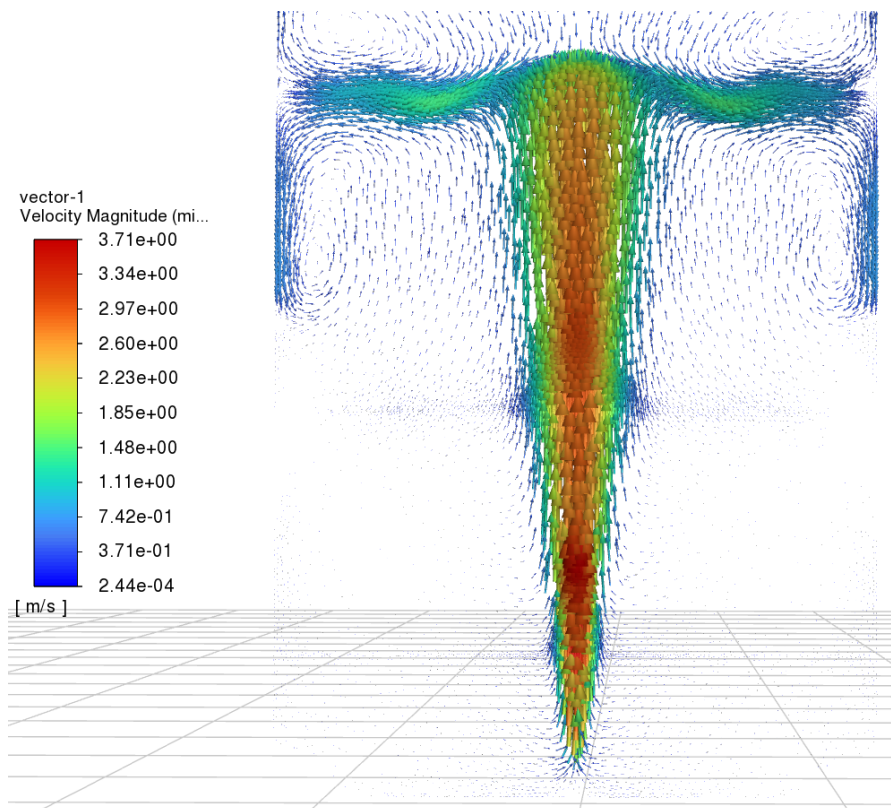


Figure 7.7: Velocity vector representation (from waterline downwards) of Rotvoll experiment

7.1.2. Above the waterline

7.1.2.1. Integral model

From the Rotvoll experiment only an average concentration measurement can be used for validation of the part above the waterline. This is due to the concentration measurements at locations further away from the centerline showed interference with the walls of the basin. A comparison for the concentration measurements of the Rotvoll experiment and the average concentration predictions of the integral model is shown in Table 7.1. In this experiment a helium-air mixture with the density of methane gas was released at 0.068 kg/s.

In order to have a broader validation base, results of the integral model are also compared against concentration measurements from an experiment in which methane gas was released at 50m water depth. Figure 7.8 shows the comparison between the average concentrations measured from the experiment [40] and the integral model. It should be noted that instantaneous concentrations measurements were taken at 0.5m above the water surface. These measurements seem to correspond well to average concentrations within a control volume with z (see Equation 5.24 and Figure 5.9) equal to half the radius of the plume at the surface. This z -value is derived from a mass balance over the control volume. Due to the large buoyancy of the methane gas, the largest concentration is found directly above the water surface. The concentration gradient changes rapidly above the surface but at heights of 0.5m or more above the waterline the concentrations change less fast. Therefore average concentrations predictions from the integral model match well with instantaneous measurements at these heights.

Table 7.1: Comparison concentration measurements Rotvoll experiment and integral model at 1m above the water surface

| Release rate [kg/s] | Measurement experiment [vol%] | Prediction model [vol%] |
|---------------------|-------------------------------|-------------------------|
| 0.06 | 1.8 | 1,92 |
| 0.03 | 1.65 | 1.22 |

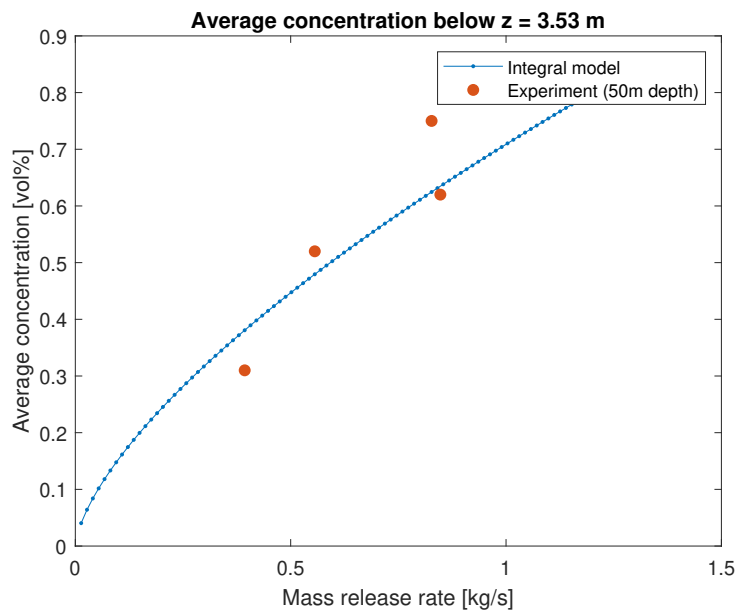


Figure 7.8: Comparison average concentrations from integral model and experiment (50m depth)

7.1.2.2. CFD model

Figure 7.9 shows a comparison between the gas concentration measurements in the Rotvoll experiment and the results from the CFD simulation with and without the solubility taken into account (time-averaged over 180s). The gas dissolution is taken into account by the user defined function shown in Appendix C. The highest concentration is not measured directly above the release point (at the center

of the plume) but at 1m away from the center. This is just outside of the fountain region (where the water is pushed upwards) which can be seen in Figure 7.6 and in the experiment [61]. In the experiment an intense boil region is seen at 1m radial position where large amount of gas escaped the water surface [61]. The gas concentrations decrease to the side and increase again at the end due to accumulation at the side walls of the basin. There seems to be an instability of the plume at the water surface. Due to the lower release rate (0.07 compared to 0.20 kg/s) the underwater gas plume is more affected by water currents. Water rises along the gas plume and flows subsequently to the side walls. Afterwards, it flows down and interacts with the plume again. This vortex pushes the plume slightly to the left, which can be seen in Figure 7.12.

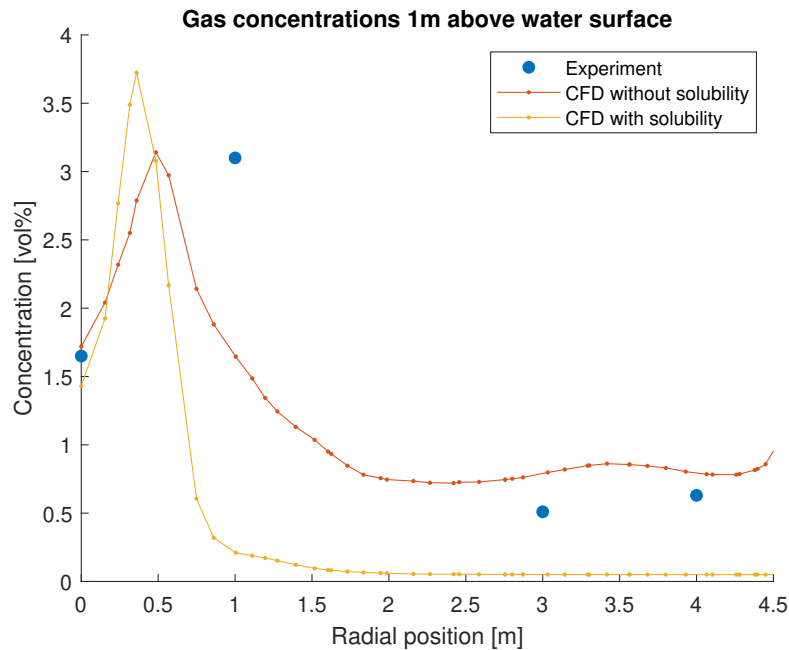


Figure 7.9: Comparison methane concentrations between the experiment and CFD for 1m above the water surface (resulting from UDF, without alteration)

There seems to be an overestimation of gas dissolution of bubbles further away from the centerline. Due to the radial flow below the waterline these bubbles have a longer residence time in the water. As seen in Figure 7.3, the velocity near the surface is underpredicted in the CFD model, which adds to the residence time. Consequently they are more likely to dissolve in the surrounding water. A reduction factor in the mass transfer from the gas to the water could be used to avoid this discrepancy. An alternative method to take the gas dissolution into account is used in Figure 7.10. The void fraction at a location below the appearance of the radial flow is compared for the case with and without gas dissolution. This location is taken at 1m below the water surface (6m above the bottom). Here, the velocity predicted by the CFD model is in good correspondence with the experiments. A surface integral for the whole plume going through $z=6\text{m}$ is taken for both cases (with and without gas dissolution). In this way the difference in mass rates, which passes through this surface, can be compared and is defined as the gas which is dissolved in the surrounding water. A gas dissolution of 6.5% is concluded from the model. This means that 93.5% of the released gas reaches the water surface. This is somewhat higher than expected but can be explained by the low release rate leading to a large rise time and consequently more gas dissolution. A possible error can be the neglect of the saturation of the surrounding water causing a higher dissolution rate. Additionally erroneous surface tension, solubility and diffusion coefficients could lead to the higher dissolution rates.

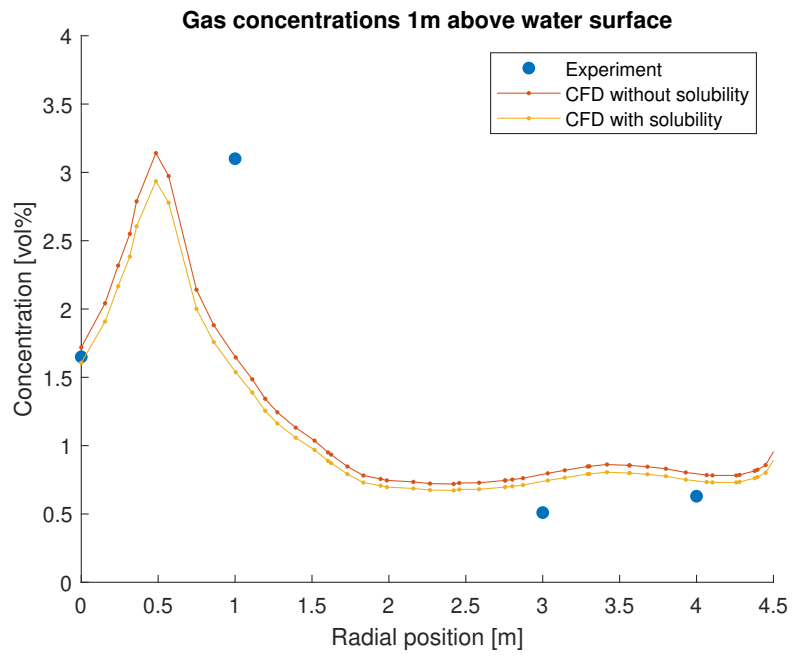


Figure 7.10: Comparison methane concentrations between the experiment and CFD for 1m above the water surface (with alteration: surfacing gas reduction)

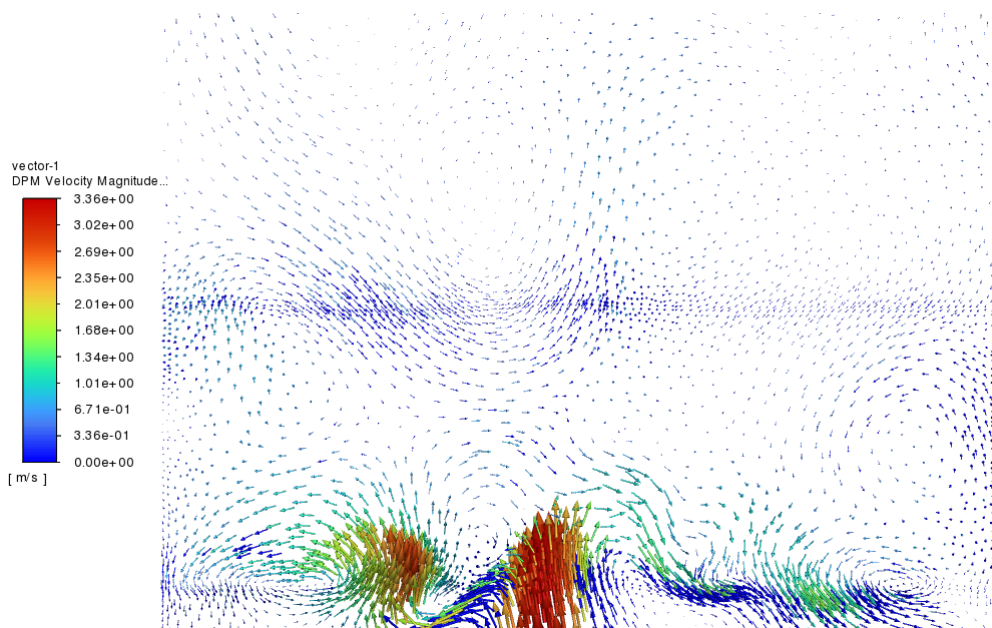


Figure 7.11: Velocity vectors Rotvoll experiment (above waterline)

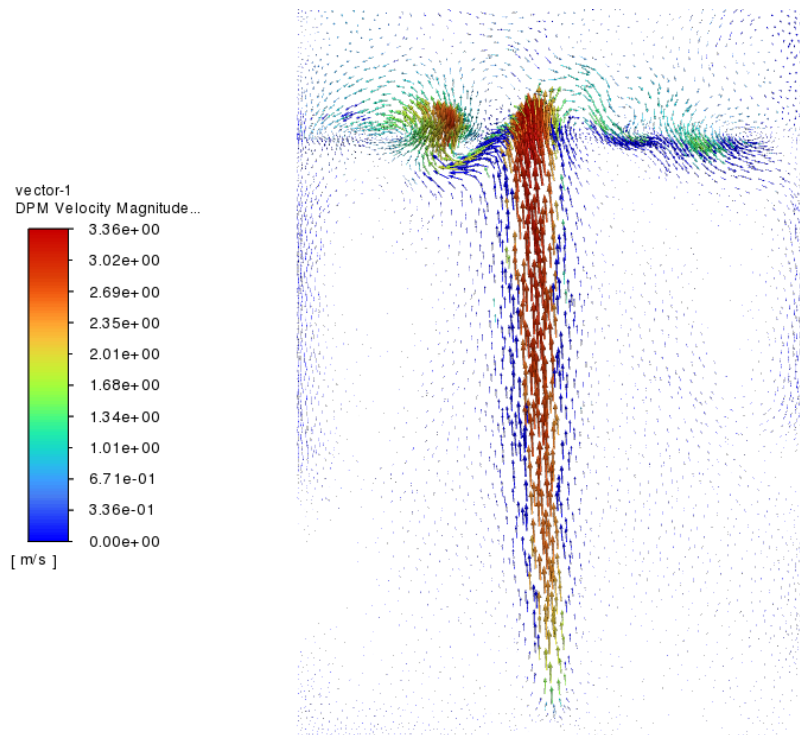


Figure 7.12: Velocity vectors Rotvoll experiment (below waterline)

7.2. Methanol full scale venting

In this section, the results of the integral and CFD model are shown for the case described in Section 6.2. This case is subdivided by the venting depth: 2.0m and 0.9m.

7.2.1. Venting depth: 2m

Firstly, the methanol concentrations above the waterline are investigated from a subsea gas release at a depth of 2m.

7.2.1.1. Integral model

The integral model from the Rotvoll experiment is adjusted to the methanol venting case. Here, the release rate is assumed to be constant and equal to the release rate at the start. This will give an error on the safe side. In reality the mass release rate will decrease over time (see Figure 6.2), consequently the surfacing mass flux and the gas concentration above the waterline are overestimated. Table 7.2 shows the input which is used for this model. Figures 7.13, 7.14 and 7.15 show the results. The results for methanol are taken as a constant fraction (0.13 for 20°C) of the result of the mixture. Due to the shallow release, a large fraction of the surfacing gas is concentrated close to the centerline. The integral model does not take into account the dissolution of methanol, consequently there is a considerable concentration of methanol (3% at 1m) above the waterline.

Table 7.2: Input for the integral model: release of methanol-nitrogen mixture

| | |
|----------------------------------|-------|
| Release rate [kg/s] | 0.32 |
| Gas density [kg/s] | 1.186 |
| Release depth (h) [m] | 2 |
| Diameter release opening (d) [m] | 0.08 |

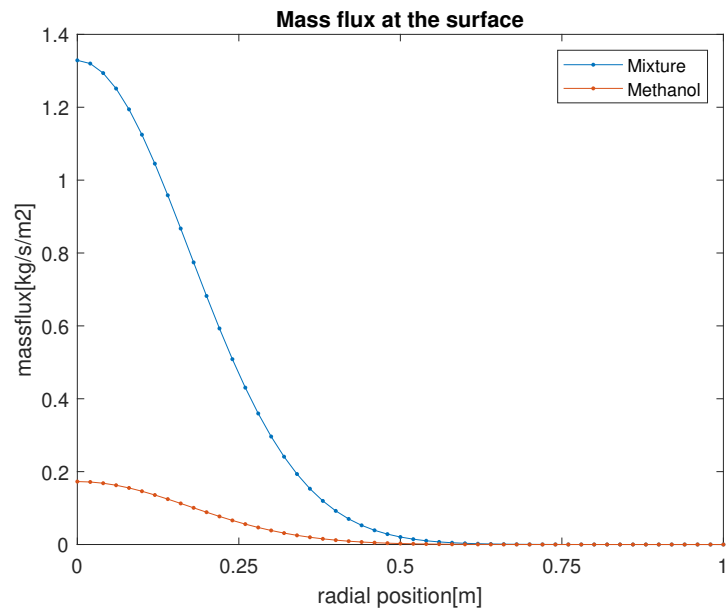


Figure 7.13: Mass flux of nitrogen-methanol mixture and methanol at the surface

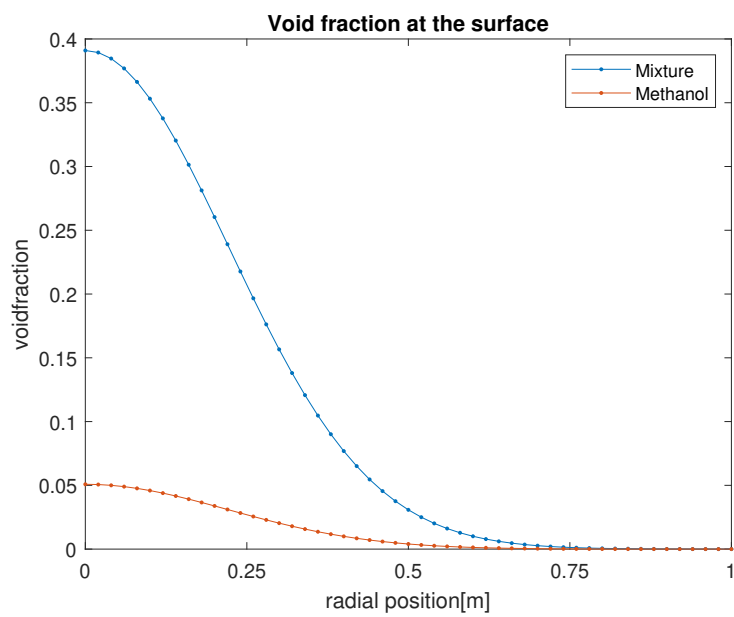


Figure 7.14: Void fraction of nitrogen-methanol mixture and methanol at the surface

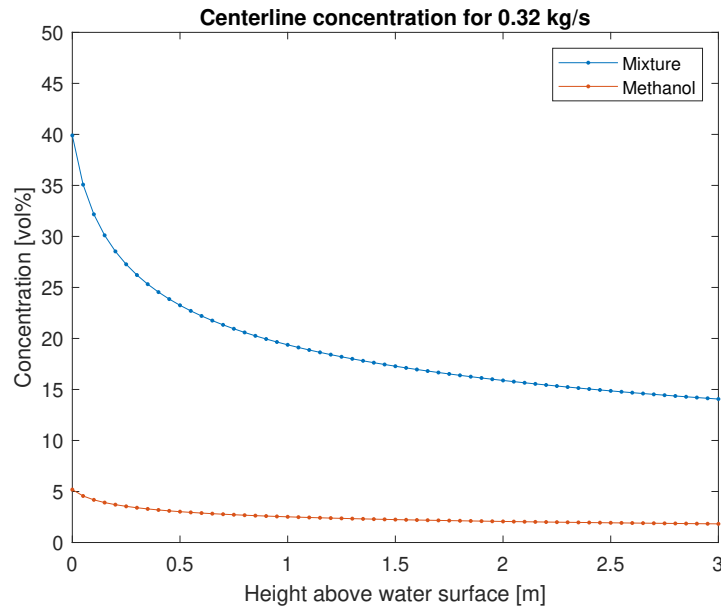


Figure 7.15: Centerline concentration of nitrogen-methanol mixture and methanol

The most plausible causes for errors in the results of the integral model are

- The empirical coefficients (α , λ , γ and u_s , see 3.2.2) are the same as in the Rotvoll experiment. They will be different for the methanol venting case, causing consequently different results. As there are no experimental measurements for the methanol venting case, it is hard to quantify these errors. For this reason, the influence of each parameter on the resulting methanol concentration is investigated. When α , λ , γ and u_s change 10%, the results changes respectively 16.7%, 1.4%, 1.8% and 1.8%. The angle under which the gas enters the water, α , clearly has a large influence. This is mainly due to its large impact on the radius of the surfacing gas. When the venting depth becomes larger, the influence of this parameter on the result increases.
- The real radius of the plume at the water surface is expected to be larger than the radius predicted by the Friedl model. Just like in the Rotvoll validation, a factor 1.3 is used (see Section 5.2). Similarly to α , this parameter has a large impact on the result. The methanol concentration will change with 12.9% when this parameter changes 10%.
- In the integral model, the gas is released from a point source. In reality the release source will have a certain diameter. This is accounted for in the integral model by changing the release depth to

$$h + \frac{d}{\alpha} \quad (7.1)$$

Where h is the initial release depth, d is the diameter of the opening and α is the angle under which the gas is released. An approximation is used in this formula where the tangent of a small angle is equal to the angle itself.

7.2.1.2. CFD model

In this section resulting concentrations from a subsea venting event are investigated both with and without the gas dissolution of methanol taken into account.

Without dissolution

A big difference to the Rotvoll experiment is the release depth. In the beginning, due to the very shallow depth, the released gas is not able to drag (lot of) water with it. Consequently, the radial movement close to the water surface is very limited and the gas escapes the surfaces almost vertically. After some time (approx. 5s) the underwater plume becomes more developed, the water starts to move and the radial movement just below the surface appears. The gas above the surface gets dragged towards the barge. That is the reason that the concentration at the deck of the barge is higher at the end of the

simulation compared to the time average.

Figure 7.16 shows the concentration at the end of the simulation 0.5m above the deck of the ship and 0.5m above the deck of the barge. Figure 7.17 shows the time-averaged concentrations at the same locations of the previous figure. The zero position (or centerline, see Figure 7.15) is straight above the injection point. The position increases (positively) towards the center of the ship. The position -1.5 is at the hull of the barge. the position decreases (negatively) towards the center of the barge. The blue and red line in Figure 7.16 represent the concentration at the location of the blue and red line in Figure 6.4. The concentrations are expressed as a multiplication factor of the IDLH-limit. The IDLH (immediately dangerous to life or health) value for methanol of 6,000 parts per million (ppm) is determined by the National Institute for Occupational Safety and Health (US) and is based on available data on the acute toxicity of methanol. The IDLH is considered the potential for immediate life-threatening effects on workers exposed to high levels of the substance.

The integral model can be compared with the CFD model by looking at the centerline concentration at 2.5m above the waterline from Figure 7.15. The resulting concentration (3 vol% or 5 times the IDLH) is an underestimation compared to 20 times the IDLH which is found in Figure 7.17.

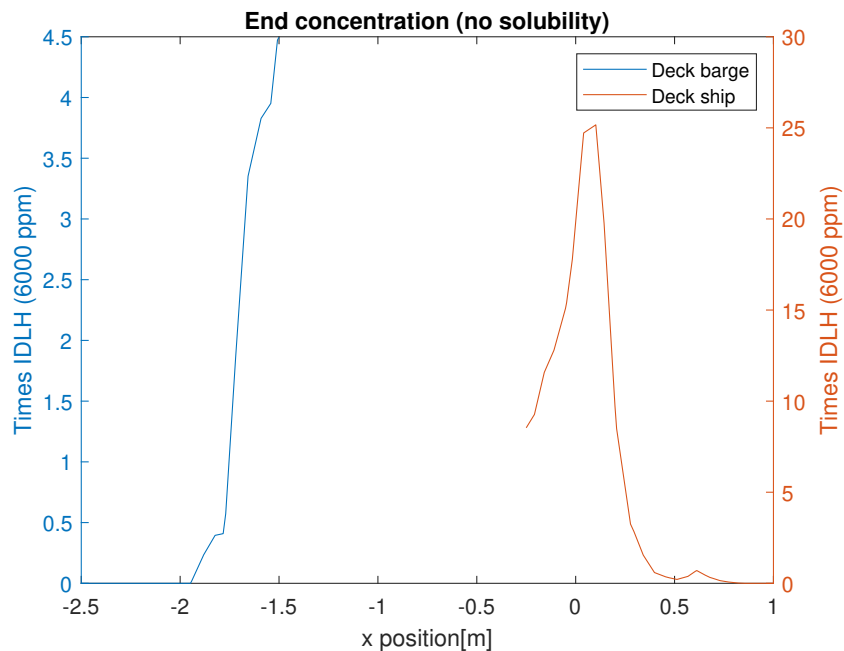


Figure 7.16: Methanol concentration at the end of the venting process, described in function of the safety threshold IDLH (Immediately Dangerous to Life or Health)

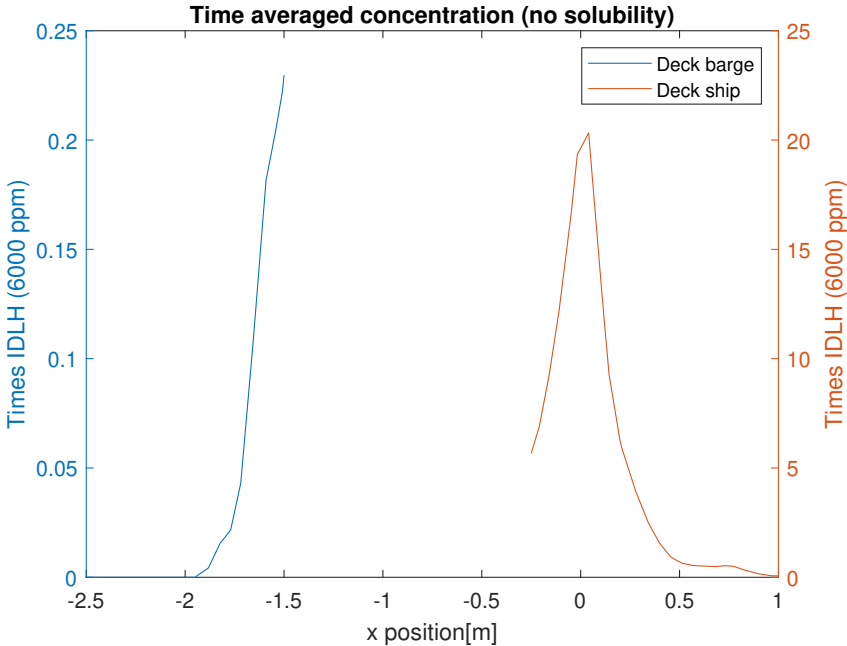


Figure 7.17: Time-averaged methanol concentration during venting

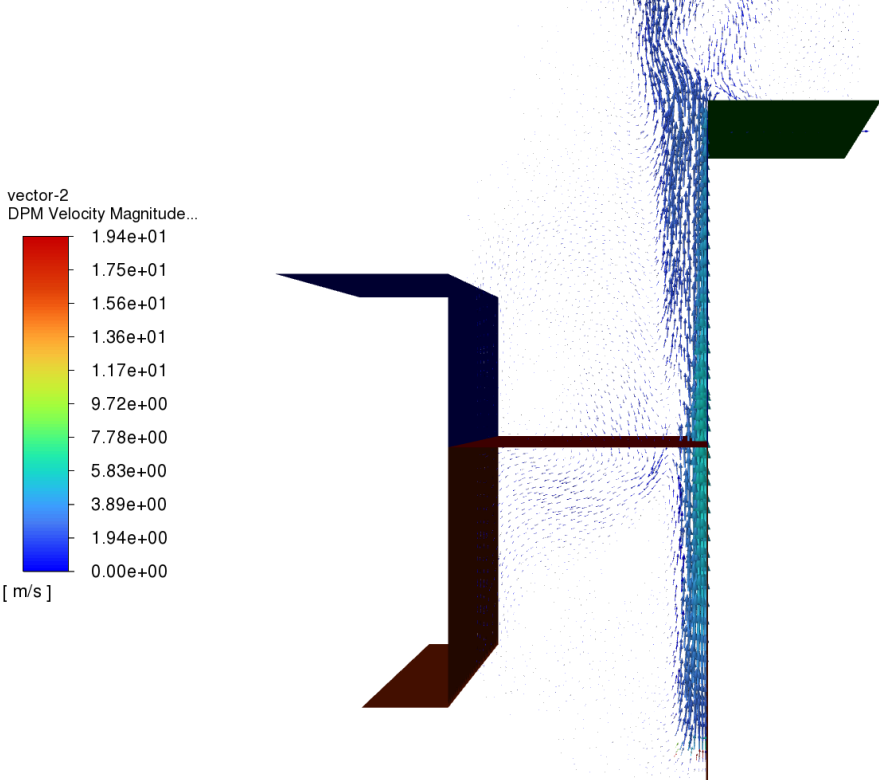


Figure 7.18: Velocity vectors during venting

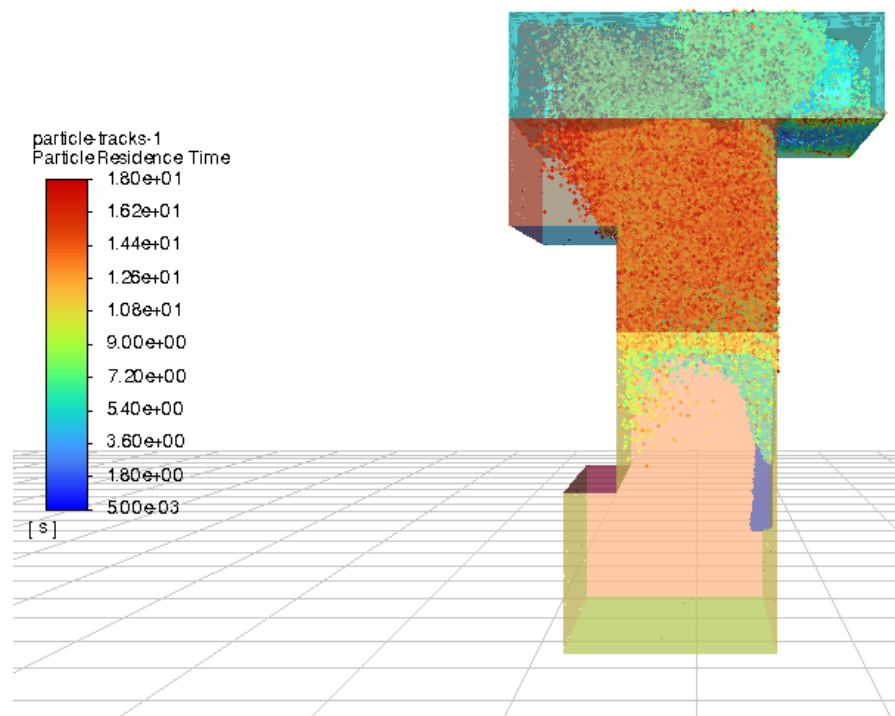


Figure 7.19: Mixture (methanol-nitrogen) vapour particles at end of venting

With dissolution

Figure 7.20 shows the particle tracks of methanol vapour at the end of a gas injection. The injection is chosen to have a duration of 18s with a release rate of 0.30 kg/s which is very conservative compared to Figure 6.2. The released vapour consists out of 100% methanol, which is an overestimation except when the bunker tank it is almost completely filled. There is a complete dissolution of the methanol in the surrounding water. Due to this gas dissolution, the methanol is not able to rise to the surface. As previously stated, the saturation of gas in the surrounding water is not taken into account. If this were the case, more methanol would be able to rise. It is still not expected that any methanol will be able to reach the water surface. Due to currents and waves, new/under saturated water will be supplied leading to a constant mass transfer of methanol vapour to the water. Figure 7.20 only shows methanol. If the released vapour would consist out of a mixture of methanol and nitrogen, there will still be nitrogen vapour above the water surface. Due to its low solubility, the gas dissolution of nitrogen is not taken into account.

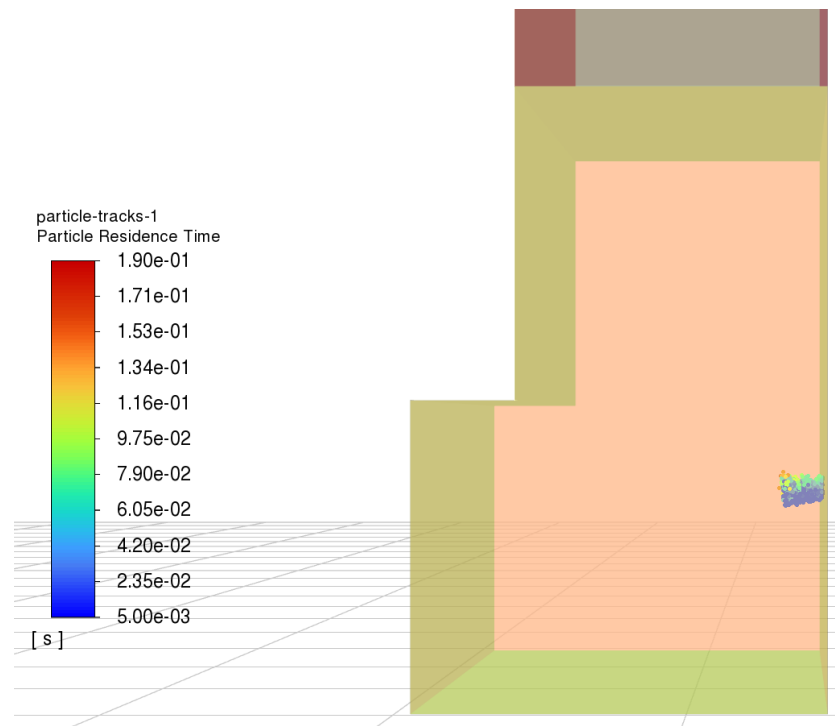


Figure 7.20: Methanol particle tracks, dissolution taken into account

7.2.2. Venting depth: 0.9m

As the closing pressure of the pressure relief valve is 9 kPa, the maximal venting depth should be 0.9m to overcome the hydrostatic pressure. Therefore the same simulation is repeated but for a lower venting depth (0.9m instead of 2m).

The used mesh (see Figure 7.21) is slightly adapted from the previous case (Figure 6.5). The air body on top of the deck of the ship is extended by 1m to reduce non-physical effect of the vicinity of the pressure outlet. The mesh consists of 730625 cells with a grid size of 3cm.

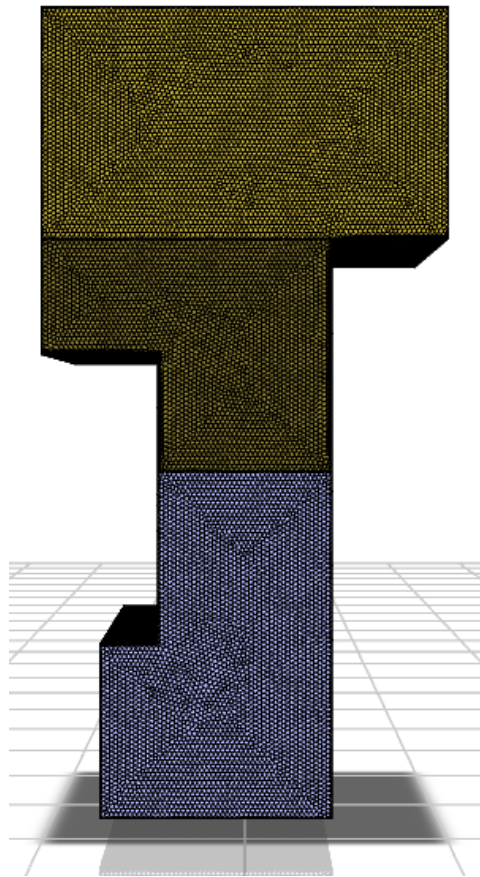


Figure 7.21: Mesh for full scale methanol-nitrogen venting at 0.9m

Without dissolution

Due to the lower release depth, the radius of the plume is much smaller compared to the venting case at 2m depth. The radial water current just below the water surface is less strong and consequently less gas above the water surface is dragged to the hull of the barge. As a result, the gas concentration levels at the deck level of the barge are much smaller compared to the venting at 2m. This is recognized by comparing Figure 7.22 with Figure 7.16 and Figure 7.23 with Figure 7.17. The gas plume will stay longer vertical and more gas will escape the simulation at the pressure outlet at the top of the mesh. Due to the much more concentrated gas plume (compared to the 2m venting depth) the methanol concentration 0,5m above the deck of the ship (in Figures 7.22 and 7.23) is higher than in Figures 7.16 and 7.17.

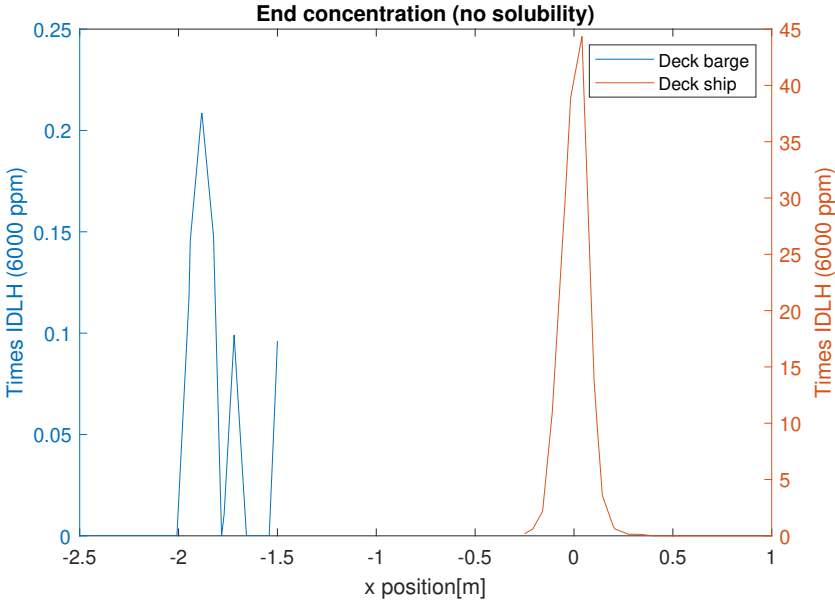


Figure 7.22: Methanol concentration at the end of the venting process

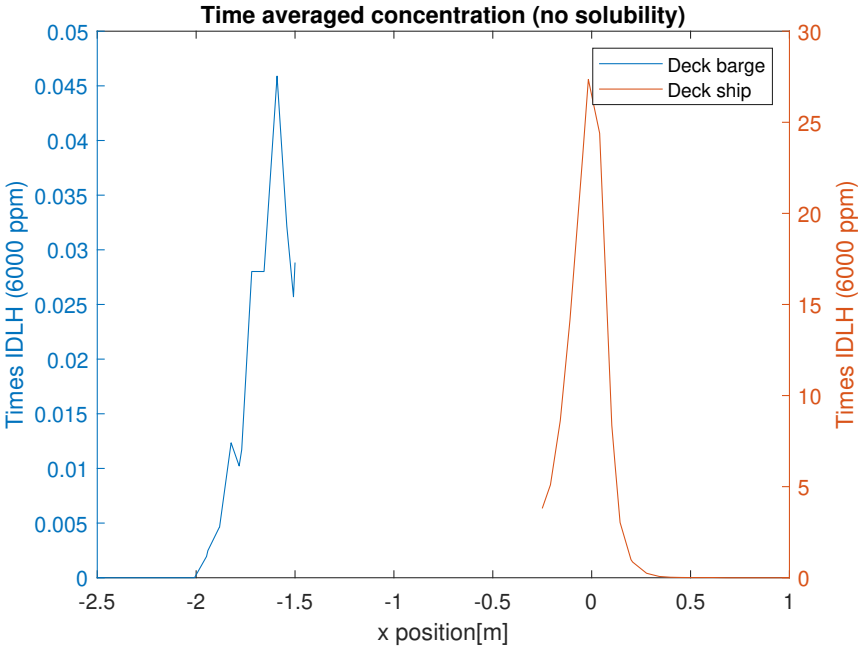


Figure 7.23: Time-averaged methanol concentration during venting

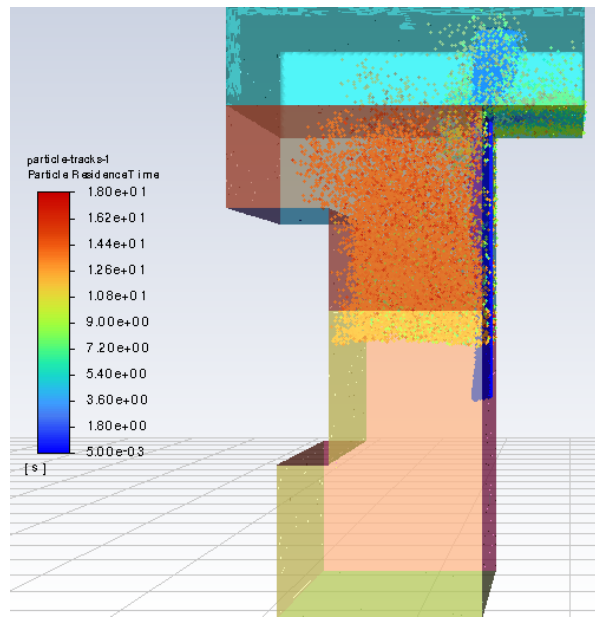


Figure 7.24: Mixture (methanol-nitrogen) vapour particles at end of venting

With dissolution

In Figure 7.20 it is clear that the methanol dissolves rapidly after the release. This is also expected when the release is closer to the water surface. This is shown in Figure 7.25. In the simulations of the Rotvoll experiment it was stated that the gas dissolution was overestimated (see Section 7.1.2.2). Therefore also the case where only half of the expected gas dissolution occurs is investigated, in other words the mass transfer in Equation 5.15 is multiplied with 0.5. By examining Figure 7.25 (b), it becomes evident that the solubility in methanol is exceedingly high, thereby constraining the significance of the reduction factor.

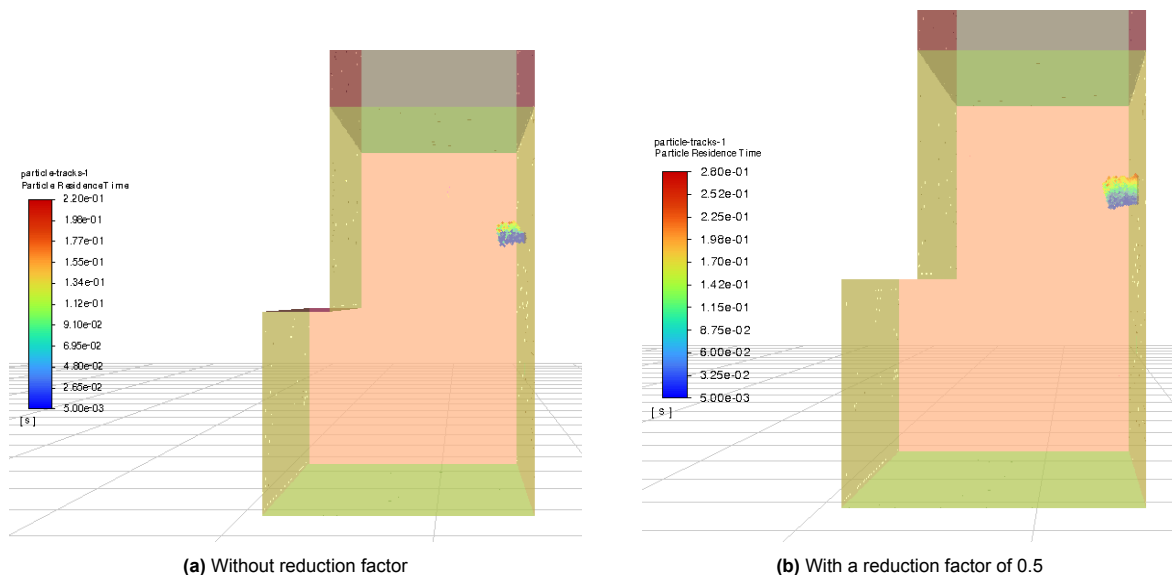


Figure 7.25: Methanol particle tracks (initial bubble size: 0.002m), dissolution taken into account

7.2.3. Influence initial bubble diameter

Due to the shallow injection depth, the bubbles have very limited time to reach the equilibrium diameter (see Section 5.1.7.2). Therefore, the initial bubble diameter is important. Illustrated in Figure 7.26 are the various regimes of bubble formation. In the scenario where methanol-nitrogen venting is employed, the velocity at which gas is injected (while the pressure relief valve is open) is that high that the current regime corresponds to jetting (e). Multiple authors have expressed the complexity of the bubble formation and focused on the importance of experiments to study the character of bubble formation in the jetting regime [19, 56, 41]. In order to reduce this uncertainty, the simulations have been repeated for an initial bubble size of 0.02m instead of 0.002m (for a venting depth of 0.9m).

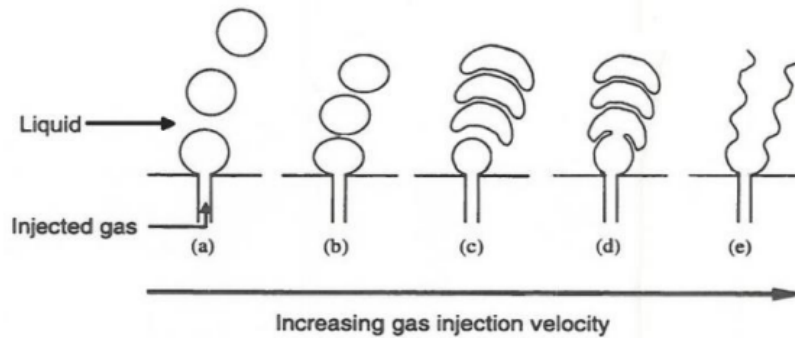


Figure 7.26: Bubble formation regimes [59]

Figure 7.27 shows the methanol particle tracks for an initial bubble diameter of 2cm. As expected, a larger bubble size leads to lower dissolution rates. This is explained in Section 5.1.7.5. Figure 7.28 shows the methanol particle tracks if the departure bubble size diameter would be equal to the diameter of the release opening (0.08m). This is most likely to represent the reality, as in the jetting regime the departure bubble size will lay close to the orifice diameter. In this case, methanol vapour is able to rise above the water surface. As an indication, the methanol peak concentration at 0.25m above the water surface is 800ppm. Higher above the water surface, the concentration decreases rapidly and at 0.5m above the the water surface only sporadic a methanol particle is found.

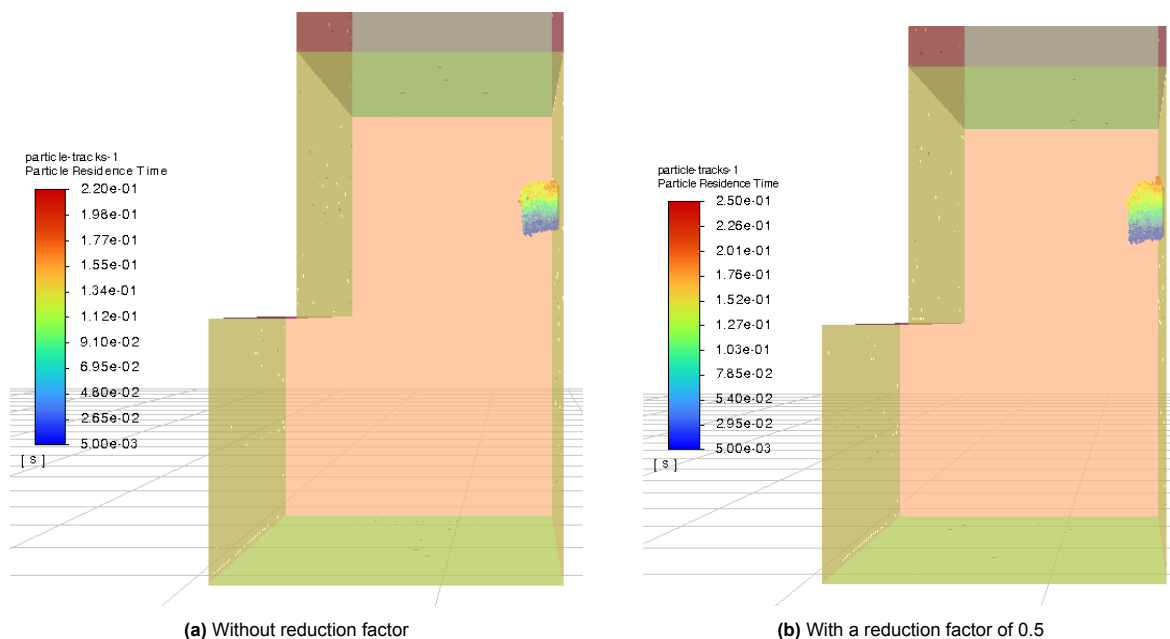


Figure 7.27: Methanol particle tracks (initial bubble size: 0.02m), dissolution taken into account

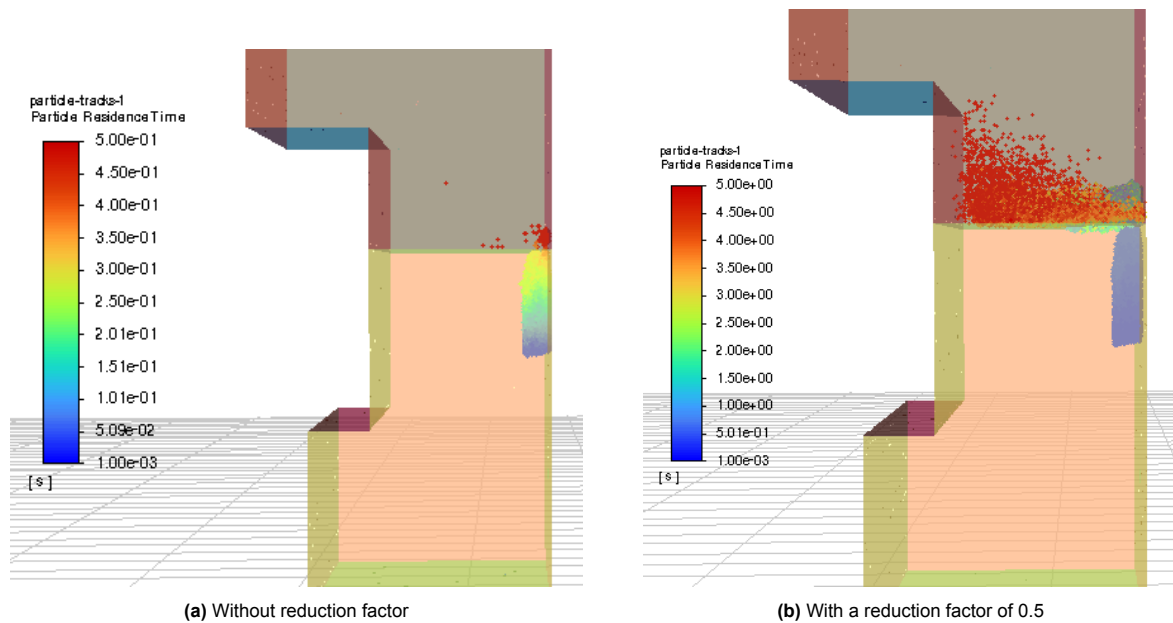


Figure 7.28: Methanol particle tracks (initial bubble size: 0.08m), dissolution taken into account

7.2.4. Influence venting depth

Vessels with a smaller draft will vent the methanol at a lower depth. The smaller the venting depth, the lower the residence time of methanol in the water leading to a lower gas dissolution rate. Figure 7.29 shows the result at the end of the venting at 0.5m below the waterline (with an initial bubble size equal to the opening diameter). Even at this lower venting depth no methanol vapour is able to reach the deck of the barge (or ship). The application of a reduction factor (of 0.5) has little influence due to the short residence time of the methanol vapour in the water. In Figure 7.30 the methanol concentration at 0.5m above the waterline is depicted. The highest methanol concentration is found close to halfway the bunker barge and the ship. The concentrations are well below the IDLH.

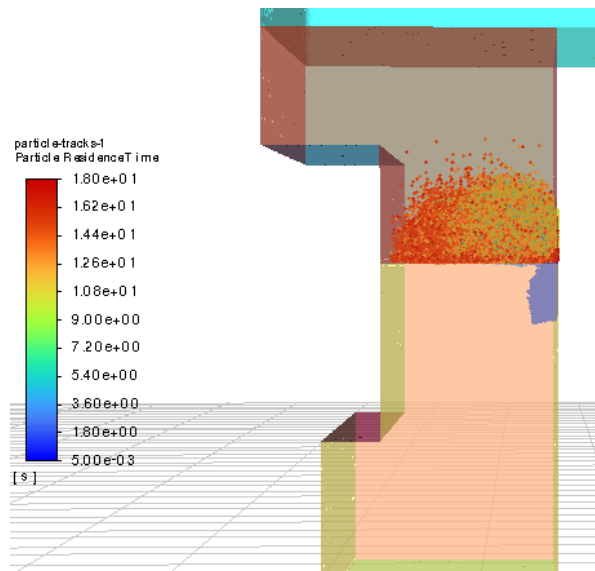


Figure 7.29: Methanol particle tracks (initial bubble size 0.08m) from the venting at 0.5m

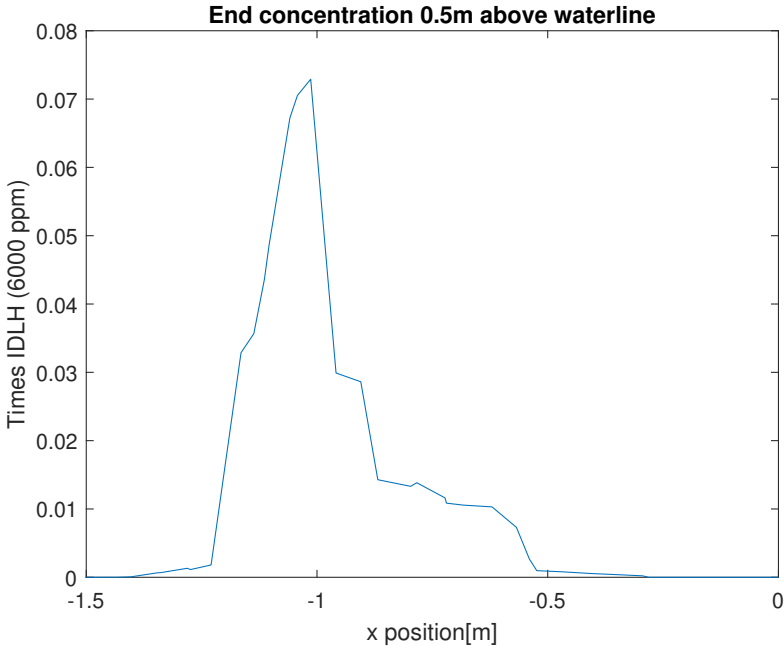


Figure 7.30: Methanol concentration at 0.5m above the waterline from the venting at 0.5m (x=0: ship, x=-1.5: barge)

7.3. Methanol small scale venting

Next to the depth, the release rate and density of the released gas, the release direction is the main difference between the small scale test and the Rotvoll experiment. After the injection, the drag force rapidly reduces the velocity of the particle. The momentum of the injection will decrease and the buoyancy will cause the plume to rise. Despite the fact that the plume will not rise from a single point, the plume will still develop in a conical shape. In the case of a very shallow release, this will be much less pronounced than for deep releases where the plume has time to develop. If the density of the released gas would be larger (for example due to a higher fraction of methanol), the momentum would increase and the upward turn would occur further away from the injection point. The jet (zone of flow establishment) and buoyant (zone of established flow, see Figure 3.1) stage is more clearly distinguished than in the vertical release case. An example of a horizontal release where air is injected at 200 m/s is shown in Figure 7.31. The CFD simulation and this experiment show a similar gas plume in the water.

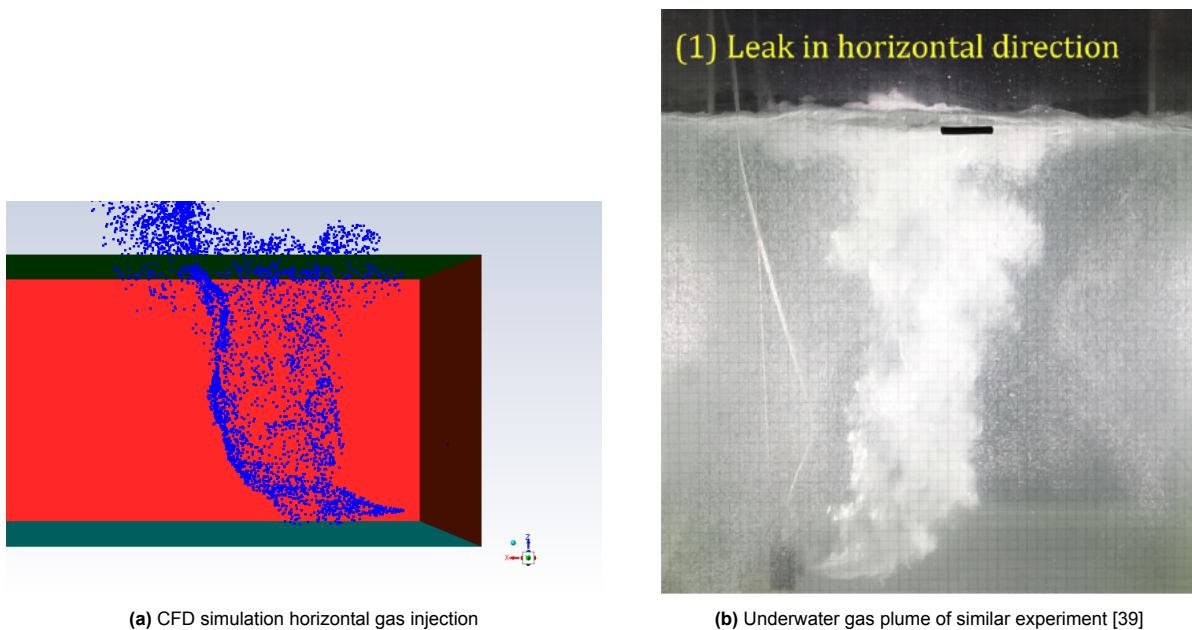
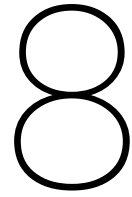


Figure 7.31: Comparison CFD model and similar experiment for the horizontal gas injection

Figure 7.32 shows the simulation of the experiment described in 6.3. The dark blue part represents the water body and the light blue is the surrounding air body. The initial bubble diameter is taken equal to the diameter of the release opening (10mm). It is clear that all the methanol vapour dissolves in the surrounding water. The conical shape of the plume is more pronounced than in the full scale venting due to the absence of the wall interaction. Also, in this case the saturation is not taken into account. This might be more problematic than in the full scale venting due to the absence of water currents and supply of fresh water. As the solubility limit of methanol in water is much higher than the injected amount of methanol, the water will not saturate. Nevertheless, the mass transfer from high to low concentration will be inhibited.



Figure 7.32: Methanol particle tracks, dissolution taken into account



Comparison underwater and on deck venting

The concentration of methanol on deck due to venting above the water line is derived from the IEC code (60079-10-1). This code gives a hazardous distance for an explosion risk. The model is adjusted for toxicity, for which the limit is lower than for flammability. A critical concentration of 6000 ppm (0.6 vol%) is used which corresponds to the immediate danger to life and health of methanol (IDLH) [47]. This value is 10% of the lower flammability limit. Equation 2.2 is used with 0.32 kg/s as gas release rate, 1.33 kg/m³ as density and 0.006 as LFL/toxicity limit. Taken into account that only 13 vol% of the released gas is methanol, the release characteristic becomes 5.21 m³/s. The corresponding hazardous distance is 9.5m (see Figure 2.5).

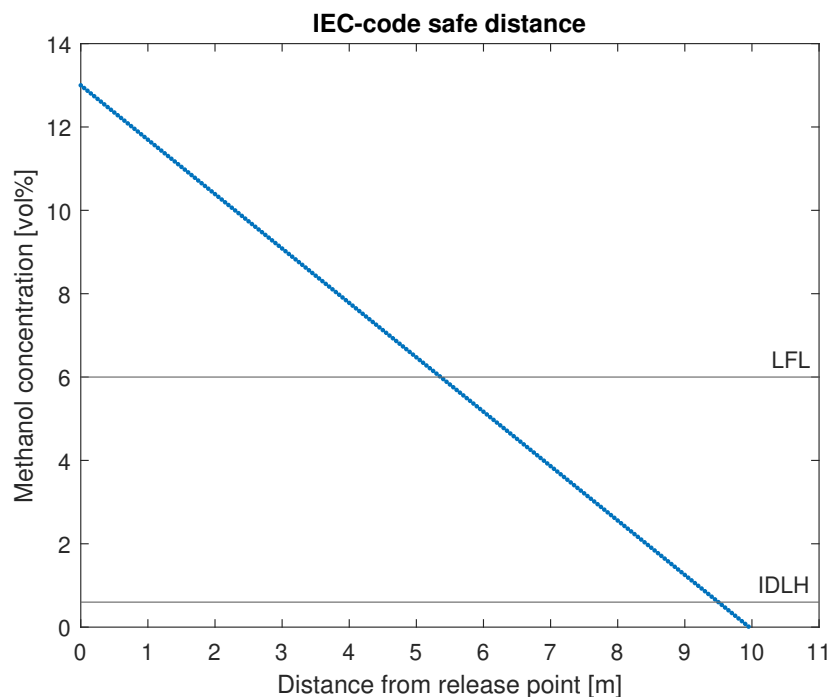


Figure 8.1: Concentration methanol in function of distance from release point

The venting above deck (IEC-code) and below the waterline (CFD results) can now be compared by placing the venting point (for the IEC-code) at the side of the ship straight above the venting point for

the underwater venting. Figure 8.2 shows the concentrations on deck (in function of the IDLH) where the zero position is at the side of the ship (port or starboard side) and the x position is increasing to the midship. Both the venting depth of 0.9m and 2.0m is shown in the figure. In reality, when the gas dissolution is taken into account, the methanol vapour is not able to reach the deck of the ship (for the venting at 0.5, 0.9 and 2.0m). It is clear that, even without taken the solubility of methanol into account, a lower safety distance can be considered for the case of venting below deck compared to the hazardous areas described in Section 2.2.2. The restrictions on the position of air intakes could also be made less stringent.

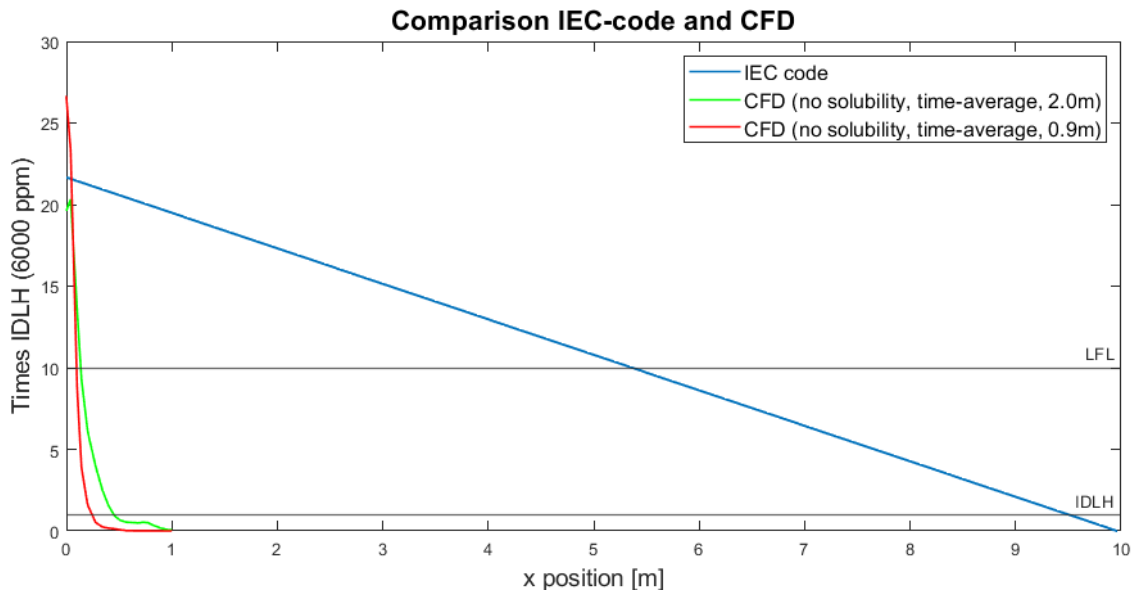


Figure 8.2: Comparison of methanol concentration resulting from venting above and below the waterline without taking the gas dissolution into account

The underwater venting might also have some drawbacks:

- The simultaneous intake of water and venting of methanol vapours might rise safety concerns. Seawater is used on board of ships for ballast water, cooling water, firefighting purposes and desalination purposes (in order to produce fresh water). Especially the intake of seawater with the aim of fresh water production might be problematic. Therefore caution should be paid to the location of water intakes in respect to the outlet of the subsea venting system.
- An opening in the hull can create additional resistance to the flow of water, resulting in increased drag and decreased fuel efficiency.
- The opening in the hull is exposed to seawater, which can cause corrosion over time. Regular maintenance and inspection are required to prevent damage.
- The opening in the hull will reduce the structural integrity of the ship.

Conclusions and recommendations

Methanol is a promising marine fuel due to its numerous advantages over traditional fossil fuels. Firstly, methanol is a clean-burning fuel that emits lower levels of pollutants such as sulphur oxides, nitrogen oxides, and particulate matter compared to conventional marine fuels. Moreover, it has a lower carbon footprint than fossil fuels, making it an environmentally-friendly option that can help reduce greenhouse gas emissions from the shipping industry. Secondly, methanol can be produced from a variety of sources, including natural gas, coal, biomass, and renewable energy sources such as wind and solar power, making it a versatile and sustainable fuel option. It should be noted that only green methanol (produced from green hydrogen and captured CO₂) has a significant reduction in well-to-wake emissions. Thirdly, methanol is a liquid fuel that is compatible with existing ship engines and fuel infrastructure, which means that retrofitting ships to use methanol is relatively straightforward compared to other alternative fuels. Furthermore, methanol can be blended with other fuels to provide a more gradual transition to using solely methanol.

However, despite these benefits, there are also some disadvantages and challenges that should be considered. For instance, methanol has a lower energy density (both gravimetric and volumetric) compared to conventional marine fuels. Additionally, its high flammability and toxicity complicate storage and handling, and it can be corrosive to some types of materials. Finally, the current limited availability to bunker methanol may pose a challenge for widespread adoption.

In case there is an overpressure in the methanol bunker tank (e.x. due to fire or a blocked vapour return line), the pressure relief valve emits methanol (and nitrogen) vapour on deck. This poses a flammability and toxicity hazard. Therefore, regulations prescribe a dangerous area zone around the venting point on deck. These areas are inaccessible for the crew and form an adversity for the ship design. Hence, in this thesis an alternative, the underwater venting of methanol vapour, is investigated. The aim of this thesis was to develop a numerical model which is able to predict the methanol concentration above the waterline after the release of methanol vapour below the waterline. The general research approach was as follows: firstly, a previously conducted experiment, where gas has been released below the waterline, is simulated. The results (e.x. the gas concentration below and above the waterline) from the numerical model and experiment are compared. Secondly, the numerical model is adjusted to the case where methanol (and nitrogen) is vented below the waterline. Thirdly, a small scale experiment, which is planned to be executed, is simulated. Finally, the consequences resulting from venting below the waterline and above deck are compared.

Two models, which represent the physics of subsea gas releases, are described in this research. The gas concentration above the waterline in the integral model follows from the gas flow rate reaching the surface and the radial inflow rate of air. The integral model is a cheap and efficient tool to predict average gas concentrations. However, it is highly dependent on the selection of appropriate values for the empirical coefficients (for example the entrainment coefficient). Also, it has other limitations, like the lack of surface interaction or the absence of gas dissolution. Modelling the surface area and reflection could significantly improve the results.

Next to the integral model, also an Eulerian-Lagrangian, transient, 3D CFD model was presented. This model tracks parcels (group of bubbles with the same properties) by using the force balance in the discrete phase model. This is the differential equation which describes the speed of parcels by function of the gravity, buoyancy and drag force. The drag force, bubble size distribution and gas dissolution are added to the CFD model by means of user defined functions. The CFD model demonstrated its capability to predict gas concentrations above the waterline resulting from a subsea gas release by successfully validating against experimental data where methane was released in the water. This capability is used to answer the research questions.

9.1. Conclusions

The conclusions of this research can be drawn by answering the (sub) research questions.

"What is the concentration of methanol at deck level when methanol is ventilated below the waterline?"

The methanol concentration above the waterline is strongly dependent on the gas release rate, venting depth and the initial bubble size of the released gas. When the initial bubble size is small (e.g. 1 cm), the methanol vapour will quickly dissolve after the release. For larger bubble sizes, the venting depth plays an important role. In the most conservative case (8cm initial bubble size and venting depth of 0.5m), the methanol does not fully dissolve in the water but no methanol vapour is able to reach the deck level of the barge or the ship.

- *"In subsea ventilation experiments, what is the concentration of methanol vapour above the waterline?"*

At the time of writing, the lab scale experiment, where a mixture of methanol and nitrogen is vented in a water tank, is yet to be executed. This experiment is drawn up in order to check the reliability of the CFD model. The simulation of this experiment points to the full dissolution of methanol in the water.

- *"How do predictions from an integral and CFD model compare with results from the experiments?"*

The validity of the integral model and CFD model have been tested against an experiment (carried out in 1997) where methane vapour is injected in a water tank. Results indicated that both models performed well in predicting velocity and void fraction measurements below the waterline. However, the integral model was found to be less reliable in predicting gas concentrations above the waterline due to several limitations. The model's lack of consideration for solubility, coupled with the difficulty in estimating coefficients, restricted its general applicability. In contrast, the CFD model's predictions were in good agreement with the gas measurements obtained in the experiment. Although the CFD model over-predicted gas dissolution, this was accounted for by introducing a mass reduction factor.

Overall, the study demonstrated that while the integral model is useful for certain applications, such as those involving vertical releases of non-soluble gases, it may not be suitable for simulating more complex scenarios. In contrast, the CFD model proved to be a more robust and versatile approach, capable of accurately predicting gas behaviour.

- *"How do consequences of underwater venting compare to consequences of venting on deck?"*

The comparison between the methanol concentration on deck due to venting above the waterline, as dictated by the IEC-code, and the methanol concentration on deck due to venting below the waterline, as predicted by the CFD model, has yielded some interesting results. As mentioned

earlier, venting below the waterline does not lead to any methanol vapours on deck, thus eliminating any potential hazards resulting from toxic or explosive methanol vapours. In contrast, venting on deck can contribute to a toxic and/or explosive area on deck, thereby requiring adherence to hazardous area and safety distance guidelines to ensure the safety of all personnel on board.

In the light of these findings, it becomes evident that venting below the waterline can provide a significant advantage in terms of safety. It allows for a reduction in the hazardous areas and safety distances on deck, leading to improved safety for crew members and other personnel on board. This reduction in hazardous areas and safety distances can also result in improved operational efficiency, as it allows for greater flexibility in the placement and operation of equipment and machinery on board the vessel.

9.2. Recommendations

Throughout this research some questions arose which can be used as suggestions for further research. The most important recommendation is the execution of a small (or ideally full scale) experiment wherein a mixture of methanol and nitrogen is vented below the waterline. The reasons why this experiment could be beneficial are described below.

9.2.1. Conditions

The models (integral and CFD) and the experiment are performed in laboratory conditions. Environmental conditions like wind, water movements, temperature differences etc. are not taken into account. Especially currents and surface waves will have an impact on the surfacing plume. These factors might influence the results, but are not expected to give totally different results. The influence of these environmental conditions should be investigated in gas dispersion (CFD) studies. Also, full scale experiments (taken into account these factors) are recommended.

This research is performed for gas releases from medium-sized bunker tanks at relative shallow depths. Large ships will have larger bunker tanks and as a result also higher mass venting rates. The physics of this underwater gas release and consequently also the gas concentrations could be different. It is recommended that full scale experiments are performed to investigate this.

9.2.2. Bubble size

The importance of bubble size is mentioned multiple times in this thesis (see Section 5.1.7.2). The rise velocity and gas dissolution rate are strongly dependent on the bubble diameter. In shallow gas releases, the bubbles have little time to coalesce or break up towards their equilibrium diameter. This emphasises the importance of the bubble diameter of the gas at the subsea injection point. The initial size of the gas bubbles in the methanol-nitrogen mixture is unknown and is dependent on the geometry of the venting arrangement. Therefore further investigation should be done on the bubble population model and the initial bubble sizes of subsea gas releases.

9.2.3. Solubility methanol

The solubility of methanol vapour into the surrounding water is taken into account by a gas dissolution model designed for the methane hydrate dissolution. The mass transfer coefficient of methanol (derived from this model) is compared against the same coefficient derived from the Sherwood number. Both methods returned similar results. Further research should be done on the applicability of these models on methanol and on the correspondence of these models with the reality. Especially the influence of nitrogen gas on the gas dissolution of methanol should be investigated.

9.2.4. Mitigating measures

Some measures which could decrease the likelihood that methanol vapours arise above the waterline are described below.

- Decrease the opening pressure setting of the pressure relief valve. The methanol mass release rate will be lower, the methanol will rise less fast in the water column and more methanol vapour

will dissolve in the surrounding water. When the closing pressure setting is kept the same, the venting process will be shorter, but will be repeated more.

- Decrease the temperature of the methanol fuel. The lower temperature will decrease the vapour pressure of methanol and consequently the methanol fraction in methanol-nitrogen mixture will also decrease.
- Use a sparger (or baffle plate) with multiple small orifices. The sparger will release bubbles with a small diameter which increases the surface area of the bubble with the surrounding water and consequently improves the gas dissolution.
- Use a premixing chamber. This will increase the contact time between the methanol vapour and the water. Additionally a packed bed and surfactants can be used in this chamber. A packed bed uses a packing material to spread out the gas and increase the contact time. Surfactants reduce the surface tension leading to an increased gas dissolution.

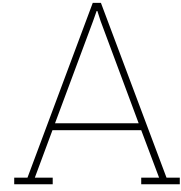
References

- [1] Wojciech P. Adamczyk et al. "Comparison of the standard Euler–Euler and hybrid Euler–Lagrange approaches for modeling particle transport in a pilot-scale circulating fluidized bed". In: *Particology* 15 (2014). Energy storage: Materials and processes, pp. 129–137. ISSN: 1674-2001. DOI: <https://doi.org/10.1016/j.partic.2013.06.008>. URL: <https://www.sciencedirect.com/science/article/pii/S1674200113001788>.
- [2] AIChE. "DIPPR database," in: (2021).
- [3] Moustafa Hussein Ali Hussein Ali. "Investigating the gas dispersion from subsea gas releases in shallow waters". MA thesis. Texas A & M University, 2018.
- [4] Alphasense. "AAN 301-04: Introduction to Photolonisation Detection (PID)". In: 2010.
- [5] Inc. ANSYS. *ANSYS Fluent Theory Guide*. 2013.
- [6] K. De Baere. *Advanced oil course: Inert gas*. Antwerp Maritime Academy. 2017.
- [7] K. De Baere. *Advanced oil course: Venting*. Antwerp Maritime Academy. 2017.
- [8] Mikkel Bakli. "Evaluation of Gas and Oil Dispersion during Subsea Blowouts". MA thesis. NTNU - Trondheim, Norwegian University of Science and Technology, 2014.
- [9] R. Bhaskaran and L. Collins. *Introduction to CFD Basics*. 2012.
- [10] Allan Bozek. "Application of IEC 60079-10-1 Edition 2.0 for Hazardous Area Classification". In: *IEEE Transactions on Industry Applications* 54.2 (Mar. 2018), pp. 1881–1889. DOI: 10.1109/tia.2017.2785258.
- [11] J. A. V. Butler, C. N. Ramchandani, and D. W. Thomson. "58. The solubility of non-electrolytes. Part I. The free energy of hydration of some aliphatic alcohols". In: *Journal of the Chemical Society (Resumed)* (1935), p. 280. DOI: 10.1039/jr9350000280.
- [12] PH Calderbank. "Physical Rate Processes in Industrial Fermentation, Part I". In: *Trans. Inst. Chem. Engrs. (London)* 36 (1958), p. 443.
- [13] United Nations Framework Convention on Climate Change. *The Paris Agreement*. 2015. URL: <https://unfccc.int/process-and-meetings/the-paris-agreement/the-paris-agreement> (visited on 07/08/2022).
- [14] Schalk Cloete, Jan Erik Olsen, and Paal Skjetne. "CFD modeling of plume and free surface behavior resulting from a sub-sea gas release". In: *Applied Ocean Research* 31.3 (July 2009), pp. 220–225. DOI: 10.1016/j.apor.2009.09.005.
- [15] Pauline M Doran. *Bioprocess Engineering Principles*. en. 2nd ed. San Diego, CA: Academic Press, 2006.
- [16] Dräger. *Dräger Sensor and Portable Instruments Handbook*. KGaA. Co and AG Safety Dräger: 2022.
- [17] R. Roberts E. Medina. *Methanol safe handling manual*. 5th ed. Methanol Institute, 2020.
- [18] Ahmed M. Ellethy et al. "Modelling and Assessment of Accidental Gas Release from Damaged Subsea Pipelines". In: *International Journal of Environmental Science and Development* 12.6 (2021), pp. 162–168. DOI: 10.18178/ijesd.2021.12.6.1335.
- [19] S.E. Forrester and C.D. Rielly. "Bubble formation from cylindrical, flat and concave sections exposed to a strong liquid cross-flow". In: *Chemical Engineering Science* 53.8 (1998), pp. 1517–1527. ISSN: 0009-2509. DOI: [https://doi.org/10.1016/S0009-2509\(98\)00019-0](https://doi.org/10.1016/S0009-2509(98)00019-0). URL: <https://www.sciencedirect.com/science/article/pii/S0009250998000190>.
- [20] M.J Friedl and T.K Fanneløp. "Bubble plumes and their interaction with the water surface". In: *Applied Ocean Research* 22.2 (Apr. 2000), pp. 119–128. DOI: 10.1016/s0141-1187(99)00022-x.

- [21] A. Gupta. "MODELING AND SIMULATION OF GAS RELEASE FROM RUPTURE OF SUBSEA SURFACE GAS PIPE". In: 2014.
- [22] S.T. Johansen H. Laux. "A CFD analysis of the air entrainment rate due to a plunging steel jet combining mathematical models for dispersed and separated multiphase flows". In: (1999).
- [23] Health and P. J. Rew Safety Executive Staff. *Dispersion of Subsea Releases*. Health and Safety Executive (HSE) Books, 1995. ISBN: 9780717609918.
- [24] S. Herman. "Chapter 18 - Fragrance". In: *Cosmetic Science and Technology*. Ed. by Kazutami Sakamoto et al. Amsterdam: Elsevier, 2017, pp. 267–283. ISBN: 978-0-12-802005-0. DOI: <https://doi.org/10.1016/B978-0-12-802005-0.00018-5>. URL: <https://www.sciencedirect.com/science/article/pii/B9780128020050000185>.
- [25] A Huser et al. "Subsea gas plumes and dispersion above sea". In: (Sept. 2013), pp. 155–162. DOI: 10.1201/b15938-24.
- [26] IEC. *IEC 60079-10-1: Explosive atmospheres – Part 10-1: Classification of areas – Explosive gas atmospheres*. 2020.
- [27] IPCC Working group III. *Climate change 2022: Mitigation of climate change*. WMO and UNEP, 2022.
- [28] IMO. "Interim guidelines for the safety of ships using methyl/ethyl alcohol as fuel". In: *MSC.1 Circ.1621* (2020), pp. 1–38.
- [29] Methanol Institute. *Renewable methanol*. 2021. URL: <https://www.methanol.org/renewable/> (visited on 09/08/2022).
- [30] P. Skjetne J.E. Olsen. *Governing physics of shallow and deep subsea gas release*. SINTEF akademisk forlag, 2015.
- [31] V. Khvorostyanov and J. Curry. "Fall Velocities of Hydrometeors in the Atmosphere: Refinements to a Continuous Analytical Power Law". In: *Journal of The Atmospheric Sciences - J ATMOS SCI* 62 (Dec. 2005), pp. 4343–4357. DOI: 10.1175/JAS3622.1.
- [32] Taewook Kim. "CFD validation of transient subsea gas plumes". MA thesis. University College of Southeast Norway, 2017.
- [33] Akshay Koodly Ravishankara. "Development of a pressure based incompressible flow solver for wind turbine applications". PhD thesis. 2021.
- [34] P. Kováts, D. Thévenin, and K. Zähringer. "Influence of viscosity and surface tension on bubble dynamics and mass transfer in a model bubble column". In: *International Journal of Multiphase Flow* 123 (2020), p. 103174. ISSN: 0301-9322. DOI: <https://doi.org/10.1016/j.ijmultiphaseflow.2019.103174>. URL: <https://www.sciencedirect.com/science/article/pii/S0301932219304264>.
- [35] P. K. Kundu and I. M. Cohen. *Fluid Mechanics*. 4th ed. Academic Press, 2008.
- [36] M.D. Lechner, ed. *Gases in Gases, Liquids and their Mixtures*. Springer Berlin Heidelberg, 2007. DOI: 10.1007/978-3-540-49718-9.
- [37] Xinhong Li. "Gas dispersion and deflagration above sea from subsea release and its impact on offshore platform". In: 2018. DOI: [.org/10.1016/j.oceaneng.2018.05.059](https://doi.org/10.1016/j.oceaneng.2018.05.059).
- [38] Xinhong Li. "Simulation and assessment of gas dispersion above sea from a subsea release: A CFD-based approach". In: 2019. DOI: [.org/10.1016/j.ijnaoe.2018.07.002](https://doi.org/10.1016/j.ijnaoe.2018.07.002).
- [39] Xinhong Li, Guoming Chen, and Faisal Khan. "Analysis of underwater gas release and dispersion behavior to assess subsea safety risk". In: *Journal of Hazardous Materials* 367 (2019), pp. 676–685. ISSN: 0304-3894. DOI: <https://doi.org/10.1016/j.jhazmat.2019.01.015>. URL: <https://www.sciencedirect.com/science/article/pii/S0304389419300159>.
- [40] M. Loes and T. K. Fannelop. "Concentration Measurements Above an Underwater Release of Natural Gas". In: *SPE Drilling Engineering* 4.02 (June 1989), pp. 171–178. DOI: 10.2118/16543-pa.

- [41] Karine Loubière and Gilles Hébrard. "Influence of liquid surface tension (surfactants) on bubble formation at rigid and flexible orifices". In: *Chemical Engineering and Processing: Process Intensification* 43.11 (2004). Special Issue on Gas-Liquid and Gas-Liquid-Solid Reactor Engineering, pp. 1361–1369. ISSN: 0255-2701. DOI: <https://doi.org/10.1016/j.cep.2004.03.009>. URL: <https://www.sciencedirect.com/science/article/pii/S0255270104000662>.
- [42] S.L. Ross Environmental Research Ltd. "Fate and Behavior of Deepwater Subsea Oil Well Blowouts in the Gulf of Mexico". In: 1997.
- [43] Oil companies international forum Marine safety forum. *The carriage of methanol in bulk onboard offshore vessels*. 1st ed. Marine safety forum, 2020.
- [44] DNV Maritime. "DNV Maritime Forecast to 2050 – Energy Transition Outlook 2022". In: 2022.
- [45] Methanex. *Safety data sheet methanol*. 2022. URL: https://www.methanex.com/sites/default/files/safety/SDS-2014/Europe-REACH/UL-METHANOL-EU_v3.1_eSDS_05.02.2022_English.pdf (visited on 11/08/2022).
- [46] Frank Millero. "The activity coefficients of non-electrolytes in seawater". In: *Marine Chemistry* 70.1 (2000), pp. 5–22. ISSN: 0304-4203. DOI: [https://doi.org/10.1016/S0304-4203\(00\)00011-6](https://doi.org/10.1016/S0304-4203(00)00011-6). URL: <https://www.sciencedirect.com/science/article/pii/S0304420300000116>.
- [47] National Institute for Occupational Safety and Health. "Methyl alcohol: Immediately dangerous to life or health concentrations". In: 1994.
- [48] J.E. Olsen and P. Skjetne. "Summarizing an Eulerian–Lagrangian model for subsea gas release and comparing release of CO₂ with CH₄". In: *Applied Mathematical Modelling* 79 (Mar. 2020), pp. 672–684. DOI: 10.1016/j.apm.2019.10.057.
- [49] Jan Erik Olsen and Paal Skjetne. "Current understanding of subsea gas release: A review". In: *The Canadian Journal of Chemical Engineering* 94.2 (Nov. 2015), pp. 209–219. DOI: 10.1002/cjce.22345.
- [50] International Maritime Organisation. *Adoption of amendments to the IMDG code*. Amendment 36-12. IMO, 2012.
- [51] United Nations Environment Programme World Health Organization International Labour Organisation. *Methanol - Environmental Health Criteria 196*. WHO, 1997.
- [52] International Labour Organization. *Methanol*. 2022. URL: https://www.ilo.org/dyn/icsc/showcard.display?p_lang=en&p_card_id=0057&p_version=1 (visited on 01/05/2018).
- [53] Qingqing Pan. "Modelling of turbulent flows with strong dispersed phase-continuous fluid interactions". In: (2014).
- [54] Dmitrii Riabov et al. "Influence of Gas Density and Plug Diameter on Plume Characteristics by Ladle Stirring". In: *Crystals* 11.5 (Apr. 2021), p. 475. DOI: 10.3390/cryst11050475.
- [55] S.L. Ross, SINTEF, and Wellflow Dynamics. *Assessing Risk and Modeling a Sudden Gas Release Due to Gas Pipeline Ruptures*. SL Ross, 2009.
- [56] M.C. Ruzicka et al. "Intermittent transition from bubbling to jetting regime in gas-liquid two phase flows". In: *International Journal of Multiphase Flow* 23.4 (1997), pp. 671–682. ISSN: 0301-9322. DOI: [https://doi.org/10.1016/S0301-9322\(97\)00009-8](https://doi.org/10.1016/S0301-9322(97)00009-8). URL: <https://www.sciencedirect.com/science/article/pii/S0301932297000098>.
- [57] American bureau of shipping. "Methanol as marine fuel". In: *Sustainability whitepaper 2* (2021), pp. 1–28.
- [58] Paal Skjetne and Jan Erik Olsen. "A parcel based modelling concept for studying subsea gas release and the effect of gas dissolution". In: *Progress in Computational Fluid Dynamics, An International Journal* 12.2/3 (2012), p. 187. DOI: 10.1504/pcfd.2012.047461.
- [59] S.D. Sovani. "High pressure gas-liquid flow inside an effervescent diesel injector and its effect on spray characteristics". PhD thesis. 2001.
- [60] O. Stråby. *Maersk methanol fueled containerhips - Design for safe operation and maintenance*. 2023.

- [61] K. Sjoen T. Engebresten T. Northug and T. K. Fannelop. "Surface Flow and Gas Dispersion from a Subsea Release of Natural Gas" in *Proceedings of the 7th International Offshore & Polar Engineering Conference*. International Society of Offshore & Polar Eng, 1997. ISBN: 9781880653289.
- [62] H. Versteeg and W. Malalasekera. *An Introduction to Computational Fluid Dynamics. The Finite Volume Method (2nd Edition)*. Prentice Hall, 2007, p. 520. ISBN: 9780131274983.
- [63] K. Visser. "Fuels: chemical structure and products". In: *DE-11-1 alternative fuels 1 3: Combustion* (2021), pp. 1–22.
- [64] K. Visser. "Fuels: properties". In: *DE-11-1 alternative fuels 1 3: Combustion* (2021), pp. 1–43.
- [65] W. R. J. Marshall W. E. Ranz. "Evaporation from drops". In: *Chemical Engineering Progress* 48 (1952), pp. 48–173.
- [66] J. Werner. "Cargo vapour concentrations on board chemical tankers in the non-cargo area during normal operations". PhD thesis. Antwerp Maritime Academy, University of Antwerp, 2019.
- [67] J. L. Xia, T. Ahokainen, and L. Holappa. "Analysis of flows in a ladle with gas-stirred melt". In: *Scandinavian Journal of Metallurgy* 30.2 (Apr. 2001), pp. 69–76. DOI: 10.1034/j.1600-0692.2001.300203.x.
- [68] Poojitha D. Yapa et al. "A model to simulate the transport and fate of gas and hydrates released in deepwater". In: *Journal of Hydraulic Research* 48.5 (Oct. 2010), pp. 559–572. DOI: 10.1080/00221686.2010.507010.
- [69] Youxue Zhang and Zhengjiu Xu. "Kinetics of convective crystal dissolution and melting, with applications to methane hydrate dissolution and dissociation in seawater". In: *Earth and Planetary Science Letters* 213.1 (2003), pp. 133–148. ISSN: 0012-821X. DOI: [https://doi.org/10.1016/S0012-821X\(03\)00297-8](https://doi.org/10.1016/S0012-821X(03)00297-8). URL: <https://www.sciencedirect.com/science/article/pii/S0012821X03002978>.



Friedl integral model

This section is based on code from Kim Taewook [32].

```
1 clear
2 close all
3 clc
4
5 g = 9.81; %gravity[m/s2]
6 rho_w=998.2; %density of water[kg/m3]
7 rho_a=1.225; %density of air above the surface
8 rho_g=0.68; %1.225 air; 0.678 methane ; density of releasing gas[kg/m3]
9 m_release=0.035; % 0.10 (83 Nm3/s or 0.05 m3/s), 0.21 (170 Nm3/s or 0.1 m3/s), 0.92 (750 Nm3/
   s or 0.45 m3/s) for air; 0.03 , 0.06 , 0.3 for methane %mass rate[kg/s]
10 m_releaseX=0.10;
11 pi=3.14;
12 p0=101325; %atmopheric pressure[pa]
13 vs=0.35; %slip velocity[m/s]
14 h=8; %height of the water surface, taken into account that the model is designed for a point
   source (extrapolate with diameter opening)
15 hp=10.33; % 10.33 fresh water; 10 sea water
16 x1 = 0; %centerline
17 hoff=0; %h offset
18 z0=1.75; %z value where you want to know about profile at
19 z8=3.8;
20
21 %coefficients%
22
23 alpha=0.1285; %0.1285 for z=1.75; 0.11 for z=3.8; entrainment coefficient; for 50m experiment
   : use alpha=0.175
24 alpha8 = 0.11;
25 gam=1.5; % for 7m experiment: gam=1.5 ; for 50m experiment: gam=2
26 beta=0.39;%0.5;theoretical value%0.39;experimental value : for a loss-free rise;ifor
   instantneous
27 lambda=0.8;
28
29 %calculation in x(radial) direction
30
31 vs1=vs*((g*m_release*(lambda^2+1))/((h+hp)*pi*gam*rho_g*2*alpha^2))^(-1/3);
32 s1=(1+lambda^2)*vs1;
33 z1=z0/(h+hp);
34 z2=h/(h+hp);
35 v1=((25/12)^(1/3))*(z1^(-1/3))*(1+11*z1/39+511/2*(z1/39)^2)-s1*7/22*(1+345/343*z1
   /13+86175/11662*(z1/13)^2)+(s1^2)*13/121*(12/25)^(1/3)*(z1^(1/2))*(1-59489/1436*z1
   /39-2825583625/23347324*(z1/39)^2);
36 v2=((25/12)^(1/3))*(z2^(-1/3))*(1+11*z2/39+511/2*(z2/39)^2)-s1*7/22*(1+345/343*z2
   /13+86175/11662*(z2/13)^2)+(s1^2)*13/121*(12/25)^(1/3)*(z2^(1/2))*(1-59489/1436*z2
   /39-2825583625/23347324*(z2/39)^2);
37 v=v1*((g*m_release*(lambda^2+1))/((h+hp)*pi*gam*rho_g*2*alpha^2))^(1/3);
38 vh=v2*((g*m_release*(lambda^2+1))/((h+hp)*pi*gam*rho_g*2*alpha^2))^(1/3);
39 b1=3/5*z1*(1-z1/13-7*(z1/13)^2)+s1*3/110*((12/25)^(1/3))*(z1^(4/3))*(1-1046/49*z1
   /39-227726/833*(z1/39)^2)-(s1^2)*48/15121*((25/12)^(1/3))*(z1^(5/3))*(1-34663/9408*z1
   +225707803/240143904*z1^2);
```

```

40 b2=3/5*z2*(1-z2/13-7*(z2/13)^2)+s1*3/110*((12/25)^(1/3))*(z2^(4/3))*(1-1046/49*z2
    /39-227726/833*(z2/39)^2)-(s1^2)*48/15121*((25/12)^(1/3))*(z2^(5/3))*(1-34663/9408*z2
    +225707803/240143904*z2^2);
41 b=b1*(2*alpha*(h+hp)); %plume width at z0
42 bh=b2*(2*alpha*(h+hp)); %plume width at the surface
43 x = [0 : 0.02: 200]; % x range- need to be set
44 y=v*exp(-(x.^2)/(b^2)); %velocity at z0
45 yh=vh*exp(-(x1^2)/(bh^2)); %velocity at the surface, at centerline
46 yh2=vh*exp(-(x.^2)/(bh^2)); %velocity at the surface
47
48 %% Script for z0=3.8
49
50 vs8 = vs*((g*m_release*(lambda^2+1))/((h+hp)*pi*gam*rho_g*2*alpha8^2))^(-1/3);
51 s18=(1+lambda^2)*vs8;
52 z18 = z8/(h+hp);
53 v18 = ((25/12)^(1/3))*(z18^(-1/3))*(1+11*z18/39+511/2*(z18/39)^2)-s18*7/22*(1+345/343*z18
    /13+86175/11662*(z18/13)^2)+(s18^2)*13/121*(12/25)^(1/3)*(z18^(1/2))*(1-59489/1436*z18
    /39-2825583625/23347324*(z18/39)^2);
54 v28 = subs(v2, s1, s18);
55 v8=v18*((g*m_release*(lambda^2+1))/((h+hp)*pi*gam*rho_g*2*alpha8^2))^(1/3);
56 vh8=v28*((g*m_release*(lambda^2+1))/((h+hp)*pi*gam*rho_g*2*alpha8^2))^(1/3);
57 b18= 3/5*z18*(1-z18/13-7*(z18/13)^2)+s18*3/110*((12/25)^(1/3))*(z18^(4/3))*(1-1046/49*z18
    /39-227726/833*(z18/39)^2)-(s18^2)*48/15121*((25/12)^(1/3))*(z18^(5/3))*(1-34663/9408*z18
    +225707803/240143904*z18^2);
58 b28 = subs(b2,s1,s18);
59 b8=b18*(2*alpha8*(h+hp));
60 bh8=b28*(2*alpha8*(h+hp));
61 y8=v8*exp(-(x.^2)/(b8^2));
62 yh8=vh8*exp(-(x1^2)/(bh8^2));
63
64 hf=beta*gam*(yh.^2)/g; %the peak of fountain profile
65 hr=hf*exp(-(x.^2)/(bh^2))-hoff; %fountain profile
66
67 void_1=1/(1-z1)/((b1^2)*(v1+s1));
68 void1=void_1*(((1+lambda^2)^2)*gam*(m_release/rho_g)^2)/((pi^2)*(lambda^2)*(2^5)*(alpha^4)
    *((h+hp)^5)*g)^(1/3);
69 voidr=void1*exp(-(x1.^2)/((lambda^2)*(b.^2))); %void fraction profile at z0
70
71 void_2=1/(1-z2)/((b2^2)*(v2+s1));
72 void2=void_2*(((1+lambda^2)^2)*gam*(m_release/rho_g)^2)/((pi^2)*(lambda^2)*(2^5)*(alpha^4)
    *((h+hp)^5)*g)^(1/3);
73 voidh=void2*exp(-(x.^2)/((lambda^2)*(bh^2))); %void fraction profile at the surface
74 mflux_surf=voidh.*yh2.*rho_g; %mass flux per unit area at the surface
75
76 %% calculating total mass flux (kg/s) escaping from the surface
77
78 syms w
79 yh_w=vh*exp(-(w^2)/(bh^2)); % velocity at the surface in function of the radial position
80 voidh_w=void2*exp(-(w^2)/((lambda^2)*(bh^2))); % void fraction at the surface in function of
    the radial position
81 mflux_surf_w = vpa(voidh_w*yh_w*rho_g,2); % mass flux at the surface in function of the
    radial position
82 Mflux_surf1 = vpa(int(mflux_surf_w*2*pi*w,w,0,inf),2) % should be the same as m_release
83
84 %% calculation in z direction
85
86 initial=0; %z start
87 last=h; %z end
88 dz=0.01; %delta z
89 n=(last-initial)/dz; %the number of data
90 zarr=zeros(n,1); % n x 1 array for z
91 veloarr=zeros(n,1); %n x 1 array for velocity in z direction
92 voidarr=zeros(n,1); %n x 1 array for voidfraction in z direction
93 i=1;
94
95 for z9=initial:dz:last
96 zarr(i)=z9;
97 z1=z9/(h+hp);
98 vs1=vs*((g*m_release*(lambda^2+1))/((h+hp)*pi*gam*rho_g*2*alpha^2))^(-1/3);
99 s1=(1+lambda^2)*vs1;

```

```

100 v1_z=((25/12)^(1/3))*(z1.^(-1/3))*(1+11*z1/39+511/2*(z1/39).^2)-s1*7/22*(1+345/343*z1
    /13+86175/11662*(z1/13).^2)+(s1^2)*13/121*(12/25)^(1/3)*(z1.^(1/2))*(1-59489/1436*z1
    /39-2825583625/23347324*(z1/39).^2);
101 v_z=v1_z*((g*m_release*(lambda^2+1))/((h+hp)*pi*gam*rho_g*2*alpha^2))^(1/3); % velocity at
    centerline
102 b1_z=3/5*z1*(1-z1/13-7*(z1/13)^2)+s1*3/110*((12/25)^(1/3))*(z1^(4/3))*(1-1046/49*z1
    /39-227726/833*(z1/39)^2)-(s1^2)*48/15121*((25/12)^(1/3))*(z1^(5/3))*(1-34663/9408*z1
    +225707803/240143904*z1^2);
103 b_z=b1_z*(2*alpha*(h+hp));
104 bz(i,1)=b_z; %designate br's 'i' th value
105 veloarr_z(i,1)=v_z*exp(-(x1^2)/(b_z^2)); %designate veloarr's 'i' th value % velocity at
    centerline
106 void1_z=1/(1-z1)/((b1_z.^2)*(v1_z+s1));
107 void_z=void1_z*(((1+lambda^2)^2)*gam*(m_release/rho_g)^2)/((pi^2)*(lambda^2)*(2^5)*(alpha^4)
    *((h+hp)^5)*g))^(1/3);
108 voidz(i,1)=void_z*exp(-(x1^2)/((lambda^2)*(b_z^2))); %designate voidr's 'i' th value
109 i=i+1;
110 end
111
112 veloarr_z_av1 = mean(veloarr_z,'omitnan')
113
114 for z9X=initial:dz:last
115 zarrX(i)=z9X;
116 z1X=z9X/(h+hp);
117 vs1X=vs*((g*m_releaseX*(lambda^2+1))/((h+hp)*pi*gam*rho_g*2*alpha^2))^(1/3);
118 s1X=(1+lambda^2)*vs1X;
119 v1_zX=((25/12)^(1/3))*(z1X.^(-1/3))*(1+11*z1X/39+511/2*(z1X/39).^2)-s1X*7/22*(1+345/343*z1X
    /13+86175/11662*(z1X/13).^2)+(s1X^2)*13/121*(12/25)^(1/3)*(z1X.^(1/2))*(1-59489/1436*z1X
    /39-2825583625/23347324*(z1X/39).^2);
120 v_zX=v1_zX*((g*m_releaseX*(lambda^2+1))/((h+hp)*pi*gam*rho_g*2*alpha^2))^(1/3);
121 b1_zX=3/5*z1X*(1-z1X/13-7*(z1X/13)^2)+s1X*3/110*((12/25)^(1/3))*(z1X^(4/3))*(1-1046/49*z1X
    /39-227726/833*(z1X/39)^2)-(s1X^2)*48/15121*((25/12)^(1/3))*(z1X^(5/3))*(1-34663/9408*z1X
    +225707803/240143904*z1X^2);
122 b_zX=b1_zX*(2*alpha*(h+hp));
123 bzX(i,1)=b_zX; %designate br's 'i' th value
124 veloarr_zX(i,1)=v_zX*exp(-(x1^2)/(b_zX^2)); %designate veloarr's 'i' th value
125 void1_zX=1/(1-z1X)/((b1_zX.^2)*(v1_zX+s1X));
126 void_zX=void1_zX*(((1+lambda^2)^2)*gam*(m_releaseX/rho_g)^2)/((pi^2)*(lambda^2)*(2^5)*(alpha
    ^4)*((h+hp)^5)*g))^(1/3);
127 voidzX(i,1)=void_zX*exp(-(x1^2)/((lambda^2)*(b_zX^2))); %designate voidr's 'i' th value
128 i=i+1;
129 end
130
131 %% Calculation u_a in function of other variables
132
133 syms u_a u_g rho_g br z_c
134
135 rho = (rho_g.*u_g+rho_a*u_a)./(u_a+u_g);
136 v = (u_a+u_g)./(pi*br^2);
137 K = 2;
138 eq = (u_a*rho_a + u_g*rho_g).*v - u_g.*rho_g*vs == (rho_a-rho)*g*z_c*pi*br^2;
139 [u_a2, params, conds] = solve(eq, u_a, 'ReturnConditions', true, 'MaxDegree', 4);
140 ua_5 = u_a2(1,1);
141
142 %% Concentration above waterline
143
144 z_c = round(bh*0.5,2);
145 rho_g = 0.678;
146 br = 2*bh;
147
148 for i = 1:100;
149 u_g = 0.02*i;
150 u_a = (((2*u_g + (40*rho_g*u_g)/49)*((80*rho_g*u_g^2)/49 + u_g^2 - (157*br^2*rho_g*u_g)
    /175))/6 - (20*rho_g*u_g^3)/49 - (2*u_g + (40*rho_g*u_g)/49)^3/27 + (((20*rho_g*u_g
    ^3)/49 - ((2*u_g + (40*rho_g*u_g)/49)*((80*rho_g*u_g^2)/49 + u_g^2 - (157*br^2*rho_g*
    u_g)/175))/6 + (2*u_g + (40*rho_g*u_g)/49)^3/27 - (24180669*br^4*u_g*z_c)/500000 -
    (157*br^2*rho_g*u_g^2)/350 + (24180669*br^4*rho_g*u_g*z_c)/612500)^2 + ((80*rho_g*u_g
    ^2)/147 + u_g^2/3 - (2*u_g + (40*rho_g*u_g)/49)^2/9 - (157*br^2*rho_g*u_g)/525)^3
    ^2 + (24180669*br^4*u_g*z_c)/500000 + (157*br^2*rho_g*u_g^2)/350 - (24180669*br
    ^4*rho_g*u_g*z_c)/612500)^(1/3) - ((80*rho_g*u_g^2)/147 + u_g^2/3 - (2*u_g + (40*
    rho_g*u_g)/49)^2/9 - (157*br^2*rho_g*u_g)/525)/(((2*u_g + (40*rho_g*u_g)/49)*((80*

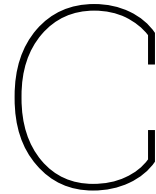
```

```
rho_g*u_g^2)/49 + u_g^2 - (157*br^2*rho_g*u_g)/175))/6 - (20*rho_g*u_g^3)/49 - (2*u_g
+ (40*rho_g*u_g)/49)^3/27 + (((20*rho_g*u_g^3)/49 - ((2*u_g + (40*rho_g*u_g)/49)
*((80*rho_g*u_g^2)/49 + u_g^2 - (157*br^2*rho_g*u_g)/175))/6 + (2*u_g + (40*rho_g*u_g
)/49)^3/27 - (24180669*br^4*u_g*z_c)/500000 - (157*br^2*rho_g*u_g^2)/350 + (24180669*
br^4*rho_g*u_g*z_c)/612500)^2 + ((80*rho_g*u_g^2)/147 + u_g^2/3 - (2*u_g + (40*rho_g*
u_g)/49)^2/9 - (157*br^2*rho_g*u_g)/525)^3)^(1/2) + (24180669*br^4*u_g*z_c)/500000 +
(157*br^2*rho_g*u_g^2)/350 - (24180669*br^4*rho_g*u_g*z_c)/612500)^(1/3) - (40*rho_g*
u_g)/147 - (2*u_g)/3;
151 ua_8 = vpa(u_a,4);
152 C = vpa(100*u_g/(u_g+ua_8),4);
153 C9(1,i) = C;
154 u_g9(1,i) = u_g;
155 end
```

B

Xia's law bubble drag

```
1 #include "udf.h"
2 DEFINE_DPM_DRAG(particle_drag_term, Re, p)
3 {
4   real drag_term;
5   real Eo;
6   real Cd;
7   real rho_water = 998.2; /* sea water: 1027.0 */
8   real surf_tension = 0.07199; /* methane: 0.06180 */
9   /* bubble shape - Xia et al. (10) */
10  Eo = 9.81*(rho_ocean - P_RHO(p))*pow(P_DIAM(p), 2) / surf_tension;
11  /* drag coefficient */
12  Cd = 2.0/3.0*pow((Eo/3),0.5);
13  drag_term = 18.0*Re*Cd / 24.0;
14  return (drag_term);
15 }
```



UDF bubble size and gas dissolution

This section is based on code from Bakli [8]. The code is shown for the simulation of the Rotvoll experiment. Coefficients and settings for the venting of methanol-nitrogen mixture are added as comments.

```
1
2 #include "udf.h"
3 #include "dpm.h"
4 #include <math.h>
5
6 real depth = 7.0;
7 real injection_height = 0.33;
8 real Temp = 15.0;
9 real Pressure_REF = 101325.0;
10 real MolarWeight = 16.04; /* 28.97 air, 16.04 methane, 32.04 methanol, 28.02 for nitrogen */
11 real SurfaceTension = 0.07199; /* 0.06180 air, 0.07199 methane, 0.022 methanol */
12 real C1 = 4.0;
13 real C2 = 100.0e-6;
14
15 static int position_var = 1;
16 static int position_var1 = 1;
17
18 DEFINE_EXECUTE_AT_END(bubble_size_mass_transfer) /* executed at end of every time step */
19 {
20
21 #if !RP_HOST
22 Domain *d = Get_Domain(1);
23 Injection *i, *i_all;
24 Particle *p;
25 cell_t c;
26 Thread *t;
27 real parcelmass_pre, parcelmass, P, gas_density, solubility, MDOT;
28 real x[ND_ND];
29 real dpm_frac, visc, visc_dpm, rho, d_eq, d_pre, tau, t_k, dt;
30 real eps, k;
31 real u_s, Re, Pe, k_CH4, J, A, D_CH4;
32 real M_H2O = 18.01528;
33 real red_factor = 1.0;
34 real Y_CH4_w = 0;
35 real n_CH4_sol = 0.00002; /* methane 0.00002, methanol 0.59, nitrogen 0.000011 */
36
37 P_List_Item *head, *tail, *item, *temp;
38 int np_removed=0;
39
40 i_all = Get_dpm_injections();
41 head = (P_List_Item *)malloc(sizeof(P_List_Item));
42 tail = (P_List_Item *)malloc(sizeof(P_List_Item));
43 head->next = NULL;
44 tail->next = NULL;
45
46 thread_loop_c(t, d)
47 {
```

```

48 begin_c_loop(c, t)
49 {
50
51 /* calculate volume fraction of DPM-phase */
52 C_CENTROID(x, c, t);
53 P = Pressure_REF + 9.81*C_R(c, t)*(depth - x[2]);
54 P = MAX(Pressure_REF, P);
55 gas_density = P * MolarWeight * 0.001 / (8.314 * (Temp + 273.15));
56 C_UDMI(c, t, 0) = C_DPMS_CONCENTRATION(c, t) / gas_density;
57 C_UDMI(c, t, 1) = MIN(C_UDMI(c, t, 0), 0.9);
58 }
59 end_c_loop(c, t)
60
61 /* loop through particles */
62 loop(i, i_all){
63 loop(p, i->p){
64 cell_t c0 = P_CELL(p);
65 Thread *t0 = P_CELL_THREAD(p);
66 Thread *t0_ocean = THREAD_SUB_THREAD(t0, 1);
67 Thread *t0_atmos = THREAD_SUB_THREAD(t0, 0);
68
69 if (P_POS(p)[2] < depth) {
70
71 parcelmass_pre = P_MASS(p)*P_N(p);
72
73 /* calculation of hydrostatic pressure for each bubble */
74 P = Pressure_REF + 9.81*C_R(c0, t0)*(depth - P_POS(p)[2]);
75 P = MAX(Pressure_REF, P);
76
77 /* bubble density */
78 P_RHO(p) = P * MolarWeight * 0.001 / (8.314 * (Temp + 273.15));
79
80 /* bubble size model, Pan(47) */
81 visc_dpm = 1.7849e-05; /* methane 1.7849e-05, methanol 0.98e-05 */
82 visc = C_MU_L(c0, t0_ocean);
83 eps = MAX(C_D(c0, t0), 1.0e-6);
84 k = C_K(c0, t0);
85 rho = C_R(c0, t0);
86 dpm_frac = C_UDMI(c0, t0, 1);
87 dt = CURRENT_TIMESTEP;
88
89 /* equilibrium diameter */
90 d_eq = C1 * sqrt(dpm_frac) * (pow(SurfaceTension / rho, 0.6) / pow(eps, 0.4))*(pow(visc_dpm /
    visc, 0.25)) + C2;
91 d_pre = P_DIAM(p);
92 t_k = 6.0*sqrt(visc / (rho * eps));
93 if (d_pre > d_eq) /* breakup */
94 {
95 tau = pow(d_pre, 0.66667)*pow(eps, -0.33333333);
96 }
97 else /* coalescence */
98 {
99 tau = d_pre / (0.2*6.0*MAX(1.0e-06, sqrt(dpm_frac*k)));
100 }
101
102 tau = MAX(tau, t_k);
103 P_DIAM(p) = (d_pre + d_eq*dt / tau) / (1.0 + dt / tau);
104 P_DIAM(p) = MAX(P_DIAM(p), 0.0001); /* bubble diameter */
105 P_MASS(p) = P_RHO(p) * M_PI * pow(P_DIAM(p), 3.0) / 6.0;
106
107 /*Gas Dissolution*/
108 D_CH4 = 1.3*pow(10, (-9)); /* Diffusion coefficient, methanol 2.63*pow(10, (-9)), nitrogen
    2.0*pow(10, (-9)) */
109 u_s = fabs(P_VEL(p)[2] - C_W(c0, t0)); /* slip velocity */
110 Re = (P_DIAM(p) * u_s * rho) / visc;
111 Pe = 2.0 * u_s * (P_DIAM(p) / 2.0) / D_CH4;
112
113 /* mass transfer coefficient Zhang & Xu */
114 k_CH4 = (1 + pow((1 + Pe), (1.0 / 3.0)) * (1 + (0.096*(pow(Re, (1.0 / 3.0)))) / (1.0 + 7.0 *
    pow(Re, (-2.0)))))) * (D_CH4 / P_DIAM(p));
115

```

```
116
117 /* assume Y_CH4_w = 0 */
118 J = k_CH4*rho*(n_CH4_sol*(MolarWeight / M_H2O) - Y_CH4_w);
119 A = M_PI*pow(P_DIAM(p), 2.0);
120
121 /* mass transfer with reduction factor */
122 MDOT = red_factor*A*J*P_N(p);
123
124 if ((parcelmass_pre - (CURRENT_TIMESTEP * MDOT)) >= 0.0)
125 {
126 parcelmass = parcelmass_pre - (CURRENT_TIMESTEP * MDOT);
127 }
128 else
129 {
130 parcelmass = 0.0;
131 }
132
133 /* number of particles in a parcel */
134 P_N(p) = parcelmass / P_MASS(p);
135 }
136
137 }
138 }
139 }
140 #endif /* !RP_NODE */
141 }
```

D

Specifics full scale methanol-nitrogen
venting

